**Mapping Protein-Protein Interactions in Self-Sufficient Cytochrome P450 Enzymes**

by

Dana B. Felker

A dissertation submitted in partial fulfillment
of the requirements for the degree of
Doctor of Philosophy
(Toxicology)
in the University of Michigan
2021

Doctoral Committee:

Professor Emeritus Rita Loch-Caruso, Co-Chair
Professor Yoichi Osawa, Co-Chair
Professor Emeritus Rudy Richardson
Professor Santiago Schnell

Dana B. Felker

dbfelker@umich.edu

ORCID iD: 0000-0003-3559-4315

## Dedication

This dissertation is dedicated to my brother, Fort H. Felker. Thank you for being my greatest advocate, ally, and role model. I will never stop learning from you.

## Acknowledgements

This dissertation would not have been possible without the help and support of exceptional mentors, colleagues, friends, and family. First and foremost, thank you to my mentor Yoichi Osawa for countless hours spent guiding my scientific growth. Thank you for your patience and for all the opportunities you gave me to improve as a researcher and communicator. I'm sure I will continue to discover lessons you taught me for a long time after this dissertation is complete. Thank you to my mentor Rita Loch-Caruso for helping me navigate the most difficult moments of the Ph.D. Thank you for paving the way for women in our field and for your dedication to mentorship. Thank you to Rudy Richardson for guiding me through my formative years at UM, and for introducing me to structural modeling. Thank you for your unwavering support, good cheer, and willingness to lend your expertise. Thank you to Santiago Schnell for your infectious enthusiasm, your willingness to always make time for me, and for guiding me in learning modeling. Your mentorship helped me enter an unknown field and quickly find footing – a rare experience I appreciated deeply.

Thank you to the entire Osawa lab for their time, patience, and camaraderie. Thank you to Haoming Zhang for introducing me to crosslinking and for so much guidance and good cheer over these many years. Thank you to Miranda Lau for endless technical expertise, help with navigating every aspect of lab, for being wonderful company, and for laughter and baked goods. Thank you Yoshi Morishima for your patient mentorship, teaching me assays with calm and methodical guidance. Thank you for jokes on the hard days, and for knowing where to look for even the most obscure data. Thank you to Jerry Bo for patience and laughs in the gradient assay days. Thank you to Amanda Davis for teaching me the basics during my rotation and beyond. Thank you to Josh West for troubleshooting and coffee.

Thank you to my PH200 teaching teams, and in particular Al Franzblau and Emily Youatt, for teaching me to integrate empathy and strong leadership into the academic world. I am so grateful for our time together, even the paper grading. Thank you to Justin Colacino and the ADP committee for their constant efforts in improving EHS graduate students' experience. Finally, thank you to my entire department – both administrators and faculty – for encouraging and supporting me on an unconventional research path.

Thank you to the friends who supported me outside the lab and the classroom. To the Livermore contingent, especially Matt, Jamie, Wes, and Clint, thank you for making me laugh from every time zone. To Jacob Moss, thank you for sanity checks and your unwavering confidence. To Colleen, Alex, Deanna, Sara, Jon, and the rest of the aerial/climbing community, thank you for teaching me to embrace imperfection and for keeping me exercised. Thank you to

Brandt Point for demonstrating how vibrant communities change lives. Jenn, Hillary, and Katie: thank you for limitless support and inspiration. To Ben, thank you for pushing me and for all the adventures. Thank you to Jessie for climbing trips, mobility, and unending sisterhood. Thank you Chrissie and Maddie for bouldering, perspective, and laughter I could look forward to at the end of the day. Thank you Aaron for endless support and pep talks. To Bill, Drake, Allyson, and Gabe, thank you for climbing trips and bonfires and particle detectors, and for making Ann Arbor such a hard place to leave. Thank you Laura, Neha, and Emily for infinite dad jokes, love, and acceptance. I'm better every day for your friendship and sisterhood. To Jacob Johnson, thank you for my favorite trips to the Red and the New, for your unparalleled patience and attention, for your quick wit, for keeping me fed, and for your exceptional partnership. You've been my favorite surprise in Michigan.

Finally, thank you to my family for making this degree possible. Thank you to Michele and Deday for your fearlessness. Thank you to Marcia and Tracie for teaching me to be strong and adventurous. Thank you to Jon and Liana for nurturing my love of science, and for years of invaluable guidance and mentorship. I love you all immensely. Thank you to my brother Fort for first aid in foreign countries, adventures shared both fun and challenging, and for a lifetime of friendship. I am so honored to be your sister. Most importantly, thank you to my parents Fort and Robin, who sacrificed more than I'll ever understand to build the foundations for my success. Thank you for raising me to ask questions and believe in my own capabilities, and for cheering me on at every step. Thank you for supporting me in every way as I chose my path, for friendship, for mentorship, for unconditional acceptance, for challenging me, and for a lifetime of inspiration. I couldn't have achieved any of this without you.

## Table of Contents

## List of Tables

## List of Figures

## Abstract

Cytochrome P450 (P450) proteins are heme-containing mixed function oxidase enzymes that play a critical role in the metabolism of drugs and toxicants. For P450 enzyme catalysis, a flavin-containing reductase must shuttle electrons from NADPH to the heme prosthetic group of P450. Although in most cases the reductase enzyme is a separate protein partner, there are self-sufficient P450 enzymes containing the reductase enzyme fused with the P450 enzyme in a single polypeptide chain. These self-sufficient P450 enzymes are excellent model systems to study the mechanism of P450 catalysis and electron transfer reactions. There are no crystal structures of the full-length self-sufficient P450 enzymes, although recently low-resolution cryo-EM derived structures of two self-sufficient P450 enzymes, CYP102A1 and neuronal nitric oxide synthase (nNOS), have been reported by our lab. A covalent crosslinking and mass spectrometry (CXL-MS) workflow was developed in this thesis to study interdomain and interprotein interactions within these two self-sufficient P450 enzymes, in order to learn how P450 and reductase domains interact in detail. In these studies, I refined the workflow to analyze and interpret MS data of crosslinks specifically from homodimeric proteins by utilizing existing structural data in combination with an established subtractive method to identify intra- and inter-protein crosslinks. CXL-MS of the CYP102A1 homodimer yielded 31 unique crosslinks, 26 of which mapped in accordance with the cryo-EM based structural models of the protein. Furthermore, I identified a novel conformational state of the CYP102A1 homodimer based on modeling studies of the remaining five crosslinks that likely represent a structure favorable for

electron transport to the active site heme. I then applied CXL-MS to a homodimer of nNOS bound to its regulatory protein calmodulin (CaM), which activates the enzyme for catalysis. The resulting 74 crosslinks, similar to those found for CYP102A1, are consistent with a conformation where the oxygenase and reductase domains are in closer proximity than seen in previous structural studies. My studies identify novel heme and reductase interdomain interactions for both of the analyzed self-sufficient P450 enzymes and provide insight on domain organization during catalysis. The CXL-MS workflow developed here will be applicable in investigating other homomeric multiprotein machineries. Most importantly, I have identified new interdomain and interprotein interfaces that can serve as regulatory targets in modulating these important metabolizing systems. This work provides new insights on the catalytic mechanism of these powerful mixed function oxidase enzymes, which are important protective enzymes from environmental toxicants as well as potential biocatalysts for use in environmental waste remediation.

# Chapter 1 Introduction

## Cytochrome P450 enzymes and human health

Cytochrome P450 enzymes (P450s or CYPs) are heme-containing mixed function oxidases that play a vital role in the metabolism of both endogenous and foreign compounds. P450s are involved in the oxidation and/or reduction of 95% of all chemicals that undergo these reactions in humans [Guengerich et al., 2016], making them a critically important class of proteins in the body's metabolic response. CYPs predominately function as monooxygenases in Phase I metabolism, which increases water solubility of chemicals. In most cases, metabolism of molecules by P450s facilitates their excretion from the body. This process deactivates numerous drugs, toxicants, and other chemicals absorbed following environmental exposures. Metabolism by P450 enzymes is therefore a large determinant of chemical half-life in the body.

The influence of P450s on drug metabolism has become apparent as we have gained a more detailed understanding of metabolic processes. Just five CYPs are involved in the metabolism of more than 90% of the small-molecule drugs in use today, and two CYP enzymes (CYP2D6 and CYP3A4) metabolize 40% of drugs and 21% of natural compounds in humans [Rendic & Guengerich, 2015]. Understanding the mechanisms of P450 function is an important step in understanding metabolism of foreign compounds in the body, and therefore in predicting and preventing toxic outcomes.

## Major classes of P450 enzymes

P450 enzymes are classified in broad subcategories based on the composition of their functional subunits. Class II P450s, responsible for the majority of Phase I metabolism in humans, comprise two separately expressed protein subunits: a P450 subunit and a diflavin reductase subunit containing both flavin adenine dinucleotide (FAD) and flavin mononucleotide (FMN) cofactors, which sources electrons from nicotinamide adenine dinucleotide phosphate hydrogen (NADPH) [Iyanagi & Mason, 1973]. These P450s are membrane-bound. Class VIII P450s comprised of similar oxygenase and reductase components to class II systems, however in class VIII P450s contain both oxygenase and reductase subunits fused within a single peptide chain. These "self-sufficient" P450s are soluble and therefore easier to study than their membrane-bound counterparts [Roberts et al., 2002; Finnigan et al., 2020].

Structural studies investigating class VIII P450s have proved widely applicable to understanding the mechanisms of enzymatic turnover in other classes of P450 enzymes. The study of protein-protein interfaces within class II P450 assemblies is complicated by the membrane-bound nature of these systems, and the fact that the reductase and oxygenase subunits are expressed as separate proteins. Partially due to this, some self-sufficient class VIII P450s have historically served as model systems by which the other classes of P450 proteins can be studied.

## Common features of Class III P450s

Class VIII P450 enzymes are comprised of an N-terminal oxygenase domain containing the active site cleft and prosthetic heme, a C-terminal reductase domain containing globular FMN- and FAD-binding domains linked by a flexible hinge, and a highly flexible linker region

connecting oxygenase and reductase domains (Figure 1-1A). The most studied class VIII P450s are obligate homodimers; to be active, two monomers with identical sequence assemble into a noncovalently associated multiprotein complex [Black & Martin, 1994; Neeli et al., 2005]. Their oxygenase and reductase domains directly contact one another, forming two protein-protein interfaces (Figure 1-1B, Left).

Due to the large size and high degree of flexibility between domains in these proteins, crystal structures are rarely obtained for more than one domain. No full-length class VIII P450 has been resolved by crystallography. The relatively stable oxygenase domain dimer has been resolved for several fusion P450 enzymes, along with individual FAD- and FMN-binding portions or entire FMN- and FAD-containing reductase domains. More recently, cryoelectron microscopy (cryo-EM) and negative stain EM have been applied to study the full-length proteins at lower resolution. These methods capture multiple conformational states of the proteins but do not provide sufficient resolution to determine which domains interact in each conformational state. Without orthogonal data, it can even be difficult to decipher which domain is responsible for each electron density in these structures. Complementary structural data acquired by crosslinking, hydrogen deuterium exchange (HDX), and mutagenesis greatly bolster our ability to utilize these low-resolution structural methods.

The path of electron transfer in this group of enzymes is a defining characteristic. Careful work using the model class VIII protein CYP102A1 has established that electrons are transferred individually from the NADPH donor to the FAD cofactor, then to an adjacent FMN. The FMN, bound within its own globular domain, then “shuttles” electrons to the active site heme within the oxygenase domain (Figure 1-1B, Right) [Munro et al., 1994; Neeli et al., 2005]. Based on the best-studied representatives from class VIII P450 enzymes, this second electron transfer is

believed to be the rate-limiting step, although the precise mechanism by which this transfer occurs is not fully understood. The orientation of the FMN domain relative to the heme-containing oxygenase during electron transfer has yet to be captured by crystallography or cryo-EM for any class VIII P450 enzyme. Due to the transient nature of this conformation, it is likely that it will be too difficult to capture by structural methods involving freezing (for cryo-EM) or crystallization (for x-ray crystallography). In contrast, structural methods able to capture conformational changes, such as HDX and crosslinking, are well positioned to address this deficiency.

## CYP102A1: a model class VIII P450

The first class VIII P450 to be discovered is also the most widely studied enzyme in this class, CYP102A1 (historically referred to as BM3). The Fulco group first isolated and characterized CYP102A1 from soil bacterium *Bacillus megaterium* in 1974 [Miura & Fulco, 1974; Hare & Fulco, 1975; Ho & Fulco, 1976; Matson et al. 1977]. Since its discovery, it rapidly became a model enzyme for understanding both self-sufficient and class II P450s. CYP102A1 contains an oxygenase domain with prosthetic heme that aligns closely with eukaryotic CYP2A and CYP4A families [Lewis et al. 1998]. It also contains a FAD- and FMN-containing NADPH-reductase domain with strong sequence and structural similarity to mammalian cytochrome P450 reductase [Narhi & Fulco 1986; Porter 1991; Sevrioukova & Peterson 1995; Warman et al., 2005]. Unlike the class II mammalian systems, this reductase is combined with the heme-containing oxygenase domain within a single peptide chain. The two domains, when cleaved by proteolysis, do not display a strong affinity for one another [Narhi & Fulco, 1987]. The CYP102A1 protein machinery is soluble, rather than membrane-bound like most mammalian

systems. With all the functional units of mammalian systems contained into a single soluble peptide chain, CYP102A1 is the ideal system by which to study mammalian P450s.

In addition to its role as a model for mammalian P450 systems, CYP102A1 is also a subject of intense interest due to its potential utility as a biocatalyst. CYP102A1 has the most rapid turnover of any P450 monooxygenase at ~17,000 min−1 [Noble et al., 1999; Munro et al., 2002]. With its ease of expression and high catalytic rate, numerous researchers have identified the enormous potential of this enzyme as a biochemical tool. An impressive body of work using point mutagenesis and directed evolution studies has been carried out in an effort to tailor substrate recognition and adapt CYP102A1 for use in the biotechnology field. Potential uses include use as a tool for pharmaceutical compound screening, drug metabolite production, production of synthetic compounds, and mimicry of human phase I metabolism [Warman et al., 2005; Reinen et al., 2011; Whitehouse et al., 2012; Murphy, 2015].

Despite its importance and decades of study, structure-function understanding of the full-length CYP102A1 has remained limited until recent years. Crystal structures of the complete oxygenase and reductase domains have been resolved at high resolution for some time [Ravichandran et al., 1993; Li & Poulos, 1997; Joyce et al., 2012]. An additional high-resolution structure was acquired using a truncated construct with both oxygenase and FMN domains, which included the full oxygenase domain dimer and one FMN domain associated [Sevrioukova et al., 1999]. However, these structures captured an incomplete subset of interdomain interaction during electron shuttling across the enzyme. Most critically, how these domains interact with one another during interprotein electron transfer from FMN to heme remains poorly understood. Recently, multiple conformations of the full-length CYP102A1 homodimer were captured by cryo-EM at high resolution [Su et al., 2020]. These three models allow our first close

examination of interdomain interactions, and likely represent the most stable conformations of the CYP102A1 homodimer. While these structures represent a major advance in understanding CYP102A1 domain mobility during enzymatic function, they do not capture all the interdomain movement in the CYP102A1 conformational suite or the conformation responsible for interprotein electron transfer from FMN to heme.

## Neuronal nitric oxide synthase

Nitric oxide (NO) is a critical molecule in the body involved in regulation of vascular tone, angiogenesis, and neurotransmission [Meffert et al., 1994; Ziche & Morbidelli, 2000; Moncada & Higgs, 2006; Calabrese et al., 2007; Forstermann & Sessa, 2012; Feng et al., 2014]. Insufficient NO has been cited as a leading cause of endothelial dysfunction [Feng & Hedner, 1990] and is linked to the subsequent pathogenesis of cardiovascular diseases including atherosclerosis, hypertension, and diabetes [Naseem, 2005]. Conversely, overabundant NO is toxic through the generation of oxidative and nitrosative stress, causing protein and lipid damage, DNA damage, and energy depletion in addition to direct cytotoxicity caused by NO itself [Schmidt & Walter, 1994; Brown, 2010; Król & Kepinska, 2020]. Unlike most signaling molecules, NO is a highly reactive gaseous molecule that is not compartmentalized and instead diffuses freely following its production. NO levels are therefore regulated through modulation of production by nitric oxide synthase (NOS) enzymes. Three isoforms of NOS enzyme are present in the body: inducible, endothelial, and neuronal. Each isoform serves a unique physiologic function through its production of NO in distinct tissues, and each isoform is implicated in adverse clinical outcomes when dysregulated. The three isoforms share a notable similarity in structure, making isoform-specific modulation of NOS enzymes extremely difficult.

NOS enzymes are unique among class VIII P450 proteins for several reasons beyond the gaseous product they produce; in part due to these differences, there is still some debate regarding their status as a class VIII P450. NOS enzymes are the only flavoheme proteins to use tetrahydrobiopterin (BH4) as a cofactor, and require BH4 for homodimer formation and catalysis [Panda et al., 2002; Stuehr et al., 2004]. In addition, the obligatory association of regulatory protein calmodulin (CaM) for NOS activity is unique to NOS enzymes among P450s. Due to the large differences between NOS enzymes and conventional class VIII P450s, it has been hypothesized that NOS and class VIII P450s are an example of convergent evolution [Masters et al., 1996].

Like other class VIII P450s, NOS enzymes are comprised of an N-terminal oxygenase domain and a C-terminal diflavin reductase domain. A flexible linker region connects these domains, which is the site of association with CaM (Figure 1-2A). CaM displays a different affinity for each of the three NOS isoforms, and the linker region is one of the sites of greatest sequence variability across isoforms. NOS enzymes are homodimeric, with dimerization interfaces between oxygenase domains and FAD domains. The dimerization interface of the oxygenase domain is vastly more stable [Panda et al., 2002]. Within this interface, a zinc ion is chelated to both monomers via two conserved cysteines and both tetrahydrobiopterin (BH4) cofactors are incorporated [Matter et al., 2005]. NOS reductase domains have been shown to dissociate in negative stain- and cryo-EM studies, leading to a large conformational shift from the closed to an extended conformational shape (Figure 1-2B) [Campbell et al., 2014; Yokom et al., 2014].

NOS enzymes, like CYP102A1, are diflavin monooxygenases with an electron transport mechanism that involves both monomers within the homodimer. Electrons donated from

NADPH are transferred to the FAD cofactor, and then an additional intra-protein transfer to the FMN domain occurs. These first two electron transfer steps happen within one NOS reductase domain. Next, the FMN domain shuttles electrons to the opposing monomer's oxygenase domain. The mechanism by which electrons are transferred from FMN to opposing heme remains poorly understood for all three NOS isoforms, however in all isoforms calcium-bound CaM associating with its binding helix is required for FMN to heme electron transfer [Panda et al., 2001]. Movement of the FMN domain toward the backside of the opposing monomer's active site cleft has been observed in all three NOS isoforms by cryo-EM [Campbell et al., 2014; Yokom et al., 2014] and hydrogen-deuterium exchange (HDX) studies have identified sites of likely interdomain contact in inducible and neuronal NOS [Smith et al., 2013; Hanson et al., 2018].

The neuronal isoform of NOS is responsible for NO production in the brain, and is implicated in the development of many neurodegenerative disorders. nNOS is structurally unique among NOS isoforms in containing an N-terminal PDZ domain which is connected to the oxygenase domain by a ~170 amino acid flexible tether (Figure 1-2A). This domain is responsible for presynaptic localization of the nNOS [Brenman et al., 1996]. Crystal structures of the nNOS reductase domain and dimerized oxygenase domains have been resolved, along with a low-resolution cryo-EM model of the nNOS homodimer bound to CaM [Garcin et al., 2004; Matter et al., 2005; Yokom 2014]. Despite extensive biochemical and structural studies on the nNOS, it remains unknown how domains interact during the critical stage of nNOS turnover: electron transfer from FMN to heme. In addition, whereas the interaction between CaM and its known binding helix on the nNOS is well characterized the interactions between CaM and other

regions of the full-length nNOS remain poorly understood. This knowledge gap is addressed in chapter 3 of my thesis.

## Transient conformations are missing links in understanding CYP102A1 and nNOS

Across dissimilar class VIII P450 enzymes CYP102A1 and nNOS, a common pathway of electron transfer is conserved: NADPH to FAD to FMN to heme. In addition, negative stain- and cryo-EM studies indicate a similar conformational suite of these two homodimeric protein machineries [Campbell et al., 2014; Yokom et al., 2014; Zhang et al., 2018; Su et al., 2020]. It remains unknown whether this translates to a conserved suite of interdomain interactions or conserved sites of interaction between domains in these very different protein machineries. In particular, the critical step in electron transfer from FMN to heme remains unresolved in both protein systems by high-resolution structural methods. The interdomain interactions and cofactor positioning in this conformation remain unknown for either enzyme.

## Studying protein-protein interactions using CXL-MS

Covalent crosslinking and mass spectrometry (CXL-MS) is a method by which protein-protein interactions can be examined in their endogenous states in solution. In these studies, a bifunctional small molecule with two reactive "warheads" is added to multiprotein machineries in solution. Each warhead covalently binds any compatible amino acid side chain it encounters, forming covalent bridges between compatible residues within certain proximity of one another in the protein. Once crosslinking is complete, proteins are proteolyzed and the resulting short peptides are analyzed by mass spectrometry. The peptide sequence and location of crosslink formation within the peptide can then be determined through examination of fragmentation spectra. A summary of this general CXL-MS workflow is shown in Figure 1-3.

CXL-MS has several important advantages over crystallography, cryo-EM and NMR in examining protein-protein interactions. It can be applied to protein machineries of unlimited size, unlike crystallography or NMR [Chavez & Bruce 2019]. In addition, it allows analysis to take place in solution; this provides insight into protein quaternary structure and native interprotein interactions too transient to withstand freezing or crystallization. Perhaps most importantly, exposing proteins to a crosslinker in solution allows for the sampling of numerous conformational states of the protein simultaneously [Rappsilber, 2011], and the method remains sound when applied to partially (although not completely) unfolded proteins [Chen et al., 2010]. Moreover, it allows for movement of proteins, which is critical for their function, whether in flexible linker regions or entire disordered segments [Dunker et al., 2008; Bruce, 2012]. CXL-MS is therefore unique among structural methods in its ability to examine large, highly flexible protein machineries as they undergo extensive movement in solution.

Recent advances in crosslink design and MS data analysis have allowed application of the CXL-MS method to answer increasingly detailed structural questions. Historically the method was only used for capturing the presence of protein-protein interaction, and did not contribute detailed information on where crosslinks formed between proteins. Current methods allow not only the presence of crosslinks to be determined but also their specific location within the protein backbone. The advent of MS-cleavable covalent crosslinkers, with fragmentation sites included in the covalent bridge, allow automated algorithms to search for specific crosslink fragments within MS data. This advance has largely overcome the previously prohibitive step of crosslink site identification within complex samples. With the ability to identify sites of crosslink formation, more intricate structural determinations can be undertaken. These include identification of the precise sites of protein-protein interaction within large multiprotein

machineries and sites of interaction between domains during conformational changes [Jacobsen et al., 2006; Murakami et al., 2013; Leitner et al., 2016; Sailer et al., 2018; Bellia et al., 2019; Chavez & Bruce, 2019]. CXL-MS is emerging as a technique well-suited in capturing the movements of large proteins through multiple conformational states [Gong et al., 2015].

**Homodimeric proteins present a unique challenge in CXL-MS data interpretation.**

Homodimeric protein complexes such as CYP102A1 and nNOS are comprised of two identical protein chains assembled in a quaternary structure. Because crosslink identification is performed using protein residue sequence, and the sequence of each subunit within these complexes is the same, a distinct challenge is presented in CXL-MS data interpretation in these systems. For each crosslink identified within a homodimeric complex, it cannot be determined from residue sequence alone which monomer within the complex were involved in the crosslink. Several methods have been proposed in the literature to overcome this hurdle; however, each multiprotein complex is unique and the application of each of these strategies is not always feasible.

An approach put forward by Gaber and colleagues (2019) addresses crosslink configuration within or across monomers during the structural modeling phase following MS data analysis. Through calculating both Euclidean distance and solvent accessible surface distance between residues identified in crosslinks, the ambiguity of crosslink assignment can be reduced as solvent accessible surface area better differentiates between intra-monomer and inter-monomer crosslinks than the traditional Euclidean distance measurement. However, without additional experimental information, ambiguity remained in their crosslink assignment. Additionally, these analyses require a near-complete structure resolution around all crosslinked

sites in the protein under investigation. This computational method can therefore not be applied in proteins with incomplete structures.

A method described in detail by Lima et al. (2018) addresses the ambiguity issue during sample preparation by stable isotope-labeling one monomer then reassembling the homodimer with one “light” and one “heavy” subunit. Differentiating which monomer is bound at either end of the identified crosslinks then becomes relatively simple during MS data analysis. This method, while unambiguous [Taverner et al., 2002; Pettelkau et al., 2013], is only feasible in protein complexes that can be dissociated, labeled, and subsequently properly reassembled. It is therefore not applicable to all systems requiring investigation.

Another method that experimentally addresses homodimeric crosslink ambiguity is incorporation of a monomer/dimer separation step following crosslinking and before MS analysis. This approach results in two samples: one of crosslinked monomeric protein (containing only crosslinks within one monomer) and one of crosslinked dimeric protein (containing crosslinks across monomers). All crosslinks present in the dimeric sample that are not detected within the monomer are assigned as inter-monomer crosslinks [Chu et al., 2006; Wu et al. 2013; Karagöz et al., 2017]. This method has the potential for applicability to a much wider array of homodimeric protein complexes; however, its precision has yet to be examined in detail. I investigate the efficacy of this approach in chapter two, in an examination of the homodimeric CYP102A1 complex.

## Conclusion

Cytochrome P450 protein systems are vital contributors to the metabolism of exogenous compounds including drugs and toxicants. The response of CYP450 enzymes affects the level of

toxicity humans experience from xenobiotics. Thus, understanding the mechanisms of their operation is of immense importance in modulating toxicity following toxicant or drug exposure. One of the largest mysteries in enzymatic function of P450 enzymes is their configurations during the transient conformational changes responsible for electron transfer to heme-containing active sites. To investigate the highly unstable states of P450 enzymes, the proteins must be in their native states when captured for structural examination. CXL-MS is a uniquely well-suited structural methodology to probe these large, flexible proteins in transient conformational states. Recent advances in the field of CXL-MS data analysis and reagent development allow the generation of high-confidence datasets from complex multiprotein machineries. In this dissertation work, I harness the CXL-MS methodology to understand how domains within self-sufficient P450 enzymes interact in their native states. I utilize two highly dissimilar P450 systems to determine whether there is a conserved conformational suite within this class of critical metabolic proteins. In chapter two, I utilize an extensively studied model class III P450, CYP102A1, to build and validate a robust method for examination of homodimeric proteins using CXL-MS. In chapter three, I apply this method to explore interprotein interactions within the more complex and poorly understood nNOS:CaM multiprotein machinery. This dissertation work provides valuable insight into the interprotein and interdomain mechanics of these important model P450 systems.

## References


Bellia, F.; Lanza, V.; García-Viñuales, S.; Ahmed, I. M. M.; Pietropaolo, A.; Iacobucci, C.; Malgieri, G.; D'Abrosca, G.; Fattorusso, R.; Nicoletti, V. G.; Sbardella, D.; Tundo, G. R.; Coletta, M.; Pirone, L.; Pedone, E.; Calcagno, D.; Grasso, G.; Milardi, D. Ubiquitin Binds the Amyloid β Peptide and Interferes with Its Clearance Pathways. *Chem. Sci.* **2019**, *10* (9), 2732–2742. https://doi.org/10.1039/C8SC03394C.

Black, S. D.; Martin, S. T. Evidence for Conformational Dynamics and Molecular Aggregation in Cytochrome P450 102 (BM-3). *Biochemistry* **1994**, *33* (40), 12056–12062. https://doi.org/10.1021/bi00206a007.

Brenman, J. E.; Chao, D. S.; Gee, S. H.; McGee, A. W.; Craven, S. E.; Santillano, D. R.; Wu, Z.; Huang, F.; Xia, H.; Peters, M. F.; Froehner, S. C.; Bredt, D. S. Interaction of Nitric Oxide Synthase with the Postsynaptic Density Protein PSD-95 and ␣1-Syntrophin Mediated by PDZ Domains. *Cell* **1996**, *84* (5), 757–767. https://doi.org/10.1016/s0092-8674(00)81053-3.

Brown, G. C. Nitric Oxide and Neuronal Death. *Nitric Oxide* **2010**, *23* (3), 153–165. https://doi.org/10.1016/j.niox.2010.06.001.

Bruce, J. E. In Vivo Protein Complex Topologies: Sights through a Cross-Linking Lens. *Proteomics* **2012**, *12* (10), 1565–1575. https://doi.org/10.1002/pmic.201100516.

Calabrese, V.; Mancuso, C.; Calvani, M.; Rizzarelli, E.; Butterfield, D. A.; Giuffrida Stella, A. M. Nitric Oxide in the Central Nervous System: Neuroprotection versus Neurotoxicity. *Nat Rev Neurosci.* **2007**, *8* (10), 766–775. https://doi.org/10.1038/nrn2214.

Campbell, M. G.; Smith, B. C.; Potter, C. S.; Carragher, B.; Marletta, M. A. Molecular Architecture of Mammalian Nitric Oxide Synthases. *Proc Natl Acad Sci U S A*. **2014**, *111* (35), E3614–E3623. https://doi.org/10.1073/pnas.1413763111.

Chavez, J. D.; Bruce, J. E. Chemical Cross-Linking with Mass Spectrometry: A Tool for Systems Structural Biology. *Curr Opin Chem Biol.* **2019**, *48*, 8–18. https://doi.org/10.1016/j.cbpa.2018.08.006.

Chen, Z. A.; Jawhari, A.; Fischer, L.; Buchen, C.; Tahir, S.; Kamenski, T.; Rasmussen, M.; Lariviere, L.; Bukowski-Wills, J.-C.; Nilges, M.; Cramer, P.; Rappsilber, J. Architecture of the RNA Polymerase II–TFIIF Complex Revealed by Cross-Linking and Mass Spectrometry. *EMBO J* **2010**, *29* (4), 717–726. https://doi.org/10.1038/emboj.2009.401.

Chu, F.; Maynard, J. C.; Chiosis, G.; Nicchitta, C. V.; Burlingame, A. L. Identification of Novel Quaternary Domain Interactions in the Hsp90 Chaperone, GRP94. *Protein Sci.* **2006**, *15* (6), 1260–1269. https://doi.org/10.1110/ps.052065106.

Dunker, A. K.; Oldfield, C. J.; Meng, J.; Romero, P.; Yang, J. Y.; Chen, J. W.; Vacic, V.; Obradovic, Z.; Uversky, V. N. The Unfoldomics Decade: An Update on Intrinsically Disordered Proteins. *BMC Genomics* **2008**, *9* (Suppl 2), S1. https://doi.org/10.1186/1471-2164-9-S2-S1.

Feng, C.; Chen, L.; Li, W.; Elmore, B. O.; Fan, W.; Sun, X. Dissecting Regulation Mechanism of the FMN to Heme Interdomain Electron Transfer in Nitric Oxide Synthases. *J Inorg Biochem.* **2014**, *130*, 130–140. https://doi.org/10.1016/j.jinorgbio.2013.09.005.

Feng, Q.; Hedner, T. Endothelium-Derived Relaxing Factor (EDRF) and Nitric Oxide (NO). I. Physiology, Pharmacology and Pathophysiological Implications. *Clin Physiol.* **1990**, *10* (5), 407–426. https://doi.org/10.1111/j.1475-097x.1990.tb00822.x.

Finnigan, J. D.; Young, C.; Cook, D. J.; Charnock, S. J.; Black, G. W. Cytochromes P450 (P450s): A Review of the Class System with a Focus on Prokaryotic P450s. In *Advances in Protein Chemistry and Structural Biology*; Elsevier, 2020; Vol. 122, pp 289–320. https://doi.org/10.1016/bs.apcsb.2020.06.005.

Forstermann, U.; Sessa, W. C. Nitric Oxide Synthases: Regulation and Function. *Eur Heart J* **2012**, *33* (7), 829–837. https://doi.org/10.1093/eurheartj/ehr304.

Gaber, A.; Gunčar, G.; Pavšič, M. Proper Evaluation of Chemical Cross-Linking-Based Spatial Restraints Improves the Precision of Modeling Homo-Oligomeric Protein Complexes. *BMC Bioinformatics* **2019**, *20* (1), 464. https://doi.org/10.1186/s12859-019-3032-x.

Garcin, E. D.; Bruns, C. M.; Lloyd, S. J.; Hosfield, D. J.; Tiso, M.; Gachhui, R.; Stuehr, D. J.; Tainer, J. A.; Getzoff, E. D. Structural Basis for Isozyme-Specific Regulation of Electron Transfer in Nitric-Oxide Synthase. *J Biol Chem.* **2004**, *279* (36), 37918–37927. https://doi.org/10.1074/jbc.M406204200.

Gong, Z.; Ding, Y.-H.; Dong, X.; Liu, N.; Zhang, E. E.; Dong, M.-Q.; Tang, C. Visualizing the Ensemble Structures of Protein Complexes Using Chemical Cross-Linking Coupled with Mass Spectrometry. *Biophys Rep.* **2015**, *1* (3), 127–138. https://doi.org/10.1007/s41048-015-0015-y.

Guengerich, F. P.; Waterman, M. R.; Egli, M. Recent Structural Insights into Cytochrome P450 Function. *Trends Pharmacol Sci.* **2016**, *37* (8), 625–640. https://doi.org/10.1016/j.tips.2016.05.006.

Hanson, Q. M.; Carley, J. R.; Gilbreath, T. J.; Smith, B. C.; Underbakke, E. S. Calmodulin-Induced Conformational Control and Allostery Underlying Neuronal Nitric Oxide Synthase Activation. *J Mol Biol.* **2018**, *430* (7), 935–947. https://doi.org/10.1016/j.jmb.2018.02.003.

Hare, R. S.; Fulco, A. J. Carbon Monoxide and Hydroxymercuribenzoate Sensitivity of a Fatty Acid (Omega-2) Hydroxylase from Bacillus Megaterium. *Biochem Biophys Res Commun.* **1975**, *65* (2), 665–672.

Ho, P. P.; Fulco, A. J. Involvement of a Single Hydroxylase Species in the Hydroxylation of Palmitate at the ω—1, ω—2 and ω—3 Positions by a Preparation from Bacillus Megaterium. *Biochim Biophys Acta.* **1976**, *431* (2), 249–256. https://doi.org/10.1016/0005-2760(76)90145-4.

Iyanagi, T.; Mason, H. S. Properties of Hepatic Reduced Nicotinamide Adenine Dinucleotide Phosphate-Cytochrome c Reductase. *Biochemistry* **1973**, *12* (12), 2297–2308. https://doi.org/10.1021/bi00736a018.

Jacobsen, R. B.; Sale, K. L.; Ayson, M. J.; Novak, P.; Hong, J.; Lane, P.; Wood, N. L.; Kruppa, G. H.; Young, M. M.; Schoeniger, J. S. Structure and Dynamics of Dark-State Bovine Rhodopsin Revealed by Chemical Cross-Linking and High-Resolution Mass Spectrometry. *Protein Sci* **2006**, *15* (6), 1303–1317. https://doi.org/10.1110/ps.052040406.

Joyce, M. G.; Ekanem, I. S.; Roitel, O.; Dunford, A. J.; Neeli, R.; Girvan, H. M.; Baker, G. J.; Curtis, R. A.; Munro, A. W.; Leys, D. The Crystal Structure of the FAD/NADPH-Binding Domain of Flavocytochrome P450 BM3. *FEBS J.* **2012**, *279* (9), 1694–1706. https://doi.org/10.1111/j.1742-4658.2012.08544.x.

Karagöz, G. E.; Acosta-Alvear, D.; Nguyen, H. T.; Lee, C. P.; Chu, F.; Walter, P. An Unfolded Protein-Induced Conformational Switch Activates Mammalian IRE1. *eLife* **2017**, *6* (e30700), 1–29. https://doi.org/10.7554/eLife.30700.

Król, M.; Kepinska, M. Human Nitric Oxide Synthase—Its Functions, Polymorphisms, and Inhibitors in the Context of Inflammation, Diabetes and Cardiovascular Diseases. *IJMS* **2020**, *22* (1), 56. https://doi.org/10.3390/ijms22010056.

Leitner, A.; Faini, M.; Stengel, F.; Aebersold, R. Crosslinking and Mass Spectrometry: An Integrated Technology to Understand the Structure and Function of Molecular Machines. *Trends Biochem Sci.* **2016**, *41* (1), 20–32. https://doi.org/10.1016/j.tibs.2015.10.008.

Lewis, D. F. V.; Watson, E.; Lake, B. G. Evolution of the Cytochrome P450 Superfamily: Sequence Alignments and Pharmacogenetics. *Mutat Res.* **1998**, *410* (3), 245–270. https://doi.org/10.1016/S1383-5742(97)00040-9.

Li, H.; Poulos, T. L. The Structure of the Cytochrome P450BM-3 Haem Domain Complexed with the Fatty Acid Substrate, Palmitoleic Acid. *Nat Struct Mol Biol* **1997**, *4* (2), 140–146. https://doi.org/10.1038/nsb0297-140.

Lima, D. B.; Melchior, J. T.; Morris, J.; Barbosa, V. C.; Chamot-Rooke, J.; Fioramonte, M.; Souza, T. A. C. B.; Fischer, J. S. G.; Gozzo, F. C.; Carvalho, P. C.; Davidson, W. S. Characterization of Homodimer Interfaces with Cross-Linking Mass Spectrometry and Isotopically Labeled Proteins. *Nat Protoc* **2018**, *13* (3), 431–458. https://doi.org/10.1038/nprot.2017.113.

Marletta, M. A. Nitric Oxide Synthase Structure and Mechanism. *J Biol Chem.* **1993**, *268* (17), 12231–12234. https://doi.org/10.1016/S0021-9258(18)31375-9.

Masters, B. S. S.; McMillan, K.; Sheta, E. A.; Nishimura, J. S.; Roman, L. J.; Martasek, P. Neuronal Nitric Oxide Synthase, a Modular Enzyme Formed by Convergent Evolution: Structure Studies of a Cysteine Thiolate-Liganded Heme Protein That Hydroxylates L-Arginine to Produce NO as a Cellular Signal. *FASEB J.* **1996**, *10* (5), 552–558. https://doi.org/10.1096/fasebj.10.5.8621055.

Matson, S.; Hare, S.; Fulco, J. Characteristics of a Cytochrome P-450-Dependent Fatty Acid Omega-2 Hydroxylase from Bacillus Megaterium. *Biochim Biophys Acta.* **1977**, *487* (3), 487–494. https://doi.org/10.1016/0005-2760(77)90218-1.

Matter, H.; Kumar, H. S. A.; Fedorov, R.; Frey, A.; Kotsonis, P.; Hartmann, E.; Fröhlich, L. G.; Reif, A.; Pfleiderer, W.; Scheurer, P.; Ghosh, D. K.; Schlichting, I.; Schmidt, H. H. H. W. Structural Analysis of Isoform-Specific Inhibitors Targeting the Tetrahydrobiopterin Binding Site of Human Nitric Oxide Synthases. *J. Med. Chem.* **2005**, *48* (15), 4783–4792. https://doi.org/10.1021/jm050007x.

Meffert, M. K.; Haley, J. E.; Schuman, E. M.; Schulman, H.; Madison, D. V. Inhibition of Hippocampal Heme Oxygenase, Nitric Oxide Synthase, and Long-Term Potentiation by Metalloporphyrins. *Neuron* **1994**, *13* (5), 1225–1233. https://doi.org/10.1016/0896-6273(94)90060-4.

Miura, Y.; Fulco, A. J. (ω–2) Hydroxylation of Fatty Acids by a Soluble System from Bacillus Megaterium. *J Biol Chem.* **1974**, *249* (6), 1880–1888.

Moncada, S.; Higgs, E. A. The Discovery of Nitric Oxide and Its Role in Vascular Biology. *Br J Pharmacol.* **2006**, *147* (S1), S193–S201. https://doi.org/10.1038/sj.bjp.0706458.

Munro, A. W.; Leys, D. G.; McLean, K. J.; Marshall, K. R.; Ost, T. W. B.; Daff, S.; Miles, C. S.; Chapman, S. K.; Lysek, D. A.; Moser, C. C.; Page, C. C.; Dutton, P. L. P450 BM3: The Very Model of a Modern Flavocytochrome. *Trends Biochem Sci.* **2002**, *27* (5), 250–257. https://doi.org/10.1016/S0968-0004(02)02086-8.

Munro, A. W.; Lindsay, J. G.; Coggins, J. R.; Kelly, S. M.; Price, N. C. Structural and Enzymological Analysis of the Interaction of Isolated Domains of Cytochrome P-450 BM3. *FEBS Lett.* **1994**, *343* (1), 70–74. https://doi.org/10.1016/0014-5793(94)80609-8.

Murakami, K.; Elmlund, H.; Kalisman, N.; Bushnell, D. A.; Adams, C. M.; Azubel, M.; Elmlund, D.; Levi-Kalisman, Y.; Liu, X.; Gibbons, B. J.; Levitt, M.; Kornberg, R. D. Architecture of an RNA Polymerase II Transcription Pre-Initiation Complex. *Science* **2013**, *342* (6159), 1238724–1238724. https://doi.org/10.1126/science.1238724.

Murphy, C. D. Drug Metabolism in Microorganisms. *Biotechnol Lett* **2015**, *37* (1), 19–28. https://doi.org/10.1007/s10529-014-1653-8.

Narhi, L.; Fulco, A. Characterization of a Catalytically Self-Sufficient 119,000-Dalton Cytochrome P-450 Monooxygenase Induced by Barbiturates in Bacillus Megaterium. J Biol Chem. 1986 Jun 5;261(16):7160-9. June 5, 1986.

Narhi, L.; Fulco, A. Identification and Characterization of Two Functional Domains in Cytochrome P-450BM-3, a Catalytically Self-Sufficient Monooxygenase Induced by Barbiturates in Bacillus Megaterium. J Biol Chem. 1987 May 15;262(14):6683-90. 5 1987.

Naseem, K. The Role of Nitric Oxide in Cardiovascular Diseases. *Molecular Aspects of Medicine* **2005**, *26* (1–2), 33–65. https://doi.org/10.1016/j.mam.2004.09.003.

Neeli, R.; Girvan, H. M.; Lawrence, A.; Warren, M. J.; Leys, D.; Scrutton, N. S.; Munro, A. W. The Dimeric Form of Flavocytochrome P450 BM3 Is Catalytically Functional as a Fatty Acid Hydroxylase. *FEBS Letters* **2005**, *579* (25), 5582–5588. https://doi.org/10.1016/j.febslet.2005.09.023.

Noble, M. A.; Miles, C. S.; Chapman, S. K.; Lysek, D. A.; MacKay, A. C.; Reid, G. A.; Hanzlik, R. P.; Munro, A. W. Roles of Key Active-Site Residues in Flavocytochrome P450 BM3. *Biochem J* **1999**, *339* (Pt 2), 371–379.

Panda, K.; Rosenfeld, R. J.; Ghosh, S.; Meade, A. L.; Getzoff, E. D.; Stuehr, D. J. Distinct Dimer Interaction and Regulation in Nitric-Oxide Synthase Types I, II, and III. *J Biol Chem.* **2002**, *277* (34), 31020–31030. https://doi.org/10.1074/jbc.M203749200.

Panda, K.; Ghosh, S.; Stuehr, D. J. Calmodulin Activates Intersubunit Electron Transfer in the Neuronal Nitric-Oxide Synthase Dimer. *J Biol Chem.* **2001**, *276* (26), 23349–23356. https://doi.org/10.1074/jbc.M100687200.

Pettelkau, J.; Thondorf, I.; Theisgen, S.; Lilie, H.; Schröder, T.; Arlt, C.; Ihling, C. H.; Sinz, A. Structural Analysis of Guanylyl Cyclase-Activating Protein-2 (GCAP-2) Homodimer by Stable Isotope-Labeling, Chemical Cross-Linking, and Mass Spectrometry. *J. Am. Soc. Mass Spectrom.* **2013**, *24* (12), 1969–1979. https://doi.org/10.1007/s13361-013-0734-6.

Porter, T. D. An Unusual yet Strongly Conserved Flavoprotein Reductase in Bacteria and Mammals. *Trends Biochem Sci.* **1991**, *16* (4), 154–158. https://doi.org/10.1016/0968-0004(91)90059-5.

Rappsilber, J. The Beginning of a Beautiful Friendship: Cross-Linking/Mass Spectrometry and Modelling of Proteins and Multi-Protein Complexes. *J Struct Biol.* **2011**, *173* (3), 530–540. https://doi.org/10.1016/j.jsb.2010.10.014.

Ravichandran, K.; Boddupalli, S.; Hasermann, C.; Peterson, J.; Deisenhofer, J. Crystal Structure of Hemoprotein Domain of P450BM-3, a Prototype for Microsomal P450's. *Science* **1993**, *261* (5122), 731–736. https://doi.org/10.1126/science.8342039.

Reinen, J.; van Leeuwen, J. S.; Li, Y.; Sun, L.; Grootenhuis, P. D. J.; Decker, C. J.; Saunders, J.; Vermeulen, N. P. E.; Commandeur, J. N. M. Efficient Screening of Cytochrome P450 BM3 Mutants for Their Metabolic Activity and Diversity toward a Wide Set of Drug-Like Molecules in Chemical Space. *Drug Metab Dispos* **2011**, *39* (9), 1568–1576. https://doi.org/10.1124/dmd.111.039461.

Rendic, S.; Guengerich, F. P. Survey of Human Oxidoreductases and Cytochrome P450 Enzymes Involved in the Metabolism of Xenobiotic and Natural Chemicals. *Chem Res Toxicol* **2015**, *28* (1), 38–42. https://doi.org/10.1021/tx500444e.

Roberts, G. A.; Grogan, G.; Greter, A.; Flitsch, S. L.; Turner, N. J. Identification of a New Class of Cytochrome P450 from a Rhodococcus Sp. *J Bacteriol* **2002**, *184* (14), 3898–3908. https://doi.org/10.1128/JB.184.14.3898-3908.2002.

Sailer, C.; Offensperger, F.; Julier, A.; Kammer, K.-M.; Walker-Gray, R.; Gold, M. G.; Scheffner, M.; Stengel, F. Structural Dynamics of the E6AP/UBE3A-E6-P53 Enzyme-Substrate Complex. *Nat Commun* **2018**, *9* (1), 4441. https://doi.org/10.1038/s41467-018-06953-0.

Schmidt, H. H. H. W.; Walter, U. NO at Work. *Cell* **1994**, *78* (6), 919–925. https://doi.org/10.1016/0092-8674(94)90267-4.

Sevrioukova, I. F.; Peterson, J. A. NADPH-P-450 Reductase: Structural and Functional Comparisons of the Eukaryotic and Prokaryotic Isoforms. *Biochimie* **1995**, *77* (7–8), 562–572. https://doi.org/10.1016/0300-9084(96)88172-7.

Sevrioukova, I. F.; Hazzard, J. T.; Tollin, G.; Poulos, T. L. The FMN to Heme Electron Transfer in Cytochrome P450BM-3: Effect Of Chemical Modification Of Cysteines Engineered At The FMN-Heme Domain Interaction Site. *J Biol Chem.* **1999**, *274* (51), 36097–36106. https://doi.org/10.1074/jbc.274.51.36097.

Smith, B. C.; Underbakke, E. S.; Kulp, D. W.; Schief, W. R.; Marletta, M. A. Nitric Oxide Synthase Domain Interfaces Regulate Electron Transfer and Calmodulin Activation. *Proc Natl Acad Sci U S A.* **2013**, *110* (38), E3577–E3586. https://doi.org/10.1073/pnas.1313331110.

Stuehr, D. J. Mammalian Nitric Oxide Synthases. *Biochim Biophys Acta.* **1999**, *1411* (2–3), 217–230. https://doi.org/10.1016/s0005-2728(99)00016-x.

Stuehr, D. J.; Santolini, J.; Wang, Z.-Q.; Wei, C.-C.; Adak, S. Update on Mechanism and Catalytic Regulation in the NO Synthases. *J Biol Chem.* **2004**, *279* (35), 36167–36170. https://doi.org/10.1074/jbc.R400017200.

Su, M.; Chakraborty, S.; Osawa, Y.; Zhang, H. Cryo-EM Reveals the Architecture of the Dimeric Cytochrome P450 CYP102A1 Enzyme and Conformational Changes Required for Redox Partner Recognition. *J Biol Chem.* **2020**, *295* (6), 1637–1645. https://doi.org/10.1074/jbc.RA119.011305.

Taverner, T.; Hall, N. E.; O'Hair, R. A. J.; Simpson, R. J. Characterization of an Antagonist Interleukin-6 Dimer by Stable Isotope Labeling, Cross-Linking, and Mass Spectrometry. *J Biol Chem.* **2002**, *277* (48), 46487–46492. https://doi.org/10.1074/jbc.M207370200.

Warman, A. J.; Roitel, O.; Neeli, R.; Girvan, H. M.; Seward, H. E.; Murray, S. A.; McLean, K. J.; Joyce, M. G.; Toogood, H.; Holt, R. A.; Leys, D.; Scrutton, N. S.; Munro, A. W. Flavocytochrome P450 BM3: An Update on Structure and Mechanism of a Biotechnologically Important Enzyme. *Biochem Soc Trans.* **2005**, *33* (4), 747–753. https://doi.org/10.1042/BST0330747.

Whitehouse, C. J. C.; Bell, S. G.; Wong, L.-L. P450 $_{BM3}$ (CYP102A1): Connecting the Dots. *Chem. Soc. Rev.* **2012**, *41* (3), 1218–1260. https://doi.org/10.1039/C1CS15192D.

Wu, B.; Peisley, A.; Richards, C.; Yao, H.; Zeng, X.; Lin, C.; Chu, F.; Walz, T.; Hur, S. Structural Basis for DsRNA Recognition, Filament Formation, and Antiviral Signal Activation by MDA5. *Cell* **2013**, *152* (1–2), 276–289. https://doi.org/10.1016/j.cell.2012.11.048.

Yokom, A. L.; Morishima, Y.; Lau, M.; Su, M.; Glukhova, A.; Osawa, Y.; Southworth, D. R. Architecture of the Nitric-Oxide Synthase Holoenzyme Reveals Large Conformational Changes and a Calmodulin-Driven Release of the FMN Domain. *J Biol Chem.* **2014**, *289* (24), 16855–16865. https://doi.org/10.1074/jbc.M114.564005.

Zhang, L.; Dawson, V. L.; Dawson, T. M. Role of Nitric Oxide in Parkinson's Disease. *Pharmacol Ther.* **2006**, *109* (1–2), 33–41. https://doi.org/10.1016/j.pharmthera.2005.05.007.

Zhang, H.; Yokom, A. L.; Cheng, S.; Su, M.; Hollenberg, P. F.; Southworth, D. R.; Osawa, Y. The Full-Length Cytochrome P450 Enzyme CYP102A1 Dimerizes at Its Reductase Domains and Has Flexible Heme Domains for Efficient Catalysis. *J Biol Chem.* **2018**, *293* (20), 7727–7736. https://doi.org/10.1074/jbc.RA117.000600.

Ziche, M.; Morbidelli, L. Nitric Oxide and Angiogenesis. *J Neurooncol.* **2000**, *50* (1–2), 139–148.

## Figures

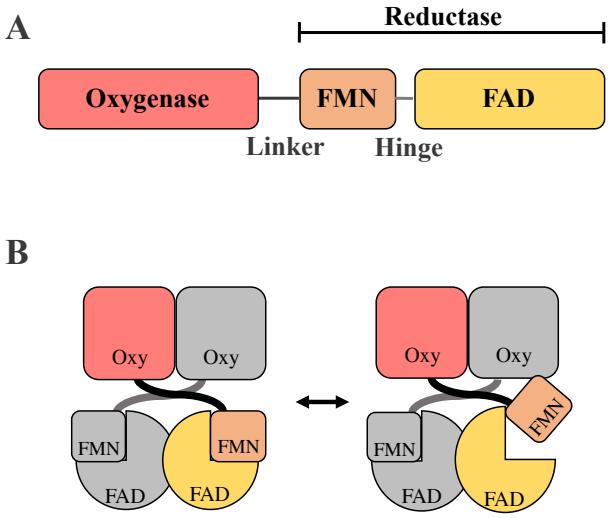


***Figure 1-1.*** *Domain organization of class VIII P450 enzymes.*

**(A)** A linear schematic of domains along a single protein's amino acid sequence. **(B)** Organization of one protein's domains within the homodimeric P450 as FMN "shuttles" between FAD and opposing oxygenase domains.

Figure adapted from the original research in Chapter 2 of this dissertation work, published as: Felker, D.; Zhang, H.; Bo, Z.; Lau, M.; Morishima, Y.; Schnell, S.; Osawa, Y. Mapping Protein-Protein Interactions in Homodimeric CYP102A1 by Crosslinking and Mass Spectrometry. *Biophysical Chemistry* **2021**, *274*, 106590. https://doi.org/10.1016/j.bpc.2021.106590.

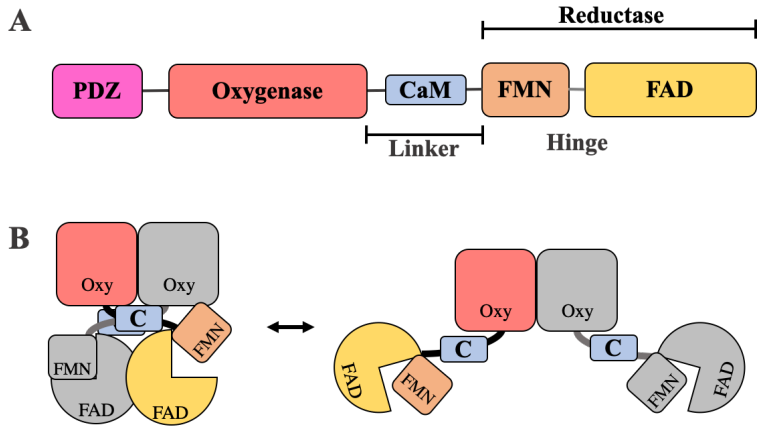


***Figure 1-2.*** *Domain organization and conformational states of CaM-bound nNOS.*

**(A)**, A linear schematic of domains along a single nNOS monomer's amino acid sequence. **(B)**, Organization of calmodulin-bound nNOS domains in the closed (left) and extended (right) conformations previously captured by negative stain- and cryo-EM studies. One monomer within the homodimer is shown in grey, with the other in color. Oxygenase domain is shown in red, calmodulin in blue, FMN in orange, and FAD in yellow.

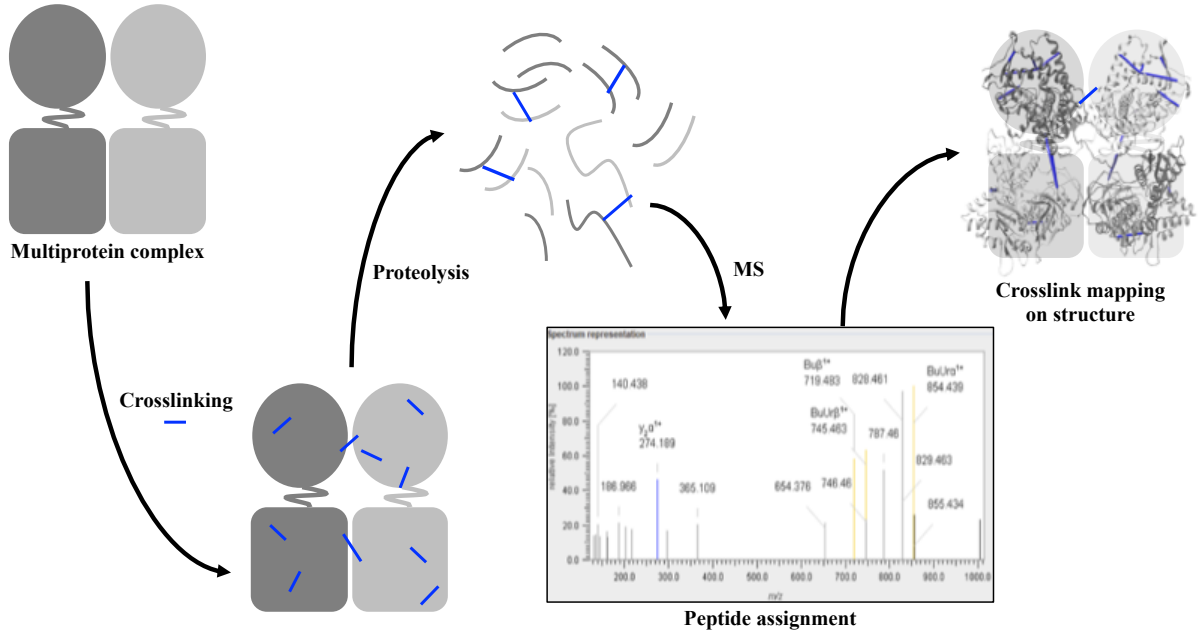


***Figure 1-3.*** *A summary of the covalent crosslinking and mass spectrometry (CXL-MS) workflow.*

A multiprotein complex is reacted with covalent crosslinker (blue), which binds residues within certain proximity in the multiprotein complex. Proteins are digested to produce peptide fragments, and mass spectrometry is used to identify fragments containing crosslinked residues. Crosslinks are then mapped to structural data to visualize crosslink formation within the larger three-dimensional protein complex.

# Chapter 2 Mapping Protein-Protein Interactions in Homodimeric CYP102A1 by Crosslinking and Mass Spectrometry


## Abstract

Covalent crosslinking and mass spectrometry techniques hold great potential in the study of multiprotein complexes, but a major challenge is the inability to differentiate intra- and inter-protein crosslinks in homomeric complexes. In the current study we use CYP102A1, a well-characterized homodimeric P450, to examine a subtractive method that utilizes limited crosslinking with disuccinimidyl dibutyric urea (DSBU) and isolation of the monomer, in addition to the crosslinked dimer, to identify inter-monomer crosslinks. The utility of this approach was examined with the use of MS-cleavable crosslinker DSBU and recently published cryo-EM based structures of the CYP102A1 homodimer. Of the 31 unique crosslinks found, 26 could be fit to the reported structures whereas 5 exceeded the spatial constraints. Not only did these crosslinks validate the cryo-EM structure, they point to new conformations of CYP102A1 that bring the flavins in closer proximity to the heme.



This section was written by D. Felker with significant intellectual contributions and editorial work from Yoichi Osawa. It was published as an original research paper in April 2021: Felker, D.; Zhang, H.; Bo, Z.; Lau, M.; Morishima, Y.; Schnell, S.; Osawa, Y. Mapping Protein-Protein Interactions in Homodimeric CYP102A1 by Crosslinking and Mass Spectrometry. *Biophysical Chemistry* **2021**, 274, 106590. https://doi.org/10.1016/j.bpc.2021.106590.

## Introduction

Covalent crosslinking and mass spectrometry (CXL-MS) is a widely used method that employs bifunctional chemical crosslinking reagents and facile peptide sequencing by high resolution mass spectrometry to identify specific amino acids that were crosslinked on the protein. This technique can be used to identify protein-protein interactions, to define interaction sites in protein complexes, as well as characterize the structure of proteins based on the crosslinker's known length. One particular challenge of this method is the inability to distinguish between inter- and intra- protein crosslinks in homomultimeric protein complexes. Lima et al. [Lima et al., 2018] has noted the prevalence and importance of homodimeric and homomultimeric proteins in biological processes and has developed a technique that utilizes stable-isotope labeling of one of the monomers in a homodimer to directly address this issue. This rigorous method to differentiate the inter- and intra- monomeric crosslinks requires the ability to express isotopically enriched protein, to purify the protein, and to reconstitute the labeled monomer with an unlabeled monomer to form a functional dimer. Unfortunately, the ability to reconstitute the dimer is dependent on the protein of interest. Another approach, albeit less rigorous, is to carefully limit the crosslinking reaction such that both crosslinked dimers and monomers can be separated by denaturing SDS-PAGE, so that the monomer, which contains only intra-monomer crosslinks, can be compared to the dimer, which contains both intra- and inter- monomer crosslinks [Bennett et al., 2000; Wu et al., 2013; Zeng-Elmore et al., 2014; Karagöz et al., 2017; Liu et al., 2014; Chu, Thornton, and Nguyen, 2018]. In this way, the intra-monomer crosslinks can be identified with certainty and essentially be subtracted from the crosslinks found in the dimeric sample, leaving a set of crosslinks for further analysis by orthologous methods. There have been only a handful of studies to employ this method [Bennett

et al., 2000; Wu et al., 2013; Zeng-Elmore et al., 2014; Karagöz et al., 2017; Liu et al., 2014; Chu, Thornton, and Nguyen, 2018].

In our study, we have utilized this subtractive CXL-MS method in the course of our structural studies on the homodimeric CYP102A1 enzyme. In particular, we wished to examine how well CXL-MS data would compare to a recently reported cryo-EM-based structural model of the full-length enzyme [Su et al., 2020] and to explore how well the subtractive CXL-MS method performed when applied to this well characterized homodimeric P450 enzyme. CYP102A1 is a self-sufficient cytochrome P450 enzyme from *Bacillus megaterium* that catalyzes the hydroxylation of fatty acids and other molecules. The catalysis involves the transfer of electrons derived from NADPH to the FMN/FAD containing reductase domain of CYP102A1 to the heme in the oxygenase domain. This allows for the sequential one-electron transfer of electrons from the FMN to the heme, a requisite one-electron acceptor, to enable dioxygen activation and insertion of one the oxygen atom into the substrate. The exact mechanism of how these electron transfer reactions occur is a topic of intense interest, especially in light of interest in utilizing CYP102A1 as a biocatalyst.

In the current study disuccinimidyl dibutyric urea (DSBU), a MS-cleavable crosslinker that allows high-confidence identification of crosslinked residues by high resolution mass spectrometry [Götze et al., 2015; Iacobucci et al., 2018], was used. The subtractive method successfully identified inter-monomeric crosslinks with residues originating in the oxygenase domain that fit in the cryo-EM derived structures of full length CYP102A1. However, the subtractive method falsely identified crosslinks spanning residues in the reductase domain as inter-monomeric crosslinks, as all crosslinks identified in this domain fit better to the cryo-EM derived structure as intra-monomeric crosslinks. Thus, the success of the subtractive method is

likely dependent on the nature of the structural domains and how they are impacted as crosslinking proceeds. Moreover, the crosslinks are consistent with the dynamic movements of the FMN domain of one monomer to the heme domain of another monomer that was proposed for CYP102A1 from the cryo-EM derived structures in open and closed conformations [Su et al., 2020]. Thus, the crosslinking studies provide important information in support of the cryo-EM derived structures as well as new evidence for a conformation that brings the FMN closer to the heme, allowing for facile electron transfer and enabling efficient catalysis.

## Materials and Methods

**Materials.** Disuccinimidyl dibutyric urea (DSBU) Lot UG281415 was purchased from Thermo Scientific. Sodium chloride Lot 16620 was from Fisher BioReagents and 1X phosphate-buffered saline pH 7.4 Lot 2052719 was from Gibco. Anhydrous DMSO Lot SHBK9388, 2-mercaptoethanol Lot SHBG9616V, and ammonium bicarbonate Lot 116K0130 were from Sigma. Bio-Safe Coomassie stain Lot BR190408, 2x Laemmli Lot 64224909, and 4-15% gradient SDS-PAGE gels Lot 64294610 were purchased from Bio-Rad.

**Protein expression, purification, and characterization.** The full-length A82F variant of CYP102A1 with an N-terminal His6 tag, referred to as full-length CYP102A1, was expressed and purified as previously described [Su et al., 2020]. This mutant is the same protein used in elucidating the cryo-EM-derived structural model of the CYP102A1 [Su et al., 2020]. The SEC-MALS analysis of full-length CYP102A1 shows a single peak with a mass of 238 ± 8.8 kDa, which is consistent with a homodimer. The full-length preparation displays NADPH consumption at ~1,220 min-1 in the presence of omeprazole [Su et al., 2020].

**Chemical crosslinking and SDS-PAGE analysis.** Purified full-length CYP102A1was diluted to a final concentration of 10 µM in 10 µl of PBS pH 7.4 supplemented with salt to give a final concentration of 255 mM NaCl. The mixture was treated with the desired amount of DSBU, which was dissolved in anhydrous DMSO, for 5 or 15 minutes at room temperature with rotation. The DMSO was always below 10% (v/v) of total reaction volume. Reactions were quenched with 2 µl 0.5 M ammonium bicarbonate and mixed for 5 minutes at 4°C, then diluted with an equal volume of 2x Laemmli Sample Buffer containing 10% (v/v) 2-mercapotethanol. Samples were boiled for 5 minutes and aliquots (3 µg of protein) were submitted for SDS-PAGE on 4-15% gradient gels typically run for 75 minutes at 50 mAmps/gel. Gels were stained for 1

hour with ProteinSafe Coomassie Stain and destained in MilliQ water. Gels were imaged with a LI-COR Odyssey Fc and bands corresponding to monomer and dimer were quantified by densitometric analysis with the use of ImageStudio software (version 5.2). A standard curve of bovine serum albumin and full-length CYP102A1 showed a linear range from 0 to 6 µg protein per lane.

**Mass spectrometry and peptide assignment.** Cross-linked protein samples were separated by SDS-PAGE. Protein bands corresponding to monomeric or dimeric CYP102A1 were submitted for in-gel trypsinolysis and subsequent analysis of the tryptic peptides on a Thermo Scientific Q Exactive HF Orbitrap MS at the University of Michigan Mass Spectrometry-Based Proteomics Resource Facility. Peptide assignments were performed using MeroX (version 2.0) to specifically search for peptides containing the signature doublet that DSBU produces upon fragmentation. MeroX software compares the experimental secondary MS to a library of all theoretically possible DSBU-crosslinked peptides and scores the results based on how well each MS/MS spectrum matches its theoretical counterpart [Götze et al., 2015; Iacobucci et al., 2018]. MS datasets were analyzed with primary and secondary fragment mass deviations of 10 and 50 ppm, respectively, with mass limits of 600-6000 Da. Score cut-offs calculated for a False Discovery Rate (FDR) < 0.01% were applied [Iacobucci and Sinz, 2017; Iacobucci et al., 2019]. The MS/MS spectra were also manually checked, as another layer of quality control, using MeroX and XCalibur (version 3.0).

**Mapping of crosslinks onto three-dimensional models of CYP102A1.** Crosslinks were mapped to recently published structural models of CYP102A1 using the Xlink Analyzer Plugin [Kosinski et al., 2015] in UCSF Chimera [Pettersen et al., 2004]. These models were derived from cryo-EM data of the same full-length A82F variant CYP102A1 used in our current study

[Su et al., 2020]. The models are the first full-length structures of the CYP102A1 and utilized the EM density as well as rigid-body fitting of the crystal structures of individual heme, FMN, and FAD domains [PDB 4KEW, 1BVY, 4DQK] [Butler et al., 2013; Sevrioukova et al., 1999; Joyce et al., 2012]. The structures represent homodimers of CYP102A1 with both heme and FAD domains in contact with each other. At least three major conformations of full-length CYP102A1 were detected representing one closed state where the FAD and FMN are in close contact and two open conformations where the FMN domain is rotated away from the FAD and is closer to the adjacent heme domain of the opposing monomer possibly favoring a trans electron transfer. Input files containing crosslinks were manually generated and 27 Å $C_\alpha$-$C_\alpha$ Euclidean distance cutoffs for the DSBU linker arm were applied in Xlink Analyzer.

## Results

**Crosslinking of CYP102A1 with DSBU leads to formation of a covalently linked dimer.** In this study we used an A82F variant of full-length CYP102A1, which is identical to that used in a recently published cryo-EM derived full-length structure of the P450 enzyme [Su et al., 2020]. This full-length CYP102A1 is highly similar to the wild-type enzyme with a molecular weight determined by MALS of 238 ± 8.8 kDa, consistent with a homodimer, and is fully functional with NADPH consumption of ~1220 min-1 in the presence of omeprazole [Su et al., 2020]. As shown in Fig. 2-1A, analysis of the full-length CYP102A1 by denaturing SDS-PAGE and Coomassie staining gives rise to a visible band migrating slightly above the 100 kDa marker, corresponding to each monomer (lane 1, *M*). Treatment of full-length CYP102A1 with 50-fold molar excess of DSBU gave a time-dependent increase in formation of one major crosslinked product, which is visible above the 250 kDa molecular weight marker (lanes 2-8, *D*). Although it migrates much higher in mass than expected for the native dimeric band, SEC analysis of the reaction mixture shows that the crosslinked product elutes with a highly similar retention time as the native dimer of untreated CYP102A1. Thus, we conclude that the SDS-PAGE does not provide the accurate molecular mass. Furthermore, analysis by a linear sucrose gradient shows that the crosslinked full-length CYP102A1 elutes in the same fractions as the native dimer (data not shown). Thus, we denote this species as the crosslinked dimer (*D*). As shown in Fig. 2-1B, the quantification of the monomer and dimer bands by densitometric analysis reveals a clear loss of the monomeric band over time (*closed squares*) and a concomitant increase in the dimeric band (*closed circles*). The sum of the densities of the monomer and dimer bands equals the total density of the starting untreated CYP102A1 band indicating that we have accounted for the major products of the crosslinking reaction. The

formation of the crosslinked dimer of CYP102A1 is dependent on the concentration of DSBU (Fig. 2-1C, lanes 1-6). The quantification of the bands once again shows that monomer is converted stoichiometrically to the crosslinked dimer product (Fig. 2-1D).

**High-resolution tandem mass spectrometric analysis of the monomer band on SDS-PAGE identifies intra-monomer crosslinked residues in CYP102A1.** Since native CYP102A1 exists as a non-covalently associated homodimer, crosslinking can give rise to either intra-monomer (within one monomer) or inter-monomer (across monomers) covalent crosslinks. We first examined the monomer band from SDS-PAGE gels after DSBU crosslinking as they can only contain intra-monomer crosslinks. We examined samples of full-length CYP102A1 after crosslinking for 5 min or 15 minutes with DSBU at 0.5 mM final concentration. Although we cannot visualize the extent of monomer crosslinking by SDS-PAGE, we do know that approximately 26% and 46% of the starting CYP102A1 was crosslinked to the dimer band after 5 min and 15 min, respectively. Bands were excised in duplicate and submitted for MS analysis, and sites of crosslinks were identified as described in Methods. As shown in Table 2-1, we found that crosslinking for a short duration gives rise to five major intra-monomer crosslinks with three of the crosslinks starting at residue K77 in the oxygenase domain. Interestingly, K77 exists on the B'-helix located above the substrate binding site of the heme binding pocket of CYP102A1 [Whitehouse, Bell, and Wong, 2012]. As shown in Fig. 2-2A, when the intra-monomer crosslinks are mapped onto a linear representation of the CYP102A1 monomer, we can readily visualize that four of the crosslinks are within the oxygenase domain with one crosslink in the linker region. At longer durations of crosslinking, we see three of the same crosslinks as in the early time sample but also crosslinks within the FAD domain concentrated around the FAD

cofactor binding site (Table 2-2 and Fig. 2-2B). We will explore how these crosslinks map to known structures of these regions in the next subsection.

**Intra-monomer crosslinks mapped to a Cryo-EM-derived structural model of full-length CYP102A1.** With the exception of one crosslink in the linker region, the intra-monomer crosslinks identified in the previous section (Fig. 2-2) spanned residues within the oxygenase domain (5 crosslinks) or the FAD domain (6 crosslinks) where high resolution crystal structures exist [Butler et al., 2013; Joyce et al., 2012].

In Fig. 3, we show the 3D structural model that was constructed by fitting the structure of the oxygenase and reductase domains as rigid bodies into the density map generated from cryo-EM studies [Su et al., 2020]. As shown in the upper half of the figure, the five crosslinks identified in the oxygenase domain were mapped onto a crystal structure of the CYP102A1 oxygenase domain as determined by Butler et al. [Butler et al., 2013] All the crosslinks mapped within the $C_\alpha$-$C_\alpha$ Euclidean distance of the DSBU linker arm of 27 Å and thus appear in close agreement with the crystal structure. The available crystal structure of the FAD domain determined by Joyce et al. [Joyce et al., 2012] contains residues for only three of the crosslinked adducts we identified. As shown in Fig. 3 lower half, the three crosslinks involving residue K1039 were mapped (*red bars*) onto structure of the FAD domain and found to have $C_\alpha$-$C_\alpha$ distances greater than 27 Å, ranging from 39.86 Å (K791-K1039) to 43.24 Å (K787-K1039). Thus, these crosslinks do not fit well to the crystal structure of the FAD domain. The remaining three FAD crosslinks involving K735, which is located on an unresolved loop on the proximal side of the cofactor binding site, as well as the crosslink on the linker region could not be mapped onto the crystal structure and we rely on cryo-EM based modeling of the regions where the crystal structures do not exist [Su et al., 2020]. Although the CYP102A1 was found in

several different conformations in the cryo-EM studies, there is only one structure where the linker region was resolved. Thus, we used this conformation to examine the remaining intra-monomeric crosslinks (Fig. 2-3). The cryo-EM derived density maps allowed the modeling of the previously unresolved loop in the FAD domain and we were able to map the three remaining FAD crosslinks from residue K735 within the DSBU distant restraint. Moreover, we also mapped the K469-K474 crosslink within the linker region to well within the DSBU distance restraint. It is noteworthy that with the exception of three crosslinks involving K1039 within the FAD domain, all the intra-monomeric crosslinks are consistent with the full-length cryo-EM derived model of the CYP102A1 structure as well as the available crystal structures of the subdomains.

**High-resolution tandem mass spectrometric analysis of the dimer band identifies both inter- and intra- monomer crosslinked residues in CYP102A1.** We now focus on the mass spectrometry data derived from the dimer band generated after crosslinking with DSBU. The crosslinks from the dimeric band comprise a mixture of intra- and inter- monomeric crosslinks with those formed at 5 min and 15 min treatments with DSBU shown in Tables 2-3 and 2-4, respectively. As a starting point for our analysis, we used an approach used by others that subtracts the crosslinks found in the monomer band, which are intra-monomer crosslinks, from the crosslinks found from the dimer band to give a data set of putative inter-monomer crosslinks [Bennett et al., 2000; Wu et al., 2013; Zeng-Elmore et al., 2014; Karagöz et al., 2017; Liu et al., 2014; Chu, Thornton, and Nguyen, 2018]. Thus, we have greyed out from Tables 2-3 and 2-4 the intra-monomer crosslinks identified from the monomer band. We have also verified by use of the cryo-EM derived dimer structure that these intra-monomer crosslinks indeed are better mapped as intra- and not inter- monomer crosslinks (data not shown). Although some

studies have utilized the subtractive method to assign the remaining crosslinks as inter-monomer crosslinks, we more carefully examine this assumption by mapping the remaining crosslinks to the cryo-EM derived structures of the CYP102A1 dimer.

**Analysis of crosslinks obtained from the dimer band with the use of the cryo-EM structural models of the CYP102A1 homodimer.** Our overall approach was to map dimer-specific crosslinks as either intra- or inter- monomer crosslinks onto the three published cryo-EM derived structural models [Su et al., 2020] to determine the $C_\alpha$-$C_\alpha$ Euclidean distance of each crosslink scenario. As shown in Table 2-5, the crosslinks that were not greyed out from Tables 2-3 and 2-4 are listed along with the location of the crosslinks with respect to the domains. A structure of the closed conformation, which was utilized above to map the intra-monomer crosslinks, was used (Closed) in addition to two open conformations (Open I and Open II) representing structures where the FMN domain appears to rotate away from the FAD domain in varying degrees, resulting in its closer proximity to the heme. A simplified model of the CYP102A1 homodimer in these three conformations is shown in Figure 2-4. For each crosslink, the $C_\alpha$-$C_\alpha$ Euclidean distance for each structure mapped as the inter-monomer or intra-monomer crosslink was determined. Since the homodimers are not symmetrical in these conformations, each crosslink can have two inter-monomeric possibilities arbitrarily denoted as α-β and β-α, as well as two intra-monomeric possibilities denoted as α-α and β-β. The distance is depicted in bold type in those cases where the distance is equal to or less than the 27 Å $C_\alpha$-$C_\alpha$ linker distance.

*Oxygenase domain crosslinks (#1-8)* – Six of the eight crosslinks originating in the oxygenase domain (#1,3-5,7,8) could be mapped within the linker distance of 27 Å as inter-monomer crosslinks to at least one of the three conformations, with the closed conformation

fulfilling five of the crosslinks. While all conformations could map crosslink #4, interestingly crosslink #8 was best only mapped to the Open II conformation. Two of these oxygenase domain crosslinks (#2,6) did not map to any of the conformations within the linker distance of 27 Å; however, the shortest distances were clearly mapped as the inter-monomer. In fact, all the crosslinks originating in the oxygenase domain were better fit as inter-monomer. Thus, for the mapping of the oxygenase domain contacts, the subtraction method utilizing the crosslinks found in the monomer band was fully validated. It appears that the Closed and Open II conformations captured the extremes of the crosslinks while the Open I conformation was intermediate between these extremes with regard to the crosslinks.

*Reductase domain crosslinks (#9-19)* – In sharp contrast to that found for the crosslinks originating from the oxygenase domain, crosslinks entirely within the reductase domain (containing the FMN and FAD subdomains) fit within a linker distance of 27 Å as intra-monomer crosslinks and not inter-monomer crosslinks. Moreover, all the crosslinks found could be fit to at least one conformation. Interestingly, seven of the eleven crosslinks could be fit on what we designated as the β-monomer of all three conformations whereas the α-monomer fit the four remaining crosslinks better.

To better understand the crosslinks in relation to the dynamic nature of the CYP102A1 structure as well as define what monomers were depicted as α and β, we have mapped all of the above crosslinks within the 27 Å linker distance (bolded values from Table 2-5) onto the Closed and Open II structures since they appear to be the extremes of the conformations with respect to the mapping of the crosslink distances (Fig. 2-5). Figure 2-5A shows the inter-monomeric crosslinks on the structure of CYP102A1 in the Closed conformation in all 10 possible combinations between the α-monomer (*light grey*) and β-monomer (*dark grey*). There is a tight

association of the oxygenase domains containing the heme prosthetic group (*red*) to form the dimeric structure as well as seemingly looser association with the FMN (*orange*) and FAD (*yellow*) containing reductase domains of the other monomer forming a trans-type configuration of the dimer. There are eight crosslinks bridging oxygenase and reductase domains, as well as two crosslinks across the oxygenase domains. As shown in Fig. 2-5B, the Open II conformation of the CYP102A1 reveals the same two crosslinks that are preserved between the oxygenase domains. However, the open conformation reflects a large conformational change in the reductase domain of α-monomer with the FMN (*orange*) moving in closer proximity to the heme (*red*) of the β-monomer. This leads to a loss of the eight crosslinks found in the Closed conformation but a new crosslink between residue Y695 of the FAD domain and residue K313 of the oxygenase domain is able to fit the structure. There are crosslinks between these same residues that are only 28 Å in the Closed conformation so this is likely not specific to the open conformation. However, there is a crosslink between S66-K1039 (Table 2-5, #2) that is 35.5 Å in distance in the Open II conformation (Fig 2-5B, *red bar*) but is much longer (51 Å) in the Closed conformation (not shown). It is possible that crosslink sampled a conformation where these residues are much closer than they appear in the Open II conformation and likely reflects a conformation where the heme and FMN are much closer than captured by the Open II structure. We will examine the crosslinks that could not be assigned within the distance constraint as a group in the Discussion.

We also mapped the intra-monomer crosslinks (Table 2-5, #9-19) to the structure of the closed and open conformations of CYP102A1 in a similar manner. As shown in Fig. 2-5C, the Closed conformation maps eight of the eleven intra-monomer crosslinks on each monomer. On the β-monomer (*dark grey*), we can see three main groups of crosslinks at residue K508,

centered around residue K573, and one short crosslink at residue K691. Although the reductase domains in the dimer are not symmetrical, we can still observe that these crosslinks are essentially mirrored on the α-monomer (*light grey*). There is an additional crosslink at residue 516 on the α-monomer and the β-monomer has an analogous crosslink that failed to meet our distance cutoff by only 0.7 Å. In Fig. 2-5D, the intra-monomer crosslinks were mapped on the Open II conformation. The β-monomer (*dark grey*) is highly similar to that found for the β-monomer of the Closed conformation and the three sets of crosslinks are present. In contrast, the α-monomer undergoes large conformational changes involving the movement of the FMN prosthetic group (*orange*) with a notably different pattern of crosslinks present. In fact, all three of the remaining crosslinks at residues S507, K508, and K561 that were not accounted for by the closed conformation are compatible with the open conformations.

## Discussion

In the current study, DSBU was used in CXL-MS experiments to map CYP102A1 residues that are close enough to be spanned by the crosslinker when the CYP102A1 homodimer is in its native state. Although modern mass spectrometry methods can readily identify the crosslinked residues, it is more difficult to determine if the residues are the result of inter- or intra- monomer crosslinks as both monomers have identical amino acid sequences. In lieu of technological challenges of isotopically labeling one monomer, we chose to follow a subtractive method used previously in several CXL-MS studies of homomeric proteins [Bennett et al., 2000; Wu et al., 2013; Zeng-Elmore et al., 2014; Karagöz et al., 2017; Liu et al., 2014; Chu, Thornton, and Nguyen, 2018]. Specifically, we carefully controlled the reaction to obtain a mixture of crosslinked dimers and monomers, which could be separated by SDS-PAGE. The crosslinked monomers were utilized to study intra-monomeric crosslinks, which mapped nicely to known structures of the protein. The crosslinked residues found in the dimer sample comprise inter-monomer as well as intra-monomer crosslinks. This subtractive method worked well for the crosslinks involving at least one residue in the heme-containing oxygenase domain of CYP102A1, as evident by mapping to a recently reported cryo-EM derived structural model of the full-length dimeric protein [Su et al., 2020]. The remaining crosslinks, which bridged residues entirely in the reductase domain, could not be mapped as inter-monomeric crosslinks. Even though these crosslinks were not found in the monomer sample data set, they appear to fit more consistently as intra-monomer crosslinks in the cryo-EM structures. This may reflect the inherent conformational flexibility of the reductase domain and its ability to sample different conformations more often after inter-monomer crosslinks are formed that lock the monomers together. Alternatively, perhaps once certain intra-monomeric crosslinks are formed, the

CYP102A1 reductase domain can no longer stay in the dimeric state. In either case, we are left with a monomer band that does not give rise to the same intra-monomer crosslinks as the dimer band. Thus, this subtractive method has its limitations and is certainly not as rigorous as labeling one monomer with a stable isotope [Lima et al., 2018].

Of the 31 total unique crosslinks identified, we successfully mapped 26 to the cryo-EM structure, suggesting a high degree of correspondence between these two methods. However, we could not map five crosslinks within the 27 Å distance restraint of the DSBU linker arm. As shown in Fig. 2-6, we have mapped these five crosslinks to the residues representing the shortest distance in the Open II conformation of the CYP102A1. Four of these crosslinks involved K1039 crosslinked to either a residue in the oxygenase domain (S66) or to three residues closely clustered on the reductase domain (K787, K791, K797) near the FAD. The distances between these residues vary between 31.8 Å to 43.2 Å in the cryo-EM derived structures. Although the low resolution of the cryo-EM structure precludes definitive statements, it's possible that conformational flexibility in these regions is reflected by the crosslinking but not apparent in the structural studies. This is noteworthy as electrons donated from NADPH must shuttle from the FAD to FMN to heme for catalytic activity [Munro et al., 1994; Munro et al., 1996; Munro et al., 2002; Neeli et al., 2005; Girvan et al., 2011]. More specifically, a further extension of the Open II conformation of the CYP102A1 homodimer would bring the residue pairs S66-K1039 and K310-K691 closer to each other giving rise to a conformation where perhaps the FAD moves closer to the prosthetic heme in solution. Interestingly, a crystal structure of a truncated CYP102A1 with the oxygenase and part of the reductase domain showed the FMN domain directly in contact with the opposing oxygenase domain [Sevrioukova et al., 1999]. The direct interaction of reductase and opposing oxygenase domain is further supported by recent

hydrogen-deuterium exchange studies [Jeffreys et al., 2020]. More recently, a computational modeling study of the interaction of CYP1A1 with cytochrome P450 reductase suggests that transient interactions between heme and FAD domain are likely [Mukherjee, Nandekar, and Wade, 2021]. Thus, perhaps both FMN and FAD can be closer to the heme during catalysis than is apparent from the current cryo-EM derived structures.

## References


Bennett, K. L.; Kussmann, M.; Björk, P.; Godzwon, M.; Mikkelsen, M.; Sørensen, P.; Roepstorff, P. Chemical Cross-Linking with Thiol-Cleavable Reagents Combined with Differential Mass Spectrometric Peptide Mapping--a Novel Approach to Assess Intermolecular Protein Contacts. *Protein Sci* **2000**, *9* (8), 1503–1518. https://doi.org/10.1110/ps.9.8.1503.

Butler, C. F.; Peet, C.; Mason, A. E.; Voice, M. W.; Leys, D.; Munro, A. W. Key Mutations Alter the Cytochrome P450 BM3 Conformational Landscape and Remove Inherent Substrate Bias. *J. Biol. Chem.* **2013**, *288* (35), 25387–25399. https://doi.org/10.1074/jbc.M113.479717.

Chu, F.; Thornton, D. T.; Nguyen, H. T. Chemical Cross-Linking in the Structural Analysis of Protein Assemblies. *Methods* **2018**, *144*, 53–63. https://doi.org/10.1016/j.ymeth.2018.05.023.

Girvan, H. M.; Dunford, A. J.; Neeli, R.; Ekanem, I. S.; Waltham, T. N.; Joyce, M. G.; Leys, D.; Curtis, R. A.; Williams, P.; Fisher, K.; Voice, M. W.; Munro, A. W. Flavocytochrome P450 BM3 Mutant W1046A Is a NADH-Dependent Fatty Acid Hydroxylase: Implications for the Mechanism of Electron Transfer in the P450 BM3 Dimer. *Archives of Biochemistry and Biophysics* **2011**, *507* (1), 75–85. https://doi.org/10.1016/j.abb.2010.09.014.

Götze, M.; Pettelkau, J.; Fritzsche, R.; Ihling, C. H.; Schäfer, M.; Sinz, A. Automated Assignment of MS/MS Cleavable Cross-Links in Protein 3D-Structure Analysis. *J. Am. Soc. Mass Spectrom.* **2015**, *26* (1), 83–97. https://doi.org/10.1007/s13361-014-1001-1.

Iacobucci, C.; Götze, M.; Ihling, C. H.; Piotrowski, C.; Arlt, C.; Schäfer, M.; Hage, C.; Schmidt, R.; Sinz, A. A Cross-Linking/Mass Spectrometry Workflow Based on MS-Cleavable Cross-Linkers and the MeroX Software for Studying Protein Structures and Protein–Protein Interactions. *Nat Protoc* **2018**, *13* (12), 2864–2889. https://doi.org/10.1038/s41596-018-0068-8.

Iacobucci, C.; Piotrowski, C.; Aebersold, R.; Amaral, B. C.; Andrews, P.; Bernfur, K.; Borchers, C.; Brodie, N. I.; Bruce, J. E.; Cao, Y.; Chaignepain, S.; Chavez, J. D.; Claverol, S.; Cox, J.; Davis, T.; Degliesposti, G.; Dong, M.-Q.; Edinger, N.; Emanuelsson, C.; Gay, M.; Götze, M.; Gomes-Neto, F.; Gozzo, F. C.; Gutierrez, C.; Haupt, C.; Heck, A. J. R.; Herzog, F.; Huang, L.; Hoopmann, M. R.; Kalisman, N.; Klykov, O.; Kukačka, Z.; Liu, F.; MacCoss, M. J.; Mechtler, K.; Mesika, R.; Moritz, R. L.; Nagaraj, N.; Nesati, V.; Neves-Ferreira, A. G. C.; Ninnis, R.; Novák, P.; O'Reilly, F. J.; Pelzing, M.; Petrotchenko, E.; Piersimoni, L.; Plasencia, M.; Pukala, T.; Rand, K. D.; Rappsilber, J.; Reichmann, D.; Sailer, C.; Sarnowski, C. P.; Scheltema, R. A.; Schmidt, C.; Schriemer, D. C.; Shi, Y.; Skehel, J. M.; Slavin, M.; Sobott, F.; Solis-Mezarino, V.; Stephanowitz, H.; Stengel, F.; Stieger, C. E.; Trabjerg, E.; Trnka, M.; Vilaseca, M.; Viner, R.; Xiang, Y.; Yilmaz, S.; Zelter, A.; Ziemianowicz, D.; Leitner, A.; Sinz, A. First Community-Wide, Comparative Cross-Linking Mass Spectrometry Study. *Anal. Chem.* **2019**, *91* (11), 6953–6961. https://doi.org/10.1021/acs.analchem.9b00658.

Iacobucci, C.; Sinz, A. To Be or Not to Be? Five Guidelines to Avoid Misassignments in Cross-Linking/Mass Spectrometry. *Anal. Chem.* **2017**, *89* (15), 7832–7835. https://doi.org/10.1021/acs.analchem.7b02316.

Jeffreys, L. N.; Pacholarz, K. J.; Johannissen, L. O.; Girvan, H. M.; Barran, P. E.; Voice, M. W.; Munro, A. W. Characterization of the Structure and Interactions of P450 BM3 Using Hybrid Mass Spectrometry Approaches. *Journal of Biological Chemistry* **2020**, *295* (22), 7595–7607. https://doi.org/10.1074/jbc.RA119.011630.

Joyce, M. G.; Ekanem, I. S.; Roitel, O.; Dunford, A. J.; Neeli, R.; Girvan, H. M.; Baker, G. J.; Curtis, R. A.; Munro, A. W.; Leys, D. The Crystal Structure of the FAD/NADPH-Binding Domain of Flavocytochrome P450 BM3. *The FEBS Journal* **2012**, *279* (9), 1694–1706. https://doi.org/10.1111/j.1742-4658.2012.08544.x.

Karagöz, G. E.; Acosta-Alvear, D.; Nguyen, H. T.; Lee, C. P.; Chu, F.; Walter, P. An Unfolded Protein-Induced Conformational Switch Activates Mammalian IRE1. *eLife* **2017**, *6*. https://doi.org/10.7554/eLife.30700.

Kosinski, J.; von Appen, A.; Ori, A.; Karius, K.; Müller, C. W.; Beck, M. Xlink Analyzer: Software for Analysis and Visualization of Cross-Linking Data in the Context of Three-Dimensional Structures. *Journal of Structural Biology* **2015**, *189* (3), 177–183. https://doi.org/10.1016/j.jsb.2015.01.014.

Lima, D. B.; Melchior, J. T.; Morris, J.; Barbosa, V. C.; Chamot-Rooke, J.; Fioramonte, M.; Souza, T. A. C. B.; Fischer, J. S. G.; Gozzo, F. C.; Carvalho, P. C.; Davidson, W. S. Characterization of Homodimer Interfaces with Cross-Linking Mass Spectrometry and Isotopically Labeled Proteins. *Nat Protoc* **2018**, *13* (3), 431–458. https://doi.org/10.1038/nprot.2017.113.

Liu, Z.; Szarecka, A.; Yonkunas, M.; Speranskiy, K.; Kurnikova, M.; Cascio, M. Crosslinking Constraints and Computational Models as Complementary Tools in Modeling the Extracellular Domain of the Glycine Receptor. *PLoS One* **2014**, *9* (7). https://doi.org/10.1371/journal.pone.0102571.

Mukherjee, G.; Nandekar, P. P.; Wade, R. C. An Electron Transfer Competent Structural Ensemble of Membrane-Bound Cytochrome P450 1A1 and Cytochrome P450 Oxidoreductase. *Commun Biol* **2021**, *4* (1), 55. https://doi.org/10.1038/s42003-020-01568-y.

Munro, A. W.; Leys, D. G.; McLean, K. J.; Marshall, K. R.; Ost, T. W. B.; Daff, S.; Miles, C. S.; Chapman, S. K.; Lysek, D. A.; Moser, C. C.; Page, C. C.; Dutton, P. L. P450 BM3: The Very Model of a Modern Flavocytochrome. *Trends in Biochemical Sciences* **2002**, *27* (5), 250–257. https://doi.org/10.1016/S0968-0004(02)02086-8.

Munro, A. W.; Daff, S.; Coggins, J. R.; Lindsay, J. G.; Chapman, S. K. Probing Electron Transfer in Flavocytochrome P-450 BM3 and Its Component Domains. *European Journal of Biochemistry* **1996**, *239* (2), 403–409. https://doi.org/10.1111/j.1432-1033.1996.0403u.x.

Munro, A. W.; Lindsay, J. G.; Coggins, J. R.; Kelly, S. M.; Price, N. C. Structural and Enzymological Analysis of the Interaction of Isolated Domains of Cytochrome *P* -450 BM3. *FEBS Letters* **1994**, *343* (1), 70–74. https://doi.org/10.1016/0014-5793(94)80609-8.

Neeli, R.; Girvan, H. M.; Lawrence, A.; Warren, M. J.; Leys, D.; Scrutton, N. S.; Munro, A. W. The Dimeric Form of Flavocytochrome P450 BM3 Is Catalytically Functional as a Fatty Acid Hydroxylase. *FEBS Letters* **2005**, *579* (25), 5582–5588. https://doi.org/10.1016/j.febslet.2005.09.023.

Pettersen, E. F.; Goddard, T. D.; Huang, C. C.; Couch, G. S.; Greenblatt, D. M.; Meng, E. C.; Ferrin, T. E. UCSF Chimera—A Visualization System for Exploratory Research and Analysis. *Journal of Computational Chemistry* **2004**, *25* (13), 1605–1612. https://doi.org/10.1002/jcc.20084.

Sevrioukova, I. F.; Li, H.; Zhang, H.; Peterson, J. A.; Poulos, T. L. Structure of a Cytochrome P450-Redox Partner Electron-Transfer Complex. *Proceedings of the National Academy of Sciences* **1999**, *96* (5), 1863–1868. https://doi.org/10.1073/pnas.96.5.1863.

Sevrioukova, I. F.; Hazzard, J. T.; Tollin, G.; Poulos, T. L. The FMN to Heme Electron Transfer in Cytochrome P450BM-3: Effect Of Chemical Modification Of Cysteines Engineered At The FMN-Heme Domain Interaction Site. *J. Biol. Chem.* **1999**, *274* (51), 36097–36106. https://doi.org/10.1074/jbc.274.51.36097.

Su, M.; Chakraborty, S.; Osawa, Y.; Zhang, H. Cryo-EM Reveals the Architecture of the Dimeric Cytochrome P450 CYP102A1 Enzyme and Conformational Changes Required for Redox Partner Recognition. *J. Biol. Chem.* **2020**, *295* (6), 1637–1645. https://doi.org/10.1074/jbc.RA119.011305.

Whitehouse, C. J. C.; Bell, S. G.; Wong, L.-L. P450 $_{BM3}$ (CYP102A1): Connecting the Dots. *Chem. Soc. Rev.* **2012**, *41* (3), 1218–1260. https://doi.org/10.1039/C1CS15192D.

Wu, B.; Peisley, A.; Richards, C.; Yao, H.; Zeng, X.; Lin, C.; Chu, F.; Walz, T.; Hur, S. Structural Basis for DsRNA Recognition, Filament Formation, and Antiviral Signal Activation by MDA5. *Cell* **2013**, *152* (1–2), 276–289. https://doi.org/10.1016/j.cell.2012.11.048.

Zeng-Elmore, X.; Gao, X.-Z.; Pellarin, R.; Schneidman-Duhovny, D.; Zhang, X.-J.; Kozacka, K. A.; Tang, Y.; Sali, A.; Chalkley, R. J.; Cote, R. H.; Chu, F. Molecular Architecture of Photoreceptor Phosphodiesterase Elucidated by Chemical Cross-Linking and Integrative Modeling. *Journal of Molecular Biology* **2014**, *426* (22), 3713–3728. https://doi.org/10.1016/j.jmb.2014.07.033.

## Acknowledgements

This work was supported in part by National Institutes of Health grants ES007062 (to DF), GM077430, and NS055746, as well as from the University of Michigan's Protein Folding Disease Initiative.

The University of Michigan Proteomics Resource Facility performed in-gel trypsinolysis and mass spectrometry analysis of samples.

### Author Contributions

This project was conceived by Dana Felker, Yoichi Osawa, and Haoming Zhang. Experiments were designed and performed by Dana Felker. Methodological input and resources were provided by Haoming Zhang, Zhiyuan Bo, Yoshihiro Morishima, Miranda Lau, and Santiago Schnell. Data analysis and methods for data visualization were developed and performed by Dana Felker with guidance from Santiago Schnell. Writing was carried out by Dana Felker and Yoichi Osawa. Review and editing was provided by Haoming Zhang, Yoshihiro Morishima, and Santiago Schnell.

## Tables

***Table 2-1****. Crosslinked tryptic peptides identified after analysis of the monomer band derived from CYP102A1 treated with DSBU for 5 min.*

| Site 1 | Site 2 | Peptide 1 | Peptide 2 | m/z | Score |
|---|---|---|---|---|---|
| K10 | K42 | EMPQP**K**TFGELK | IADELGEIF**K**FEAPGR | 848.691 | 169 |
| K77 | K188 | NLSQAL**K**FVR | ALDEAMN**K**LQR | 665.615 | 181 |
| K77 | K203 | NLSQAL**K**FVR | ANPDDPAYDEN**K**R | 959.150 | 87 |
| K77 | K350 | NLSQAL**K**FVR | EDTVLGGEYPLE**K**GDELMVLIPQLHR | 1081.327 | 138 |
| K469 | K474 | KIPLGGIPSPSTEQSA**K**K | **K**AEDAHDTPLLVLYGSNMGTAEGTAR | 954.100 | 21 |

*Score values are calculated as indicated in methods.*

***Table 2-2.*** *Crosslinked tryptic peptides identified after analysis of the monomer band derived from CYP102A1 treated with DSBU for 15 min.*

| Site 1 | Site 2 | Peptide 1 | Peptide 2 | m/z | Score |
|---|---|---|---|---|---|
| K25 | K365 | NLPLLNTD**K**PVQALMK IADELGEIFK | D**K**TIWGDDVEEFRPER | 1020.331 | 70 |
| K77 | K188 | NLSQAL**K**FVR | ALDEAMN**K**LQR | 665.615 | 160 |
| K77 | K203 | NLSQAL**K**FVR | ANPDDPAYDEN**K**R | 959.484 | 36 |
| K77 | K350 | NLSQAL**K**FVR | EDTVLGGEYPLE**K**GDELMVLIPQLHR | 1081.327 | 119 |
| K735 | K771 | LEAEEE**K**LAHLPLAK | AMAA**K**TVCPPHK | 640.144 | 183 |
| K735 | T772 | LEAEEE**K**LAHLPLAK | AMAAK**T**VCPPHK | 640.143 | 160 |
| K735 | K814 | LEAEEE**K**LAHLPLAK | YPACEM**K**FSEFIALLPSIRPR | 883.071 | 45 |
| K787 | K1039 | VELEALLE**K**QAYK | LWLQQLEE**K**GR | 1043.572 | 263 |
| K791 | K1039 | QAY**K**EQVLAK | LWLQQLEE**K**GR | 693.883 | 171 |
| K797 | K1039 | EQVLA**K**R | LWLQQLEE**K**GR | 610.344 | 135 |

*Score values are calculated as indicated in methods.*

***Table 2-3.*** *Crosslinked tryptic peptides identified after analysis of the dimer band derived from CYP102A1 treated with DSBU for 5 min.*

| Site 1 | Site 2 | Peptide 1 | Peptide 2 | m/z | Score |
|---|---|---|---|---|---|
| S66 | K1039 | LIKEABDE**S**R | LWLQQLEE**K**GR | 704.617 | 165 |
| K77 | K188 | NLSQAL**K**FVR | ALDEAMN**K**LQR | 665.615 | 175 |
| K290 | K691 | NPHVLQ**K**AAEEAAR | HLEIELP**K**EASYQEGDHLGVIPR | 872.657 | 44 |
| T577 | K1039 | NWA**T**TYEKVPAFIDETLAAK | LWLQQLEE**K**GR | 966.515 | 83 |

*Rows emphasized in grey indicate crosslinks also detected in Tables 1 and 2. Score values are calculated as indicated in methods.*

***Table 2-4.*** *Crosslinked tryptic peptides identified after analysis of the dimer band derived from CYP102A1 treated with DSBU for 15 min.*

| Site 1 | Site 2 | Peptide 1 | Peptide 2 | m/z | Score |
|---|---|---|---|---|---|
| K10 | K42 | EMPQP**K**TFGELK | IADELGEIF**K**FEAPGR | 1131.249 | 221 |
| K25 | K365 | NLPLLNTD**K**PVQALMKIADE LGEIFK | D**K**TIWGDDVEEFRPER | 1023.531 | 119 |
| K60 | K561 | LI**K**EACDESR | QFVDWLDQASADEV**K**GVR | 1160.237 | 39 |
| S66 | K1039 | LIKEACDE**S**R | LWLQQLEE**K**GR | 704.616 | 233 |
| K70 | K561 | FD**K**NLSQALK | QFVDWLDQASADEV**K**GVR | 856.189 | 136 |
| K77 | K188 | NLSQAL**K**FVR | ALDEAMN**K**LQR | 665.614 | 159 |
| K77 | K203 | NLSQAL**K**FVR | ANPDDPAYDEN**K**R | 959.151 | 110 |
| K77 | K350 | NLSQAL**K**FVR | EDTVLGGEYPLE**K**GDELMVLIP QLHR | 1081.327 | 118 |
| K219 | K448 | VMNDLVD**K**IIADRK | ETLTLKPEGFVV**K**AK | 697.795 | 169 |
| K310 | K691 | QV**K**QLK | HLEIELP**K**EASYQEGDHLGVIPR | 892.985 | 115 |
| K310 | K735 | QV**K**QLK | LEAEEE**K**LAHLPLAK | 658.128 | 71 |
| K313 | Y695 | QL**K**YVGMVLNEALR | HLEIELPKEAS**Y**QEGDHLGVIPR | 892.677 | 122 |
| S507 | K791 | DLADIAM**S**KGFAPQVATLDS HAGNLPR | QAY**K**EQVLAK | 1042.793 | 30 |
| K508 | K735 | DLADIAMS**K**GFAPEVATLDS HAGDLPR | LEAEEE**K**LAHLPLAK | 940.691 | 46 |
| K508 | K778 | DLADIAMS**K**GFAPEVATLDS HAGDLPR | TVCPPH**K**VELEALLEK | 974.905 | 25 |
| T516 | K735 | DLADIAMSKGFAPQVA**T**LDS HAGNLPR | LEAEEE**K**LAHLPLAK | 1171.113 | 144 |
| K561 | K787 | QFVDWLDQASADEV**K**GVR | VELEALLE**K**QAYK | 1264.654 | 204 |
| K573 | Y790 | YSVFGCGD**K**NWATTYQK | VELEALLEKQA**Y**K | 939.219 | 192 |
| K573 | K791 | YSVFGCGD**K**NWATTYQK | QAY**K**EQVLAK | 850.169 | 131 |
| K573 | K1039 | YSVFGCGD**K**NWATTYQK | LWLQQLEE**K**GR | 905.697 | 171 |
| K691 | K841 | HLEIELP**K**EASYQEGDHLGVI PR | VDE**K**QASITVSVVSGEAWSGY GEYK | 1379.439 | 170 |
| K735 | K771 | LEAEEE**K**LAHLPLAK | AMAA**K**TVCPPHK | 640.144 | 162 |
| K735 | T772 | LEAEEE**K**LAHLPLAK | AMAAK**T**VCPPHK | 640.143 | 175 |
| K791 | K1039 | QAY**K**EQVLAK | LWLQQLEE**K**GR | 693.883 | 169 |
| K797 | K1039 | EQVLA**K**R | LWLQQLEE**K**GR | 610.344 | 140 |

*Rows emphasized in grey indicate crosslinks also detected in Tables 1 and 2. Score values are calculated as indicated in methods.*

***Table 2-5.*** *Distances of the crosslinked residues mapped as inter- and intra- monomer crosslinks onto the three available conformations of the full-length CYP102A1 structure.*

| *Crosslink Identity* | | | *Structural Conformation* | | | | | | | | | | | |
|---|---|---|---|---|---|---|---|---|---|---|---|---|---|---|
| | | | Closed | | | | Open I | | | | Open II | | | |
| | | | α-β | β-α | α-α | β-β | α-β | β-α | α-α | β-β | α-β | β-α | α-α | β-β |
| # | Residues | Domains | Cα-Cα Distance (Å) | | | | | | | | | | | |
| 1 | K60-K561 | Oxy-FMN | **19.3** | **19.3** | 96.7 | 96.7 | 27.9 | 41.2 | 97.6 | 93.8 | 33.0 | 41.9 | 101.9 | 95.2 |
| 2 | S66-K1039 | Oxy-FAD | 51.8 | 51.3 | 105.1 | 105.1 | 47.4 | 47.1 | 101.8 | 109.4 | 72.3 | 35.5 | 99.8 | 112.4 |
| 3 | K70-K561 | Oxy-FMN | **22.8** | **22.5** | 92.8 | 92.8 | **25.6** | 42.1 | 96.6 | 91.9 | 37.1 | 44.1 | 100.8 | 93.2 |
| 4 | K219-K448 | Oxy-Oxy | **17.9** | **17.9** | 36.5 | 36.5 | **14.3** | **16.4** | 36.5 | 36.5 | **14.0** | **15.4** | 36.5 | 36.5 |
| 5 | K290-K691 | Oxy-FAD | **26.8** | **26.4** | 57.7 | 57.7 | 32.3 | 36.1 | 61.4 | 62.6 | 52.6 | 28.0 | 61.6 | 66.0 |
| 6 | K310-K691 | Oxy-FAD | 31.4 | 31.1 | 49.1 | 49.1 | 32.6 | 37.1 | 52.2 | 54.9 | 50.5 | 31.8 | 53.3 | 57.8 |
| 7 | K310-K735 | Oxy-FAD | **23.3** | **21.4** | 46.8 | 45.1 | 29.0 | **25.8** | 39.0 | 45.8 | 34.2 | 28.0 | 46.8 | 42.4 |
| 8 | K313-Y695 | Oxy-FAD | 28.4 | 28.0 | 64.1 | 64.1 | 31.7 | 33.2 | 64.3 | 68.1 | 52.1 | **25.7** | 65.5 | 69.1 |
| 9 | S507-K791 | FMN-FAD | 79.9 | 79.8 | 27.9 | 27.9 | 79.2 | 76.5 | **22.9** | 27.8 | 78.1 | 75.2 | **22.9** | 27.8 |
| 10 | K508-K735 | FMN-FAD | 58.4 | 59.3 | **20.2** | **20.9** | 59.3 | 53.0 | **23.0** | **21.2** | 57.8 | 51.6 | **23.0** | **21.2** |
| 11 | K508-K778 | FMN-FAD | 78.2 | 78.1 | 31.3 | 31.3 | 80.7 | 74.8 | **24.5** | 31.2 | 79.2 | 73.3 | **24.5** | 31.2 |
| 12 | T516-K735 | FMN-FAD | 57.6 | 59.3 | **25.0** | 27.7 | 69.0 | 56.9 | 36.5 | 30.0 | 67.8 | 56.0 | 36.5 | 30.0 |
| 13 | K561-K787 | FMN-FAD | 97.4 | 97.2 | 35.3 | 35.3 | 96.7 | 93.3 | **16.1** | 34.5 | 95.3 | 92.2 | **16.1** | 34.5 |
| 14 | K573-Y790 | FMN-FAD | 78.3 | 78.3 | **22.3** | **22.3** | 79.3 | 82.8 | 42.4 | **21.8** | 78.0 | 81.7 | 42.4 | **21.8** |
| 15 | K573-K791 | FMN-FAD | 80.5 | 80.5 | **19.0** | **19.0** | 81.8 | 85.0 | 40.8 | **18.4** | 80.7 | 83.9 | 40.8 | **18.4** |
| 16 | K573-K1039 | FMN-FAD | 95.6 | 95.7 | **20.9** | **20.9** | 94.1 | 96.0 | **24.1** | **22.6** | 94.5 | 95.2 | **24.1** | **22.6** |
| 17 | T577-K787 | FMN-FAD | 88.2 | 88.2 | **26.9** | **26.9** | 87.6 | 90.7 | 37.2 | **25.5** | 86.4 | 89.7 | 37.2 | **25.5** |
| 18 | K577-K1039 | FMN-FAD | 100.7 | 100.8 | **17.7** | **17.7** | 99.6 | 100.2 | **20.6** | **21.8** | 99.8 | 99.6 | **20.6** | **21.8** |
| 19 | K691-K841 | FAD-FAD | 60.6 | 60.5 | **7.3** | **7.3** | 59.0 | 59.0 | **7.3** | **7.3** | 59.1 | 59.2 | **7.3** | **7.3** |

All crosslinks from Table 3 and 4 that were not greyed out were used. Since the dimer in these conformations is not symmetrical, we arbitrarily assigned one monomer α and the other β. Thus, there are four possible distances for each crosslink in each conformation. Crosslink configurations that mapped to distances within the 27 Å distance restraint for the DSBU linker arm are shown in bold.

## Figures

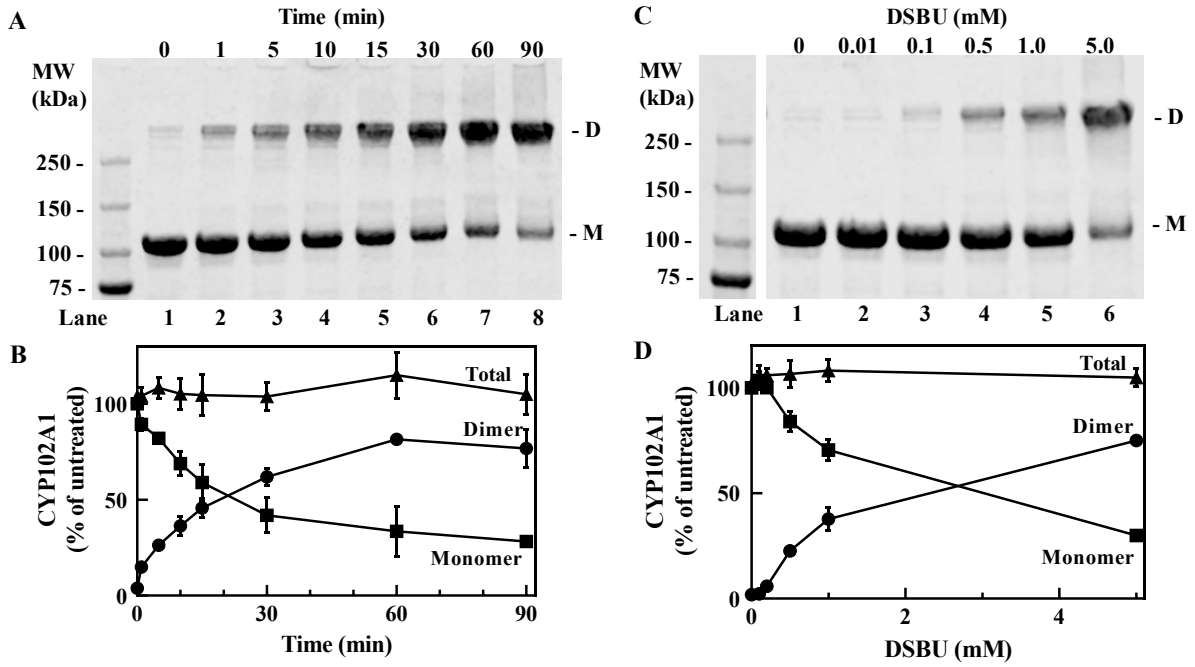


***Figure 2-1.*** *Formation of covalently crosslinked CYP102A1 dimer after treatment with DSBU.*

**(A)**, Time-dependent formation of crosslinked CYP102A1 after treatment with DSBU. Full-length CYP102A1 (10 μM) was treated with 0.5 mM DSBU for the indicated duration and aliquots (3 μg) of the reaction mixtures were submitted to SDS-PAGE and stained with Coomassie Blue as described in Methods. D, crosslinked dimeric CYP102A1; M, monomer of CYP102A1. **(B)**, Quantification of bands seen in A. Bands corresponding to the crosslinked dimer (closed circles) and monomer (closed squares) were quantified by densitometric analysis. The sum of the dimer and monomer was also calculated (closed triangle). Mean ± SD derived from three independent reaction mixtures (n=3). **(C)**, Formation of the crosslinked CYP102A1 is dependent on the concentration of DSBU. CYP102A1 was treated with the indicated concentrations of DSBU for 5 min and the reaction mixture analyzed as in A. **(D)**, Quantification of bands seen in C. The amount of dimeric CYP102A1 (closed circles), monomeric CYP102A1 (closed squares), and the sum total (closed triangles) was quantified as in B. Mean ± SD (n=3). Densities determined for all bands are within the linear range of detection.

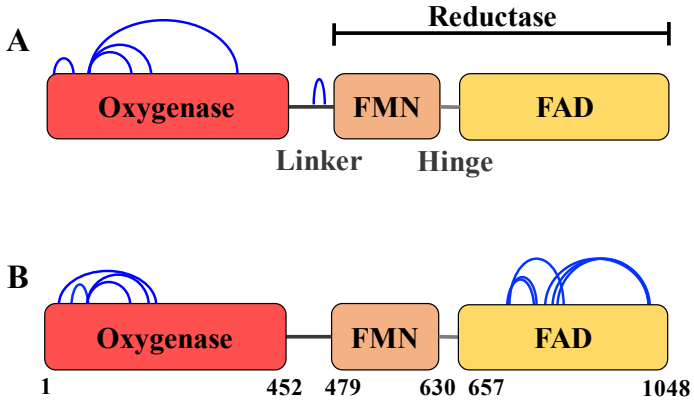


***Figure 2-2.*** *Schematic representation of the intra-monomer crosslinks found in the monomer band derived from CYP102A1 treated with DSBU for 5 min (A) or 15 min (B).*

Blue arcs, crosslinks; red, oxygenase domain; orange, FMN domain; yellow, FAD domain. The FMN and FAD domains together represent the reductase domain.

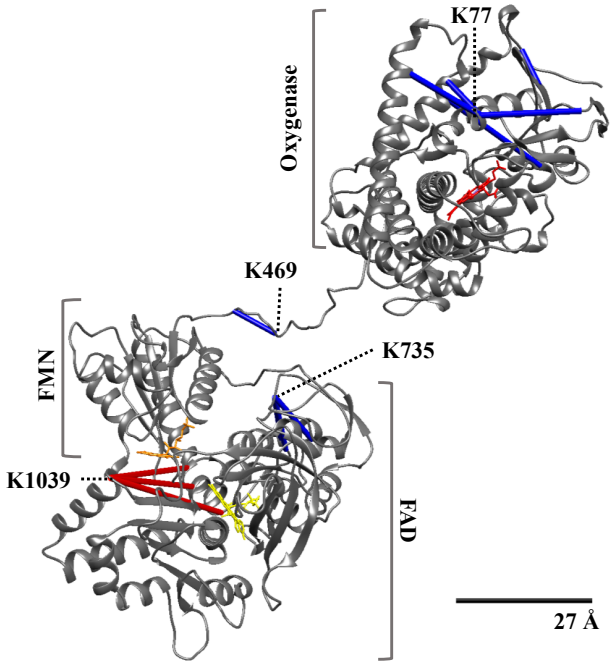


***Figure 2-3.*** *Structure of the CYP102A1 monomer derived from the cryo-EM model constructed with the use of the crystal structure of the oxygenase and reductase domain, which contains the FMN and FAD binding domains.*

Backbone ribbon model of CYP102A1 is shown in grey and the 27Å scale bar indicates the accepted $C_\alpha$-$C_\alpha$ distance restraint for the DSBU crosslinker. Blue bars, crosslinks that map within 27 Å; red bars, crosslinks that exceed 27 Å; red, heme prosthetic moiety; orange, FMN; yellow, FAD.

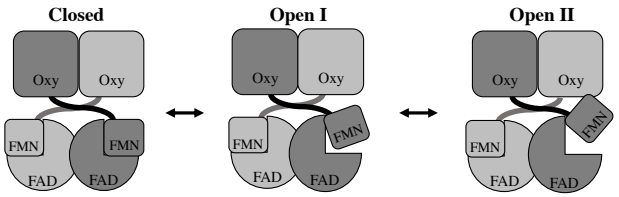


***Figure 2-4****. Three conformations of the CYP102A1 homodimer identified in Cryo-EM structural model.*

Simplified models of the homodimer in its Closed, Open I, and Open II conformational states are shown that represent conformations captured in recent cryo-EM studies of the enzyme [Su et al., 2020].

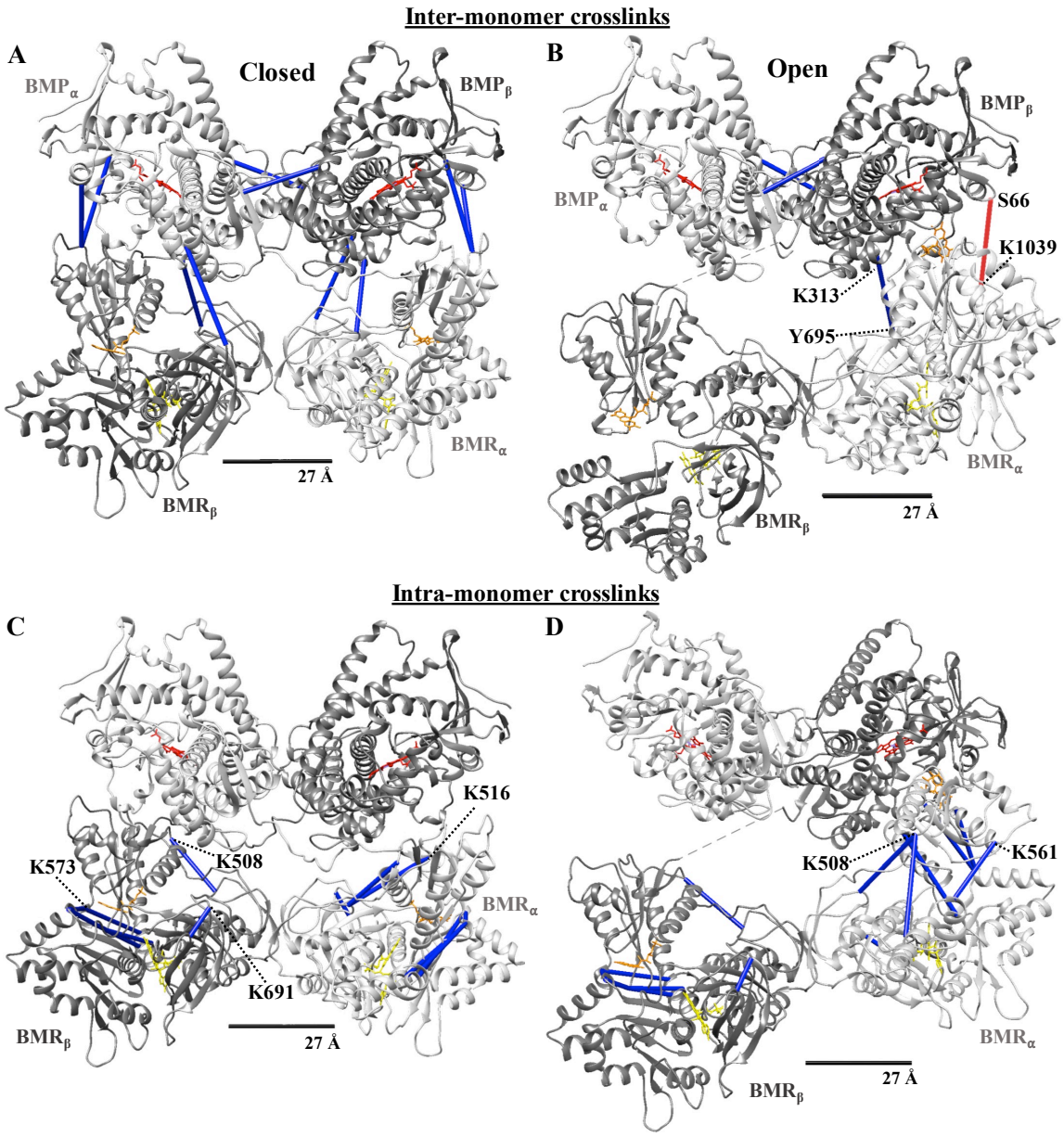


***Figure 2-5.*** *Crosslinks mapped to cryo-EM structural model of the CYP102A1 homodimer in Closed (A and C) and Open II (B and C) conformations.*

Since the dimer is not symmetrical, we arbitrary labeled one monomer α (light grey) and the other β (dark grey). The heme-containing oxygenase (BMP) and flavin-containing reductase (BMR) domains of each monomer are labeled accordingly. Cofactors and crosslinks are colored as in Figure 3. 27Å scale bar indicates the accepted $C_\alpha$-$C_\alpha$ distance restraint for the DSBU crosslinker. Crosslinks #1-8 with the exception of #6 from Table 5 are shown in **A** and **B**. Crosslinks #9-19 from Table 5 are shown in **C** and **D**.

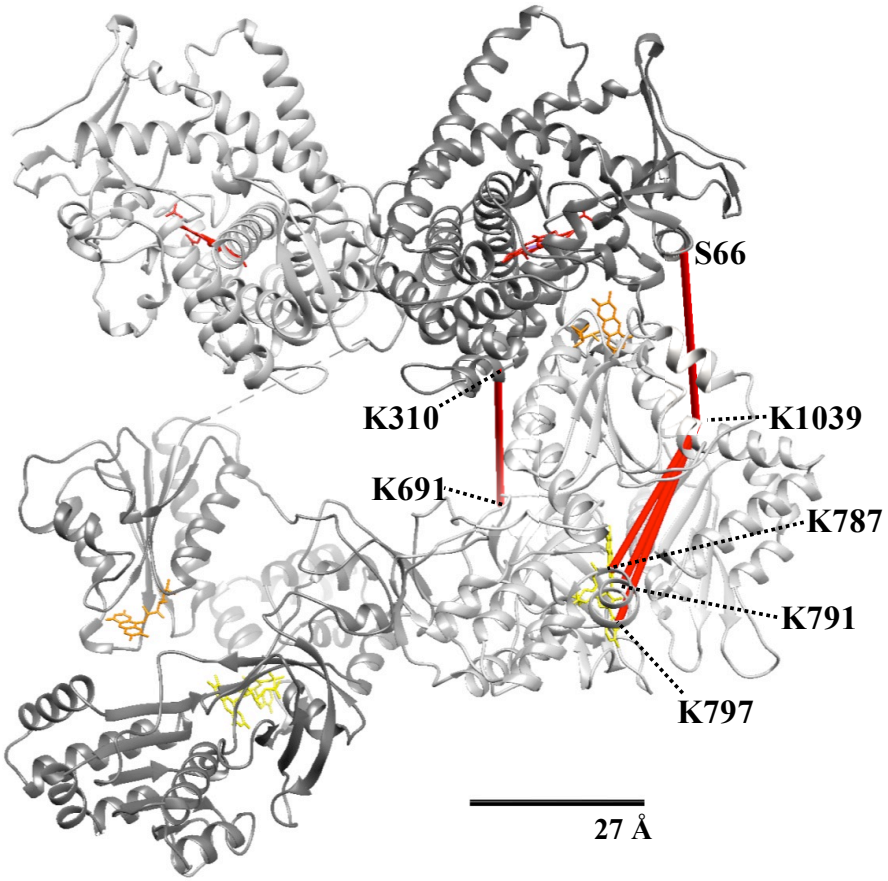


***Figure 2-6.*** *All five crosslinks that exceeded the distance restraint of the DSBU linker arm were mapped to shortest distances in the open II conformation of the CYP102A1 homodimer.*

Monomers and cofactors are colored as in Figure 4. 27Å scale bar indicates the accepted $C_\alpha$-$C_\alpha$ distance restraint for the DSBU crosslinker.

# Chapter 3 Interprotein Interactions Within Calmodulin-Bound Neuronal Nitric Oxide Synthase


## Abstract

Neuronal nitric oxide synthase (nNOS) is a cytochrome P450 enzyme responsible for the production of nitric oxide, an important neurotransmitter and signaling molecule, in the brain. nNOS is tightly regulated through several mechanisms including the formation of a stable homodimer and the association of calmodulin, which confers calcium dependence on nNOS activity *in vivo*. Although crystal structures have been successfully resolved for calmodulin's interaction with its truncated binding helix of nNOS, interactions between calmodulin and full-length functional nNOS are not known. Similarly, high-resolution structures have been resolved of individual domains of nNOS, but it remains incompletely understood how these domains interact within full-length nNOS in its native state. In this study, we utilized covalent crosslinking and mass spectrometry (CXL-MS) to identify sites of interdomain and interprotein interaction within the active nNOS:calmodulin multiprotein machinery. The nNOS:calmodulin homodimeric complex was treated with an MS-cleavable crosslinker disuccinimidyl dibutyric urea (DSBU) to produce a crosslinked complex containing both nNOS and calmodulin, which was abolished in the absence of calcium. This crosslinked complex was isolated for analysis by mass spectrometry, and thirteen unique crosslinks were identified between calmodulin and nNOS and sixty-one were identified within nNOS. Crosslinks between CaM and nNOS dictate a close proximity between CaM and the nNOS oxygenase domain as well as reductase domain. This

high degree of interconnectivity suggests calmodulin interacts with both oxygenase and reductase domains of nNOS in addition to its known binding helix between these domains. Additional crosslinks between the nNOS oxygenase and reductase domains demonstrate that both the FMN and FAD domains achieve a closer proximity to the oxygenase than previously observed in structural studies. Intermolecular docking to satisfy crosslinks detected between nNOS oxygenase and FMN domains positions the FMN domain adjacent to nNOS residue W587, consistent with the previously proposed site of electron transfer to heme. These experiments captured multiple interprotein interactions between domains of nNOS and between nNOS and its regulator, calmodulin. These data enhance our understanding of the nNOS holoenzyme's structural arrangement in solution and provide evidence for novel target sites for pharmacologic regulation of the nNOS:calmodulin multiprotein complex.

This section was written by D. Felker with significant intellectual contributions from Yoichi Osawa. Technical assistance and methodological expertise were provided by Miranda Lau and Yoshihiro Morishima. Intellectual contributions were provided by Haoming Zhang.

## Introduction

Nitric oxide (NO) is an important signaling molecule throughout the body, necessary for regulation of vascular tone and neurotransmission [Meffert et al., 1994; Schmidt 1994; Ziche & Mobidelli, 2000; Moncada & Higgs, 2006; Calabrese et al., 2007]. NO is a highly reactive molecule that freely diffuses following its production. Because of this, NO is primarily regulated through its production by nitric oxide synthase (NOS) enzymes. Three major isoforms of NOS exist: neuronal, endothelial, and inducible. Each isoform is present in specific tissues and carries out different physiologic functions through NO production. Development of isoform-specific regulators of NOS enzymes is of great clinical interest; however, because of the strong structural similarities across NOS isozymes the development of isoform-specific modulators has proved challenging.

Neuronal nitric oxide synthase (nNOS) is expressed in neural and skeletal muscle tissues, and is responsible for NO production in the brain. Dysregulation of NO production by nNOS is implicated in aggressive behavior, migraine, stroke, and the development of neurodegenerative diseases [Schmidt 1994; Zhang et al., 2006]. nNOS is an obligate homodimer composed of an N-terminal heme-containing oxygenase domain and a C-terminal diflavin reductase domain connected by a flexible linker. The association of the calcium-bound regulatory protein calmodulin (CaM) with this linker region is necessary for enzyme function. Thus, CaM confers calcium-dependence on nNOS activity *in vivo*.

For nNOS to complete enzymatic turnover, electrons are received from NADPH by the FAD cofactor within the nNOS reductase domain. An intraprotein electron transfer then occurs from FAD to FMN, and the FMN shuttles electrons to the active site heme of the opposing nNOS monomer. CaM exerts regulatory control over several stages of this process. Previous

studies have demonstrated that CaM plays a role in stabilizing FMN cofactor binding to its domain on nNOS [Panda et al., 2013] and regulates intramolecular electron transfer from FAD to FMN within the reductase domain [Matsuda & Iyanagi, 1999; Guan & Iyanagi, 2003]. Most notably, CaM is necessary for interprotein electron transfer to occur from FMN to heme [Panda et al., 2001]. The interaction of CaM with NOS enzymes differs across isoforms, and is one of the most isoform-specific mechanisms of NOS regulation. While the interaction between CaM and its truncated binding helix on nNOS has been captured at high resolution by x-ray crystallography, the interactions between CaM and other regions of the full-length nNOS remain poorly understood.

Previous studies using negative stain- and cryoelectron microscopy (cryo-EM) have shown that the nNOS:CaM homodimer samples a large conformational space that encompasses a closed configuration with both oxygenase and reductase domains dimerized, and an extended state with reductase domains hinged far apart [Yokom 2014; Hanson 2018; Smith 2013]. With numerous conformational states likely critical to biologic activity, studies examining the interdomain dynamics of the full-length nNOS in multiple conformations are crucial in understanding the mechanisms of electron shuttling through flavins to heme.

Covalent crosslinking and mass spectrometry (CXL-MS) is a highly sensitive method to identify sites of protein-protein interaction. Recent advances in covalent crosslink design and automated search algorithms allow high-confidence identification of crosslinked residues within large multiprotein machineries [Gotze 2015; Arlt 2016; Iacobucci 2018; Iacobucci 2019]. CXL-MS is optimal for the study of large and highly dynamic multiprotein complexes such as the nNOS:CaM homodimer [Gong 2015], as this method samples the entire conformational suite of proteins in their native state.

We applied this versatile methodology to study protein-protein interactions within the active nNOS:CaM complex. Our results show that CaM interacts with the oxygenase and reductase domains of nNOS in addition to its well-known binding site between domains. We also demonstrate that both components of the reductase come in closer proximity to the oxygenase domain than previous structural models of the nNOS:CaM homodimer have captured. This proximity brings both flavins closer to heme. These findings identify novel conformational states of the nNOS:CaM complex and indicate that novel interdomain and interprotein interactions occur within the nNOS:CaM conformational suite.

## Materials and Methods

**Materials.** Disuccinimidyl dibutyric urea (DSBU) (Lot UG281415) was purchased from Thermo Scientific. Sodium chloride (Lot 16620) was from Fisher BioReagents. Anhydrous DMSO (Lot SHBK9388), 2-mercaptoethanol (Lot SHBG9616V), HEPES (Lot SLBW4677), ammonium bicarbonate (Lot 116K0130), and rabbit anti-nNOS antibody (N7155) were from Sigma. The 10x Tris/Glycine/SDS (Lot 64343645), Bio-Safe Coomassie stain (Ctrl BR03262020), 2x Laemmli (Lot 64315141), and 4-15% gradient SDS-PAGE gels (Lot 64362663) were purchased from Bio-Rad. Mouse anti-calmodulin antibody was from Millipore (05-173, Lot 2829830). Goat anti-rabbit (926–32211) and goat anti-mouse (926–68020) infrared dye-conjugated antibodies were from Li-Cor.

**Protein expression and purification.** Full-length rat neuronal nitric oxide synthase (nNOS) was expressed and purified as previously described [Clapp et al., 2010]. The purified nNOS had a specific activity of 504 nmol NO/min/mg as assessed by the oxyhemoglobin method described below. The expression vector for human calmodulin containing an N-terminal His6-TEV tag was generously provided by John Tesmer (Purdue University, West Lafayette, IN). Human calmodulin was overexpressed in E. coli, purified by nickel agarose chromatography, and treated with TEV protease to remove the tag [Beyett et al., 2019].

**nNOS activity measurement using oxyhemoglobin method.** NO synthesis was determined by measuring the NO-catalyzed conversion of oxyhemoglobin to methemoglobin [Feelisch et al., 1996]. The nNOS (1.3 μg) was incubated with 100 μM $CaCl_2$, 100 μM L-arginine, 100 μM tetrahydrobiopterin, 100 units/ml catalase, 25 μM oxyhemoglobin, and an NADPH-regenerating system consisting of 400 μM NADP+, 10 mM glucose 6-phosphate, and 1 unit/ml glucose-6-phosphate dehydrogenase, expressed as final concentrations, in a total volume

of 180 µl of 50 mM Tris, pH 7.4. at 37°C. The rate of oxidation of oxyhemoglobin was measured with a microtiter plate reader as described previously [Feelisch et al., 1996; Billecke et al., 2004; Clapp et al., 2010].

**Chemical crosslinking, SDS-PAGE, and western blotting.** Purified nNOS (2 µM) was mixed with calmodulin (1.3 mg/ml), 10 µM $CaCl_2$, 10 µM tetrahydrobiopterin, and 0.1 mM NaCl in total volume of 10 µl of HEPES, pH 7.35 for 5 minutes at 4°C. The mixture was treated with the desired amount of DSBU, which was dissolved in anhydrous DMSO, at room temperature with rotation. The DMSO concentration was 10% (v/v) of the total reaction mixture. Reactions were quenched at the appropriate times with 2 µl of 0.5 M ammonium bicarbonate and gently mixed for 5 minutes at 4°C before addition of an equal volume of 2x Laemmli Sample Buffer containing 10% (v/v) 2-mercapotethanol. Samples were boiled for 5 minutes and aliquots (15 µl) were submitted to SDS-PAGE on 4-15% gradient gels run for 45 minutes at 50 mAmps/gel. Gels were Coomassie stained for 1 hour with ProteinSafe Coomassie Stain and destained in MilliQ water. Gels were imaged with a LI-COR Odyssey Fc and bands corresponding to nNOS monomer and dimer were quantified by densitometric analysis with the use of ImageStudio software (version 5.2).

Aliquots (7.5 µl) of the reaction mixtures were run on SDS-PAGE as above and further analyzed by western blotting. Gels were transferred to Immobilon-FL PVDF membranes at 100V for 2 hours in a Mini Trans-Blot Electrophoretic Transfer Cell (Bio-Rad). The membranes were blocked for 30 minutes and then incubated with anti-nNOS (0.01% v/v) or anti-CaM (1.5 µg/ml) at room temperature for 1 hour. The blots were washed and incubated with the appropriate IR-tagged secondary antibody (0.4 µg/ml anti-rabbit and 0.2 µg/ml anti-mouse) for 1 hour. The IR signal for nNOS and CAM were imaged with a LI-COR Odyssey Fc.

**Mass spectrometry and peptide assignment.** Crosslinked protein samples were separated by SDS-PAGE. Duplicate protein bands corresponding to CaM-bound dimeric nNOS were submitted for in-gel trypsinolysis and subsequent analysis on a Thermo Scientific Q Exactive HF Orbitrap MS at the University of Michigan Mass Spectrometry-Based Proteomics Resource Facility. Peptide assignments were performed using MeroX (version 2.0) to specifically search for peptides containing the signature doublet that DSBU produces upon fragmentation. MS datasets were analyzed with primary and secondary fragment mass deviations of 10 and 50 ppm, respectively, with mass limits of 600-6000 Da and s/n ratio of 1.5. Score cut-offs calculated for a False Discovery Rate (FDR) < 0.01% were applied as recommended in the literature [Iacobucci et al., 2017; Iacobucci & Sinz, 2019]. The MS/MS spectra were also manually checked, as another layer of quality control, using MeroX.

**Mapping of crosslinks onto three-dimensional models of nNOS.** A cryo-EM based structural model of the nNOS:CaM homodimer was used to guide in silico model construction for crosslink analysis. Rigid-body fitting results of crystal structures of NOS heme, FMN, and FAD domains [PDB 1RS9, 3HR4, 1TLL] into cryo-EM density of the nNOS homodimer [EMDB 5940] were generously provided by Daniel Southworth at University of California San Francisco [Yokom et al., 2014]. Crystal structures of nNOS oxygenase and FMN domains [PDB 1ZVL, $1TLL_{750\text{-}951}$] were aligned with domains in this model using UCSF Chimera (Version 1.13.1) [Pettersen et al., 2014], and original iNOS domains were removed. Human calmodulin [PDB 3HR4] was aligned to this structure using its included CaM-binding helix as a reference. The CaM-binding helix of iNOS [PDB 3GOF] was oriented using the original NOS:CaM structure as a reference and renumbered according to Blast alignments of iNOS and nNOS sequences for the region, to allow visualization of the N-terminal portion of the alpha helix in the

final model. $C_\alpha$-$C_\alpha$ Euclidean distances were mapped to the resulting models and measured using Chimera.

**Crosslink-guided molecular docking of nNOS and CaM.** Crystal structures of dimerized nNOS oxygenase domains [PDB 1ZVL], reductase domain [PDB 1TLL], and full-length calmodulin [PDB 3HR4] were obtained from the Protein Databank [Garcin et al., 2004; Matter et al., 2005; Xia et al., 2009]. Truncated FMN domain residues 750-951 were isolated from the reductase domain structure for docking. Water, heme, $BH_4$, zinc, and $Ca^{2+}$ cofactors were deleted from the structures. All structures were minimized using UCSF Chimera, then uploaded as molecules in the HADDOCK online server (version 2.4-2021.05) [van Zundert et al., 2015], with position of both chains of the oxygenase domain fixed at their original position during initial docking to maintain the $nNOS_{oxy}$ dimerization interface. All interprotein (CaM-nNOS) and interdomain crosslinks with residues present in these structures (Table 3-5 #3-5,8-10 and Table 3-6 #37,42,44) were input as ambiguous restraints to guide docking. In accordance with the accepted 27 Å $C_\alpha$-$C_\alpha$ DSBU linker arm length [Piersimoni & Sinz, 2020], distances between $C_\alpha$ atoms were set with a range of 4-29 Å. Number of partitions for random exclusion was set to 2, causing random exclusion of 50% of the guiding crosslinks in each docking iteration. Docking was performed with 1000 rigid body docking iterations, 200 semi-flexible refinements, and 200 final refinements.

## Results

**CaM addition to nNOS forms the active nNOS:CaM multiprotein complex.** In this study, we used purified nNOS that was shown by HPLC to be dimeric (data not shown). The enzyme was activated by CaM in a concentration-dependent manner, as shown in Figure 3-1A. We selected the lowest concentration of CaM that achieved maximal nNOS activation to use in crosslinking experiments (*red asterisk*), to minimize nonspecific CaM association with nNOS while ensuring our examination of the fully active CaM-bound nNOS. This nNOS:CaM complex is dissociated by denaturing SDS-PAGE and western blotting (Figure 3-1B, *Lane 1, M*), giving rise to a nNOS monomeric band migrating at 160 kDa without CaM. This indicates a noncovalent association between proteins, as expected from the literature. Treatment of this complex with DSBU results in the time-dependent crosslinking of CaM to nNOS. At early reaction times (*Lanes 2-3*), CaM migrates at ~175 kDa, in accordance with formation of a 1:1 stoichiometric CaM:nNOS monomeric species. As crosslinking continues, the majority of CaM is contained in a ~325 kDa species (*Lanes 4-8*) in accordance with inter-monomer crosslinking within the nNOS dimer, with each monomer bound to CaM. While the weight of this species appears low relative to the expected 354 kDa for the nNOS:CaM complex, analysis by a linear sucrose gradient showed the crosslinked dimer elutes in the same fractions as the native CaM-bound dimer (data not shown). Therefore, we denote this species as the crosslinked dimer (D).

**The active nNOS:CaM complex is the dominant species formed by DSBU crosslinking.** As seen in Figure 3-2A, denaturing SDS-PAGE and Coomassie staining of this complex results in a visible band migrating around 160 kDa, corresponding to the 160 kDa nNOS monomeric species (*Lane 1, M*). Treatment of the complex with a 50-fold molar excess of DSBU caused the time-dependent formation of a crosslinked product migrating around 325 kDa

(*Lanes 2-8, D*), consistent with the crosslinked bands observed by western blot (Fig. 3-1B). As seen in Figure 3-2B, densitometric analysis indicates formation of the crosslinked dimer (*circles*) corresponding to a loss of the monomeric species (*squares*). The sum of monomer and dimer was constant over the course of this shift, indicating that the monomer is converted stoichiometrically to the crosslinked dimer product over time. The formation of crosslinked dimer is also dependent on the concentration of DSBU, as shown in Fig. 3-2C (*Lanes 1-8*). Similarly, dimer formation appears to be stoichiometric (Fig. 3-2D).

To ensure the crosslinked product was not the result of nonspecific interactions in the nNOS:CaM complex, crosslinking was carried out in the absence of nNOS, CaM, and calcium (Figure 3-3). Crosslink of CaM alone did not give rise to crosslinked species within the molecular weight range of the nNOS monomer or dimer bands (*Lanes 1-2*). In the absence of CaM, crosslink of nNOS by DSBU formed a dimeric species at similar molecular weight to the nNOS:CaM species identified in Figures 3-1B (*Lanes 4-5*) and 3-2A (*Lanes 3-4*). In the absence of DSBU crosslinker, no nonspecific nNOS:CaM species formation was observed (*Lane 5*). The crosslinked nNOS:CaM dimer was shown to contain both nNOS and CaM (*Lanes 6-7, D*), and its formation was severely reduced in the presence of a calcium chelator EGTA (*Lane 8, D*). We therefore conclude that the crosslinked species is the active nNOS:CaM complex.

**High-resolution tandem mass spectrometric analysis of the nNOS:CaM homodimer.** We excised duplicate bands of the crosslinked nNOS:CaM dimer corresponding to the condition represented in Fig. 3-3, Lane 7 (D) for analysis by mass spectrometry. Formation of this crosslinked species has been shown to be time-, DSBU-, CaM-, and calcium-dependent (Figures 3-1 – 3-3). Sites of crosslink formation within this species were identified as described in

Methods and crosslinks bridging residues from CaM to nNOS within this sample are presented in Table 3-1. Crosslinks bridging residues within nNOS are shown in Table 3-2.

As shown in Figure 3-4, when CaM-nNOS crosslinks are mapped to a linear representation of the protein backbones (*red lines*), there is clear connectivity between calmodulin and regions of nNOS outside the known CaM-binding helix (*blue*). In addition to interactions with the CaM binding helix of nNOS, CaM formed one crosslink to the PDZ domain (*pink*), five crosslinks to the nNOS oxygenase domain (*red*), one to the FMN domain (*orange*), and two to the FAD domain (*yellow*).

Numerous crosslinks were also identified connecting domains within the nNOS (Fig. 3-4, *blue arcs*). A large degree of connectivity was observed between the PDZ domain and oxygenase domain, with 17 PDZ-oxygenase domain crosslinks detected. There was also one crosslink between PDZ and the CaM-binding helix, and one from the PDZ to FAD domain. The oxygenase domain showed the greatest level of connectivity with the CaM-binding helix and the FMN domain. Interestingly, there were also two crosslinks from the oxygenase domain to the FAD domain at the C-terminal portion of the protein. The FMN and FAD domains were connected by two crosslinks.

**Crosslinks between CaM and its binding helix on nNOS visualized using crystal structures.** Four crosslinks detected between CaM and its known binding helix were first examined, as this protein-protein interaction has previously been well characterized. Three of the four crosslinks involved nNOS residue K725, which has not previously been resolved in a crystal structure. To address this, the corresponding portion of the CaM binding helix from iNOS [PDB 3GOF] was sequence-aligned and overlaid with the crystal structure of the human CaM-bound iNOS [PDB 3HR4] as described in Methods. All crosslinks between CaM and the CaM binding

helix are shown mapped to these combined crystal structures in Figure 3-5. $C_\alpha$-$C_\alpha$ Euclidean distances for each crosslink were measured using this structure; all mapped to distances that were well within the accepted 27 Å distance restraint for the DSBU linker arm.

**PDZ domain crosslinks could not be interpreted using existing structural data.** While a crystal structure has been resolved of the truncated nNOS PDZ fold [Hillier et al., 1999], none of the crosslinks detected within the nNOS PDZ domain bridged residues present in this structure. Additionally, there are no structural data available regarding the 170-residue region connecting the PDZ fold to the nNOS oxygenase domain. Thus, we could not map crosslinks involving the PDZ domain (Table 3-2, *#1-32*) on existing structures. These crosslinks were therefore omitted from structural analysis.

**Crosslinks within the nNOS oxygenase domain interpreted using a crystal structure of the dimerized oxygenase domains.** Because the nNOS:CaM complex contains two nNOS proteins and two CaM proteins, each crosslinked residue on nNOS or CaM is present in the complex twice. In order to examine which configuration (within or across monomers in the homodimer) was the appropriate orientation of each crosslink, we started by examining crosslinks within the most well resolved dimer of the system: the nNOS oxygenase domain dimer, for where there is a high-resolution crystal structure available [Matter et al., 2005]. We arbitrarily assigned one nNOS monomer as α and the other as β for clarity. Given that the crystal structure of the nNOS oxygenase domain dimer is asymmetric, all crosslinks within this domain had four possible configurations within the structure: α-α, α-β, β-β, and β-α. The $C_\alpha$-$C_\alpha$ Euclidean distance of each possible orientation of these crosslinks is presented in Table 3-3. Values within the 27 Å $C_\alpha$-$C_\alpha$ distance cutoff for the DSBU linker arm are shown in bold within this table; all crosslinks within the oxygenase domain mapped to distances within this cutoff in at

least one configuration. Crosslinks mapped to the crystal structure in the configuration with the shortest $C_\alpha$-$C_\alpha$ distance for each monomer are presented in Figure 3-6A.

**nNOS reductase domain crosslinks interpreted using crystal structures aligned to cryo-EM density.** To examine reductase domain crosslinks we applied a similar method, using a cryo-EM based model of the nNOS:CaM homodimer. This model, generated as described in Methods, contained individual nNOS domain crystal structures docked into a low-resolution EM density map of the CaM-bound nNOS homodimer. The reductase domains from both monomers were isolated from this model crosslinks were mapped as both intra- and inter-protein within the reductase domain dimer, and results are reported in Table 3-4. Crosslinks mapped in the shortest $C_\alpha$-$C_\alpha$ configuration on this model are shown in Figure 3-6B. Two crosslinks involved residues not present in the cryo-EM based model that were resolved in the crystal structure of the full-length reductase domain in its shielded conformation [Garcin et al., 2004]. For these crosslinks (*#54-55*), distance values could only be measured in an intra-monomer configuration within the crystal structure and these are not mapped in Fig. 3-6B. Of all intra-reductase crosslinks identified, only one (*#57*) mapped to a distance above the 27 Å restraint for DSBU at 32.2 Å (Fig. 3-6B, *red bars*). This crosslinks bridges FMN and FAD domains, and is therefore affected by reductase domain conformation. In the crystal structure of the reductase in its shielded conformation this distance is shortened to 30.1 Å.

**CaM-nNOS crosslinks interpreted using the cryo-EM based structural model of the CaM-bound nNOS homodimer.** Crosslinks between CaM and the oxygenase and reductase domains of nNOS could only be visualized using the cryo-EM based model of the full-length nNOS:CaM homodimer. As with the intra-domain crosslinks discussed above, we measured the $C_\alpha$-$C_\alpha$ Euclidean distance of each possible configuration of CaM-nNOS crosslinks in this larger

structure in order to determine their appropriate configuration within or across monomers. These distances are presented in Table 3-5. Crosslinks mapped from $CaM_{\alpha}$ to nNOS at the shortest possible distance are shown in Figure 3-7. All five crosslinks from CaM to nNOS oxygenase domain were well above the 27 Å restraint regardless of configuration (Fig. 3-7, *red*). One crosslink to the FMN domain mapped to a distance that was compatible with the linker arm length of DSBU (*orange*). The two remaining crosslinks between CaM and the nNOS FAD domain are shown in *yellow*; both were above the restraint of the DSBU linker arm. Thus, all CaM-oxygenase and CaM-FAD domain crosslinks were incompatible with the existing structural model.

**nNOS-nNOS interdomain crosslinks visualized using the cryo-EM based model of the nNOS:CaM homodimer.** The remaining subset of crosslinks, which bridged different domains of nNOS, were also analyzed using the cryo-EM based holoenzyme structure. All possible $C_{\alpha}$-$C_{\alpha}$ distances for these crosslinks are presented in Table 3-6. All nNOS-nNOS crosslinks mapped to the homodimeric structure are presented in Figure 3-8, with intra-domain crosslinks included in both monomers (*blue*) and inter-domain crosslinks shown once mapped to the shortest possible distance (*red*). A large degree of connectivity between nNOS oxygenase and reductase domains is represented by entirely trans-configured crosslinks.

Five crosslinks were observed between oxygenase and reductase domains of nNOS; three of these five were between oxygenase and FMN domains, reflecting the increased interaction between oxygenase and FMN domains relative to oxygenase-FAD. The large distances spanned by all five oxygenase-reductase crosslinks on the current model of the homodimer demonstrate the oxygenase domain achieves a closer proximity to the reductase than represented by the cryo-EM model.

**Crosslink-guided intermolecular modeling of nNOS and $CaM_{\alpha}$.** To determine whether a different conformation of the nNOS:CaM would satisfy crosslinks that were not compatible with the existing nNOS:CaM cryo-EM based model, crosslink-guided intermolecular docking was performed using HADDOCK. Crystal structures of the nNOS oxygenase domain dimer, FMN domain, and CaM were isolated from the cryo-EM model (Figure 3-9A) and positioned using all crosslinks within these regions that were not compatible with the existing structure (Figure 3-9B). The resulting configuration of $CaM_{\alpha}$ and $FMN_{\alpha}$ relative to the oxygenase domain dimer is shown in Figure 3-9C. This configuration substantially shortened all nNOS-CaM and nNOS oxygenase-reductase crosslinks relative to the existing model, and satisfied all crosslinks between nNOS oxygenase and FMN domains. Only two of the crosslinks between CaM and nNOS oxygenase domains were above the distance restraint in the resulting model (*#3 & #4*), bridging 45.7 Å and 31.8 Å respectively. CaM interacted exclusively with nNOS $oxygenase_{\alpha}$ in the docking result, contacting nNOS along the proximal surface below the opening to the substrate cleft.

The FMN cofactor (*magenta*) was oriented directly adjacent to the proposed site of electron transfer suggested in the literature (Figure 3-9D, *purple*) [Tejero et al., 2010; Hanson et al., 2018]. The distance between FMN and heme iron was shortened to 21.0 Å in the docking result, compared to 69.4 Å in the cryo-EM model conformation. This is slightly above the accepted distance for electron tunneling for this transfer [Moser et al., 2008; Stuchebrukhov, 2010; Tejero et al., 2010]. This configuration is therefore vastly more favorable for electron transport than the configuration represented by cryo-EM density. It is likely that this FMN configuration represents a conformational state close to that under which electron transfer from FMN to the opposing heme occurs.

## Discussion

This study applied CXL-MS to investigate inter-domain and inter-protein interactions within the nNOS:CaM multiprotein complex in its native state. By crosslinking with the MS-cleavable reagent DSBU and carefully controlling reaction conditions, we were able to obtain a dataset of high-confidence crosslinks capturing interactions within and across domains in nNOS, along with crosslinks between nNOS and CaM. The crosslinks bridging residues within previously resolved crystal structures of the nNOS oxygenase and reductase domains were compatible with the conformations captured in those structures. Similarly, the crosslinks between CaM and its binding helix within the nNOS linker mapped nicely to crystal structures of the region.

Crosslinks between other domains of nNOS and CaM, as well as crosslinks between oxygenase and reductase domains of nNOS, were examined using a low-resolution cryo-EM based model of the homodimer, which is the only existing model of the full-length nNOS:CaM complex. These crosslinks were incompatible with the spacing between the nNOS oxygenase domains and both CaM and reductase as captured in the model. These crosslinks formed in a conformational state with CaM in close proximity with the nNOS oxygenase domain, as well as both flavin-containing reductase domains closer to the heme. Additional conformational states of all three NOS isoforms observed by negative stain- and cryo-EM are consistent with the entire reductase undergoing large conformational shifts relative to oxygenase domains [Zhou & Zhu, 2009; Feng et al., 2014; Campbell et al., 2014].

To model the conformation under which the crosslinks between nNOS oxygenase and both FMN and CaM formed, intermolecular docking was used with crosslinks guiding protein orientation. The predicted configuration of CaM and FMN domain in relation to the nNOS

oxygenase domain from this docking model (Figure 3-9D) includes very limited direct contact between the oxygenase domain and CaM. CaM localizes below the opening to the substrate cleft in the oxygenase domain, burying nNOS surface residues R299-K302, Q500, E503, Q507, Q508, and V715. A CaM-induced shielding of the R299-K302 segment was detected by HDX studies of the iNOS oxygenase domain; however, no CaM-induced shielding or deshielding in any of these residues was observed in the neuronal isoform [Smith et al., 2013; Hanson et al., 2018]. This may indicate a transient association of CaM with the nNOS oxygenase was captured by the crosslinking, or perhaps the crosslinks reflect CaM occupying a close proximity with the nNOS oxygenase without direct protein-protein contact.

The position of FMN domain and bound cofactor in the docking result is consistent with the location of electron transfer from FMN to opposing heme surrounding W587, as proposed previously in mutagenic and HDX studies [Tejero et al., 2010; Hanson et al., 2018]. The residues buried within the FMN domain interaction interface in the docking model include segment Q420-K423, which was heavily deshielded in response to CaM binding and which is the proposed lower "lip" of the heme access point for electron transfer [Hanson et al., 2018]. While we do not propose the docking configuration acquired here is the precise electron transfer configuration of the oxygenase-FMN complex, it represents a transient conformation of the nNOS with FMN vastly closer to heme (21.0 Å) than in the conformation captured by cryo-EM (69.4 Å).

The connectivity observed in these experiments between nNOS oxygenase and reductase domains is highly consistent with the proposed FMN domain configuration for electron transfer to heme, and demonstrate that additional conformations of the nNOS:CaM complex occur in solution with both flavins closer to heme than captured by current structural models. We also

showed that CaM is in close proximity to the nNOS oxygenase domain in addition to its well-documented interaction with the CaM-binding helix in the nNOS linker region. These experiments improve our understanding of the interdomain and interprotein interactions that occur within the nNOS:CaM complex in its native state, and identify potential sites of interprotein interaction to serve as targets for pharmacologic control of the enzyme. More study is needed to determine whether these sites of interprotein interaction serve a regulatory function, and whether there are isoform-specific characteristics of these sites across NOS isozymes.

## References


Arlt, C.; Götze, M.; Ihling, C. H.; Hage, C.; Schäfer, M.; Sinz, A. Integrated Workflow for Structural Proteomics Studies Based on Cross-Linking/Mass Spectrometry with an MS/MS Cleavable Cross-Linker. *Anal. Chem.* **2016**, *88* (16), 7930–7937. https://doi.org/10.1021/acs.analchem.5b04853.

Beyett, T. S.; Fraley, A. E.; Labudde, E.; Patra, D.; Coleman, R. C.; Eguchi, A.; Glukhova, A.; Chen, Q.; Williams, R. M.; Koch, W. J.; Sherman, D. H.; Tesmer, J. J. G. Perturbation of the Interactions of Calmodulin with GRK5 Using a Natural Product Chemical Probe. *Proc Natl Acad Sci U S A.* **2019**, *116* (32), 15895–15900. https://doi.org/10.1073/pnas.1818547116.

Billecke, S. S.; Draganov, D. I.; Morishima, Y.; Murphy, P. J. M.; Dunbar, A. Y.; Pratt, W. B.; Osawa, Y. The Role of Hsp90 in Heme-Dependent Activation of Apo-Neuronal Nitric-Oxide Synthase. *J Biol Chem.* **2004**, *279* (29), 30252–30258. https://doi.org/10.1074/jbc.M403864200.

Calabrese, V.; Mancuso, C.; Calvani, M.; Rizzarelli, E.; Butterfield, D. A.; Giuffrida Stella, A. M. Nitric Oxide in the Central Nervous System: Neuroprotection versus Neurotoxicity. *Nat Rev Neurosci.* **2007**, *8* (10), 766–775. https://doi.org/10.1038/nrn2214.

Campbell, M. G.; Smith, B. C.; Potter, C. S.; Carragher, B.; Marletta, M. A. Molecular Architecture of Mammalian Nitric Oxide Synthases. *Proc Natl Acad Sci U S A.* **2014**, *111* (35), E3614–E3623. https://doi.org/10.1073/pnas.1413763111.

Clapp, K. M.; Peng, H.-M.; Morishima, Y.; Lau, M.; Walker, V. J.; Pratt, W. B.; Osawa, Y. C331A Mutant of Neuronal Nitric-Oxide Synthase Is Labilized for Hsp70/CHIP (C Terminus of HSC70-Interacting Protein)-Dependent Ubiquitination. *J Biol Chem.* **2010**, *285* (44), 33642–33651. https://doi.org/10.1074/jbc.M110.159178.

Feelisch, M; Kubitzek, D; Werringloer, J.
M. Feelisch, J.S. Stamler (Eds.), Methods in Nitric Oxide Research, John Wiley & Sons, Inc., New York (**1996**), pp. 472-473

Feng, C.; Chen, L.; Li, W.; Elmore, B. O.; Fan, W.; Sun, X. Dissecting Regulation Mechanism of the FMN to Heme Interdomain Electron Transfer in Nitric Oxide Synthases. *J Inorg Biochem.* **2014**, *130*, 130–140. https://doi.org/10.1016/j.jinorgbio.2013.09.005.

Garcin, E. D.; Bruns, C. M.; Lloyd, S. J.; Hosfield, D. J.; Tiso, M.; Gachhui, R.; Stuehr, D. J.; Tainer, J. A.; Getzoff, E. D. Structural Basis for Isozyme-Specific Regulation of Electron Transfer in Nitric-Oxide Synthase. *J Biol Chem.* **2004**, *279* (36), 37918–37927. https://doi.org/10.1074/jbc.M406204200.

Gong, Z.; Ding, Y.-H.; Dong, X.; Liu, N.; Zhang, E. E.; Dong, M.-Q.; Tang, C. Visualizing the Ensemble Structures of Protein Complexes Using Chemical Cross-Linking Coupled with Mass Spectrometry. *Biophys Rep.* **2015**, *1* (3), 127–138. https://doi.org/10.1007/s41048-015-0015-y.

Götze, M.; Pettelkau, J.; Fritzsche, R.; Ihling, C. H.; Schäfer, M.; Sinz, A. Automated Assignment of MS/MS Cleavable Cross-Links in Protein 3D-Structure Analysis. *J. Am. Soc. Mass Spectrom.* **2015**, *26* (1), 83–97. https://doi.org/10.1007/s13361-014-1001-1.

Guan, Z.-W.; Iyanagi, T. Electron Transfer Is Activated by Calmodulin in the Flavin Domain of Human Neuronal Nitric Oxide Synthase. *Arch Biochem Biophys.* **2003**, *412* (1), 65–76. https://doi.org/10.1016/S0003-9861(03)00009-2.

Hanson, Q. M.; Carley, J. R.; Gilbreath, T. J.; Smith, B. C.; Underbakke, E. S. Calmodulin-Induced Conformational Control and Allostery Underlying Neuronal Nitric Oxide Synthase Activation. *J Mol Biol.* **2018**, *430* (7), 935–947. https://doi.org/10.1016/j.jmb.2018.02.003.

Hillier, B. J.; Christopherson, K. S.; Prehoda, K. E.; Bredt, D. S.; Lim, W. A. Unexpected Modes of PDZ Domain Scaffolding Revealed by Structure of NNOS-Syntrophin Complex. *Science.* **1999**, *284* (5415), 812–815. https://doi.org/10.1126/science.284.5415.812.

Iacobucci, C.; Götze, M.; Ihling, C. H.; Piotrowski, C.; Arlt, C.; Schäfer, M.; Hage, C.; Schmidt, R.; Sinz, A. A Cross-Linking/Mass Spectrometry Workflow Based on MS-Cleavable Cross-Linkers and the MeroX Software for Studying Protein Structures and Protein–Protein Interactions. *Nat Protoc.* **2018**, *13* (12), 2864–2889. https://doi.org/10.1038/s41596-018-0068-8.

Iacobucci, C.; Piotrowski, C.; Aebersold, R.; Amaral, B. C.; Andrews, P.; Bernfur, K.; Borchers, C.; Brodie, N. I.; Bruce, J. E.; Cao, Y.; Chaignepain, S.; Chavez, J. D.; Claverol, S.; Cox, J.; Davis, T.; Degliesposti, G.; Dong, M.-Q.; Edinger, N.; Emanuelsson, C.; Gay, M.; Götze, M.; Gomes-Neto, F.; Gozzo, F. C.; Gutierrez, C.; Haupt, C.; Heck, A. J. R.; Herzog, F.; Huang, L.; Hoopmann, M. R.; Kalisman, N.; Klykov, O.; Kukačka, Z.; Liu, F.; MacCoss, M. J.; Mechtler, K.; Mesika, R.; Moritz, R. L.; Nagaraj, N.; Nesati, V.; Neves-Ferreira, A. G. C.; Ninnis, R.; Novák, P.; O'Reilly, F. J.; Pelzing, M.; Petrotchenko, E.; Piersimoni, L.; Plasencia, M.; Pukala, T.; Rand, K. D.; Rappsilber, J.; Reichmann, D.; Sailer, C.; Sarnowski, C. P.; Scheltema, R. A.; Schmidt, C.; Schriemer, D. C.; Shi, Y.; Skehel, J. M.; Slavin, M.; Sobott, F.; Solis-Mezarino, V.; Stephanowitz, H.; Stengel, F.; Stieger, C. E.; Trabjerg, E.; Trnka, M.; Vilaseca, M.; Viner, R.; Xiang, Y.; Yilmaz, S.; Zelter, A.; Ziemianowicz, D.; Leitner, A.; Sinz, A. First Community-Wide, Comparative Cross-Linking Mass Spectrometry Study. *Anal. Chem.* **2019**, *91* (11), 6953–6961. https://doi.org/10.1021/acs.analchem.9b00658.

Iacobucci, C.; Sinz, A. To Be or Not to Be? Five Guidelines to Avoid Misassignments in Cross-Linking/Mass Spectrometry. *Anal. Chem.* **2017**, *89* (15), 7832–7835. https://doi.org/10.1021/acs.analchem.7b02316.

Matsuda, H.; Iyanagi, T. Calmodulin Activates Intramolecular Electron Transfer between the Two £avins of Neuronal Nitric Oxide Synthase Flavin Domain. *Biochim Biophys Acta.* **1999**, *1473* (2–3), 345–355. https://doi.org/10.1016/s0304-4165(99)00193-2.

Matter, H.; Kumar, H. S. A.; Fedorov, R.; Frey, A.; Kotsonis, P.; Hartmann, E.; Fröhlich, L. G.; Reif, A.; Pfleiderer, W.; Scheurer, P.; Ghosh, D. K.; Schlichting, I.; Schmidt, H. H. H. W. Structural Analysis of Isoform-Specific Inhibitors Targeting the Tetrahydrobiopterin Binding

Site of Human Nitric Oxide Synthases. *J. Med. Chem.* **2005**, *48* (15), 4783–4792. https://doi.org/10.1021/jm050007x.

Meffert, M. K.; Haley, J. E.; Schuman, E. M.; Schulman, H.; Madison, D. V. Inhibition of Hippocampal Heme Oxygenase, Nitric Oxide Synthase, and Long-Term Potentiation by Metalloporphyrins. *Neuron* **1994**, *13* (5), 1225–1233. https://doi.org/10.1016/0896-6273(94)90060-4.

Moncada, S.; Higgs, E. A. The Discovery of Nitric Oxide and Its Role in Vascular Biology. *Br J Pharmacol.* **2006**, *147* (S1), S193–S201. https://doi.org/10.1038/sj.bjp.0706458.

Moser, C. C.; Chobot, S. E.; Page, C. C.; Dutton, P. L. Distance Metrics for Heme Protein Electron Tunneling. *Biochim Biophys Acta.* **2008**, *1777* (7–8), 1032–1037. https://doi.org/10.1016/j.bbabio.2008.04.021.

Panda, K.; Ghosh, S.; Stuehr, D. J. Calmodulin Activates Intersubunit Electron Transfer in the Neuronal Nitric-Oxide Synthase Dimer. *J Biol Chem.* **2001**, *276* (26), 23349–23356. https://doi.org/10.1074/jbc.M100687200.

Panda, S. P.; Polusani, S. R.; Kellogg, D. L.; Venkatakrishnan, P.; Roman, M. G.; Demeler, B.; Masters, B. S. S.; Roman, L. J. Intra- and Inter-Molecular Effects of a Conserved Arginine Residue of Neuronal and Inducible Nitric Oxide Synthases on FMN and Calmodulin Binding. *Arch Biochem Biophys.* **2013**, *533* (1–2), 88–94. https://doi.org/10.1016/j.abb.2013.03.004.

Pettersen, E. F.; Goddard, T. D.; Huang, C. C.; Couch, G. S.; Greenblatt, D. M.; Meng, E. C.; Ferrin, T. E. UCSF Chimera—A Visualization System for Exploratory Research and Analysis. *J Comput Chem.* **2004**, *25* (13), 1605–1612. https://doi.org/10.1002/jcc.20084.

Piersimoni, L.; Sinz, A. Cross-Linking/Mass Spectrometry at the Crossroads. *Anal Bioanal Chem* **2020**, *412* (24), 5981–5987. https://doi.org/10.1007/s00216-020-02700-x.

Schmidt, H. H. H. W.; Walter, U. NO at Work. *Cell* **1994**, *78* (6), 919–925. https://doi.org/10.1016/0092-8674(94)90267-4.

Smith, B. C.; Underbakke, E. S.; Kulp, D. W.; Schief, W. R.; Marletta, M. A. Nitric Oxide Synthase Domain Interfaces Regulate Electron Transfer and Calmodulin Activation. *Proc Natl Acad Sci U S A.* **2013**, *110* (38), E3577–E3586. https://doi.org/10.1073/pnas.1313331110.

Stuchebrukhov, A. A. Long-Distance Electron Tunneling in Proteins: A New Challenge for Time-Resolved Spectroscopy. *Laser Phys.* **2010**, *20* (1), 125–138. https://doi.org/10.1134/S1054660X09170186.

Tejero, J.; Hannibal, L.; Mustovich, A.; Stuehr, D. J. Surface Charges and Regulation of FMN to Heme Electron Transfer in Nitric-Oxide Synthase. *J Biol Chem.* **2010**, *285* (35), 27232–27240. https://doi.org/10.1074/jbc.M110.138842.

van Zundert, G. C. P.; Melquiond, A. S. J.; Bonvin, A. M. J. J. Integrative Modeling of Biomolecular Complexes: HADDOCKing with Cryo-Electron Microscopy Data. *Structure* **2015**, *23* (5), 949–960. https://doi.org/10.1016/j.str.2015.03.014.

Xia, C.; Misra, I.; Iyanagi, T.; Kim, J.-J. P. Regulation of Interdomain Interactions by Calmodulin in Inducible Nitric-Oxide Synthase. *J Biol Chem.* **2009**, *284* (44), 30708–30717. https://doi.org/10.1074/jbc.M109.031682.

Yokom, A. L.; Morishima, Y.; Lau, M.; Su, M.; Glukhova, A.; Osawa, Y.; Southworth, D. R. Architecture of the Nitric-Oxide Synthase Holoenzyme Reveals Large Conformational Changes and a Calmodulin-Driven Release of the FMN Domain. *J Biol Chem.* **2014**, *289* (24), 16855–16865. https://doi.org/10.1074/jbc.M114.564005.

Zhang, L.; Dawson, V. L.; Dawson, T. M. Role of Nitric Oxide in Parkinson's Disease. *Pharmacol Ther.* **2006**, *109* (1–2), 33–41. https://doi.org/10.1016/j.pharmthera.2005.05.007.

Zhou, L.; Zhu, D.-Y. Neuronal Nitric Oxide Synthase: Structure, Subcellular Localization, Regulation, and Clinical Implications. *Nitric Oxide* **2009**, *20* (4), 223–230. https://doi.org/10.1016/j.niox.2009.03.001.

Ziche, M.; Morbidelli, L. Nitric Oxide and Angiogenesis. *J Neurooncol.* **2000**, *50* (1–2), 139–148. https://doi.org/10.1023/a:1006431309841.

## Acknowledgements

This work was supported by National Institutes of Health grants ES007062, GM077430, GM007767, NS055746, and ES030791 as well as from the University of Michigan Medical School's Protein Folding Disease Initiative.

The University of Michigan Proteomics Resource Facility was used to trypsinize samples and analyze by mass spectrometry.

The FP7 WeNMR (project# 261572), H2020 West-Life (project# 675858), the EOSC-hub (project# 777536) and the EGI-ACE (project# 101017567) European e-Infrastructure projects are acknowledged for the use of their web portals, which make use of the EGI infrastructure with the dedicated support of CESNET-MCC, INFN-PADOVA-STACK, INFN-LNL-2, NCG-INGRID-PT, TW-NCHC, CESGA, IFCA-LCG2, UA-BITP, SURFsara and NIKHEF, and the additional support of the national GRID Initiatives of Belgium, France, Italy, Germany, the Netherlands, Poland, Portugal, Spain, UK, Taiwan and the US Open Science Grid.

## Tables

***Table 3-1.*** *Crosslinks identified between CaM and nNOS following treatment with DSBU.*

| CaM Residue | nNOS Residue | Peptide 1 | Peptide 2 | m/z |
|---|---|---|---|---|
| K22 | K725 | EAFSLFD**K**DGDGTITTK | GTNGTPT**K**R | 743.869 |
| T30 | K733 | EAFSLFDKDGDGTIT**T**K | **K**LAEAVK | 700.371 |
| T35 | K613 | DGDGTITTKELG**T**VMR | **K**MDLDMR | 943.779 |
| K95 | Y604 | EAFRVFD**K**DGNGYISAAELR | **Y**NILEEVAK | 883.697 |
| K95 | K771 | VFD**K**DGDGYISAAELR | SQAYA**K**TLCEIFK | 878.193 |
| K95 | S1077 | VFD**K**DGDGYISAAELR | NTALGVI**S**NWKDESR | 910.712 |
| Y100 | K1080 | VFDKDGDG**Y**ISAAELR | NTALGVISNW**K**DESR | 911.207 |
| T111 | K302 | HVM**T**NLGEKLTDEEVDEMIR | FL**K**VK | 797.916 |
| T111 | K469 | HVM**T**NLGEKLTDEEVDEMIR | TDG**K**HDFR | 706.943 |
| K116 | K469 | HVMTNLGE**K**LTDEEVDEMIR | TDG**K**HDFR | 883.176 |
| K116 | K725 | HVMTNLGE**K**LTDEEVDEMIR | GTNGTPT**K**R | 872.68 |
| T118 | K38 | L**T**DEEVDEMIR | ERVS**K**PPVIISDLIR | 1089.578 |
| T118 | K725 | HVMTDLGEKL**T**DEEVDEMIR | GTNGTPT**K**R | 872.68 |

***Table 3-2.*** *Crosslinks identified within nNOS following DSBU treatment.*

| # | Residue 1 | Residue 2 | Peptide 1 | Peptide 2 | m/z |
|---|---|---|---|---|---|
| 1 | *M1 | K38 | *MEENTFGVQQIQPNVISVR | VS**K**PPVIISDLIR | 956.023 |
| 2 | K24 | K229 | **K**VGGLGFLVK | AEM**K**DTGIQVDR | 644.606 |
| 3 | K24 | K242 | **K**VGGLGFLVK | DLDG**K**SHK | 528.803 |
| 4 | K24 | S368 | **K**VGGLGFLVK | EFLDQYYS**S**IKR | 691.381 |
| 5 | K33 | S140 | VGGLGFLV**K**ER | AVDLSHQP**S**ASKDQSLAVDR | 699.577 |
| 6 | K33 | K188 | VGGLGFLV**K**ER | ST**K**ANLQDIGEHDELLK | 657.159 |
| 7 | K33 | K225 | VGGLGFLV**K**ER | GGPA**K**AEMK | 565.316 |
| 8 | K33 | S243 | VGGLGFLV**K**ER | **S**HKAPPLGGDNDR | 684.118 |
| 9 | K33 | K302 | VGGLGFLV**K**ER | FL**K**VK | 501.808 |
| 10 | K33 | K452 | VGGLGFLV**K**ER | YATN**K**GNLR | 602.339 |
| 11 | K33 | K732 | VGGLGFLV**K**ER | AIGF**K**K | 509.055 |
| 12 | S215 | K229 | EIEPVLSILNSG**S**KATNR | AEM**K**DTGIQVDR | 872.208 |
| 13 | K225 | K302 | GGPA**K**AEMK | FL**K**VK | 430.249 |
| 14 | K225 | K469 | GGPA**K**AEMK | TDG**K**HDFR | 515.509 |
| 15 | K229 | S243 | AEM**K**DTGIQVDR | **S**HKAPPLGGDNDR | 585.091 |
| 16 | K229 | K406 | AEM**K**DTGIQVDR | DTELIYGA**K**HAWR | 780.144 |
| 17 | K229 | K1320 | AEM**K**DTGIQVDR | EPDRP**K**K | 607.565 |
| 18 | K242 | S367 | DLDG**K**SHK | EFLDQYY**S**SIKR | 661.586 |
| 19 | S243 | K245 | **S**HKAPPLGGDNDR | DLDGKSH**K**APPLGGDNDR | 690.942 |
| 20 | K245 | K245 | SH**K**APPLGGDNDR | SH**K**APPLGGDNDR | 731.364 |
| 21 | K245 | K302 | SH**K**APPLGGDNDR | FL**K**VK | 439.443 |
| 22 | K245 | K344 | SH**K**APPLGGDNDR | **K**PEDVR | 576.294 |
| 23 | K245 | K370 | SH**K**APPLGGDNDR | EFLDQYYSSI**K**R | 622.511 |
| 24 | K245 | K620 | SH**K**APPLGGDNDR | **K**TSSLWK | 602.817 |
| 25 | S280 | K302 | EQ**S**PTSGK | FL**K**VK | 416.484 |
| 26 | T282 | K302 | EQSP**T**SGK | FL**K**VK | 554.976 |
| 27 | K285 | T289 | EQSPTSG**K**QSPTK | EQSPTSGKQSP**T**K | 736.870 |
| 28 | S287 | K302 | EQSPTSGKQ**S**PTK | FL**K**VK | 735.406 |
| 29 | T289 | K302 | EQSPTSGKQSP**T**K | FL**K**VK | 441.647 |
| 30 | T289 | K370 | EQSPTSGKQSP**T**K | EFLDQYYSSI**K**R | 780.393 |
| 31 | K290 | K302 | QSPT**K**NGSPSR | FL**K**VK | 497.781 |
| 32 | S295 | K302 | NGSP**S**R | FL**K**VK | 483.270 |
| 33 | K302 | K344 | FL**K**VK | **K**PEDVR | 393.986 |
| 34 | K302 | T724 | FL**K**VK | GTNGTP**T**KR | 588.003 |
| 35 | K302 | K725 | FL**K**VK | GTNGTPT**K**R | 441.253 |
| 36 | K302 | K733 | FL**K**VK | **K**LAEAVK | 530.002 |
| 37 | K302 | K932 | FL**K**VK | TWA**K**K | 488.300 |
| 38 | K344 | K469 | **K**PEDVR | TDG**K**HDFR | 479.244 |
| 39 | K351 | Y394 | T**K**DQLFPLAK | LEEVNKEIESTST**Y**QLK | 842.701 |
| 40 | K351 | K469 | T**K**DQLFPLAK | TDG**K**HDFR | 467.050 |
| 41 | K370 | K406 | EFLDQYYSSI**K**R | DTELIYGA**K**HAWR | 826.670 |
| 42 | K406 | K842 | DTELIYGA**K**HAWR | SY**K**VR | 602.573 |
| 43 | K406 | S1410 | DTELIYGA**K**HAWR | LR**S**ESIAFIEESK | 816.675 |
| 44 | K452 | K842 | YATN**K**GNLR | SY**K**VR | 471.759 |
| 45 | K452 | K1302 | YATN**K**GNLR | N**K**GVFR | 488.770 |
| 46 | K469 | K725 | TDG**K**HDFR | GTNGTPT**K**R | 701.682 |
| 47 | K550 | K620 | HP**K**FDWFK | **K**TSSLWK | 538.037 |
| 48 | K555 | K613 | FDWF**K**DLGLK | **K**MDLDMR | 593.802 |
| 49 | K612 | K620 | YNILEEVA**K**K | **K**TSSLWK | 563.565 |
| 50 | K620 | K660 | **K**TSSLWK | VTIVDHHSATESFI**K**HMENEYR | 738.373 |
| 51 | T724 | K732 | GTNGTP**T**KR | AIGF**K**K | 597.667 |
| 52 | K725 | K733 | GTNGTPT**K**R | **K**LAEAVK | 629.352 |
| 53 | K778 | K932 | TLCEIF**K**HAFDAK | TWA**K**K | 602.818 |
| 54 | S833 | K856 | HPN**S**VQEER | **K**SSGDGPDLR | 581.284 |
| 55 | K842 | S857 | SY**K**VR | **S**SGDGPDLR | 584.299 |
| 56 | K856 | K1320 | **K**SSGDGPDLR | EPDRP**K**K | 524.775 |
| 57 | K932 | S1083 | TWA**K**K | NTALGVISNWKDE**S**R | 840.112 |
| 58 | K932 | Y1135 | TWA**K**K | LLVLSKGLQE**Y**EEWK | 666.869 |
| 59 | K989 | S1077 | LTYVAEAPDLTQGLSNVH**K**K | NTALGVI**S**NWKDESR | 814.830 |
| 60 | K989 | S1083 | LTYVAEAPDLTQGLSNVH**K**K | NTALGVISNWKDE**S**R | 814.629 |
| 61 | Y1292 | K1321 | IDHI**Y**REETLQAK | **K**YVQDVLQEQLAESVYR | 1293.658 |

**Crosslink formed to N-terminal amine of residue M1.*

***Table 3-3.*** *$C_\alpha$-$C_\alpha$ Euclidean distances of crosslinks detected within the nNOS oxygenase domain mapped in each possible configuration to the crystal structure of the nNOS oxygenase domain homodimer.*

| | ***Crosslink Identity*** | | ***Crosslink Configuration*** | | | |
|---|---|---|---|---|---|---|
| | | | **α-α** | **α-β** | **β-β** | **β-α** |
| **#** | **Residue 1** | **Residue 2** | **Cα-Cα Distance (Å)** | | | |
| 33 | K302 | K344 | 35.1 | **19.8** | 33.7 | **18.2** |
| 38 | K344 | K469 | **16.8** | 60.5 | **17.4** | 58.9 |
| 39 | K351 | Y394 | **10.0** | 62.5 | **10.5** | 62.2 |
| 40 | K351 | K469 | **16.0** | 67.1 | **17.9** | 65.5 |
| 41 | K370 | K406 | **17.6** | 60.1 | **17.4** | 60.0 |
| 47 | K550 | K620 | **25.7** | **16.2** | **25.6** | **16.2** |
| 48 | K555 | K613 | **11.5** | 28.4 | **11.7** | 28.5 |
| 49 | K612 | K620 | **13.8** | 28.0 | **13.4** | 28.1 |
| 50 | K620 | K660 | 40.8 | **19.4** | 40.6 | **19.4** |

Crosslinks that satisfied the DSBU distance restraint are shown in **bold**.

***Table 3-4.*** *$C_\alpha$-$C_\alpha$ Euclidean distances of crosslinks detected within the nNOS reductase domain mapped in each possible configuration to the cryo-EM based model of the reductase domain homodimer.*

| | ***Crosslink Identity*** | | ***Crosslink Configuration*** | | | |
|---|---|---|---|---|---|---|
| | | | **α-α** | **α-β** | **β-β** | **β-α** |
| **#** | **Residue 1** | **Residue 2** | **Cα-Cα Distance (Å)** | | | |
| 53 | K778 | K932 | **13.3** | 57.1 | **13.3** | 57.1 |
| 54 | S833 | K856 | ***19.3** | NS | ***19.3** | NS |
| 55 | K842 | S857 | ***25.6** | NS | ***25.6** | NS |
| 56 | K856 | K1320 | NS | NS | NS | NS |
| 57 | K932 | S1083 | 32.2 | 44.7 | 32.2 | 44.7 |
| 58 | K932 | Y1135 | **12** | 66.6 | **12** | 66.6 |
| 59 | K989 | S1077 | 28.1 | **16.2** | 28.1 | **16.2** |
| 60 | K989 | S1083 | **12** | **25.5** | **12** | **25.5** |
| 61 | Y1292 | K1321 | **19.3** | 111.4 | **19.3** | 111.4 |

Crosslinks that satisfied the DSBU distance restraint are shown in **bold**.
*Structural information only available in crystal structure 1TLL, not resolved in cryo-EM based reductase dimer.
NS = No structural information available for one or both residues.

***Table 3-5**. $C_\alpha$-$C_\alpha$ Euclidean distances of CaM-nNOS crosslinks mapped in each possible configuration to the cryo-EM based model of the nNOS:CaM homodimer.*

| | ***Crosslink Identity*** | | | | ***CaM-nNOS Crosslink Configuration*** | | | |
|---|---|---|---|---|---|---|---|---|
| | | | | | **Cα-Nα** | **Cα-Nβ** | **Cβ-Nβ** | **Cβ-Nα** |
| **#** | **CaM Residue** | **CaM Lobe** | **nNOS Residue** | **nNOS Domain** | **Cα-Cα Distance (Å)** | | | |
| 1 | K22 | N-Lobe | K725 | CaM Helix | **14.7** | 34.0 | **14.7** | 34.0 |
| 2 | T30 | N-Lobe | K733 | CaM Helix | **21.3** | 45.6 | **21.3** | 45.6 |
| 3 | T35 | N-Lobe | K613 | Oxygenase | 100.1 | 97.9 | 100.2 | 97.5 |
| 4 | K95 | C-Lobe | Y604 | Oxygenase | 72.9 | 67.7 | 73.1 | 67.2 |
| 5 | K95 | C-Lobe | K771 | FMN | **16.1** | 38.7 | **16.1** | 38.7 |
| 6 | K95 | C-Lobe | S1077 | FAD | 34.0 | 33.7 | 34.0 | 33.7 |
| 7 | Y100 | C-Lobe | K1080 | FAD | 46.2 | 47.1 | 46.2 | 47.1 |
| 8 | T111 | C-Lobe | K302 | Oxygenase | 53.2 | 54.5 | 52.5 | 55.3 |
| 9 | T111 | C-Lobe | K469 | Oxygenase | 56.4 | 61.2 | 58.0 | 59.7 |
| 10 | K116 | C-Lobe | K469 | Oxygenase | 54.9 | 63.7 | 56.5 | 62.2 |
| 11 | K116 | C-Lobe | K725 | CaM Helix | **11.8** | **23.0** | **11.8** | **23.0** |
| 12 | T118 | C-Lobe | K38 | PDZ | NS | NS | NS | NS |
| 13 | T118 | C-Lobe | K725 | CaM Helix | **13.4** | **25.3** | **13.4** | **25.3** |

Crosslink configurations mapped in Figure 5 have underlined distance values above.
Crosslinks that satisfied the DSBU distance restraint are shown in **bold**.
NS = No structural information available for one or both residues.

***Table 3-6.*** *$C_\alpha$-$C_\alpha$ Euclidean distances of nNOS-nNOS crosslinks mapped in each possible configuration to the cryo-EM derived model of the nNOS:CaM homodimer.*

| | ***Crosslink Identity*** | | ***Crosslink Configuration*** | | | |
|---|---|---|---|---|---|---|
| | | | **α-α** | **α-β** | **β-β** | **β-α** |
| **#** | **Residue 1** | **Residue 2** | **Cα-Cα Distance (Å)** | | | |
| 34 | K302 | T724 | NS | NS | NS | NS |
| 35 | K302 | K725 | 61.9 | 58.1 | 61.4 | 59.1 |
| 36 | K302 | K733 | 46.1 | 49.6 | 45.6 | 50.5 |
| 37 | K302 | K932 | 61.2 | 74.3 | 60.4 | 73.8 |
| 42 | K406 | K842 | 83.4 | 73.1 | 82.7 | 72.4 |
| 43 | K406 | S1410 | 88.8 | 85.8 | 88.1 | 85.0 |
| 44 | K452 | K842 | 104.2 | 85.7 | 103.3 | 85.6 |
| 45 | K452 | K1302 | 153.8 | 132.0 | 153.0 | 131.6 |
| 46 | K469 | K725 | 52.5 | 72.7 | 54.1 | 74.2 |
| 47 | K550 | K620 | **25.7** | **16.2** | **25.6** | **16.2** |
| 48 | K555 | K613 | **11.5** | 28.4 | **11.7** | 28.5 |
| 49 | K612 | K620 | **13.8** | 28.0 | **13.4** | 28.1 |
| 50 | K620 | K660 | 40.8 | **19.4** | 40.6 | **19.4** |
| 51 | T724 | K732 | NS | NS | NS | NS |
| 52 | K725 | K733 | **18.6** | 35.5 | **18.6** | 35.5 |

Crosslinks that satisfied the DSBU distance restraint are shown in **bold**.
NS = No structural information available for one or both residues.

## Figures

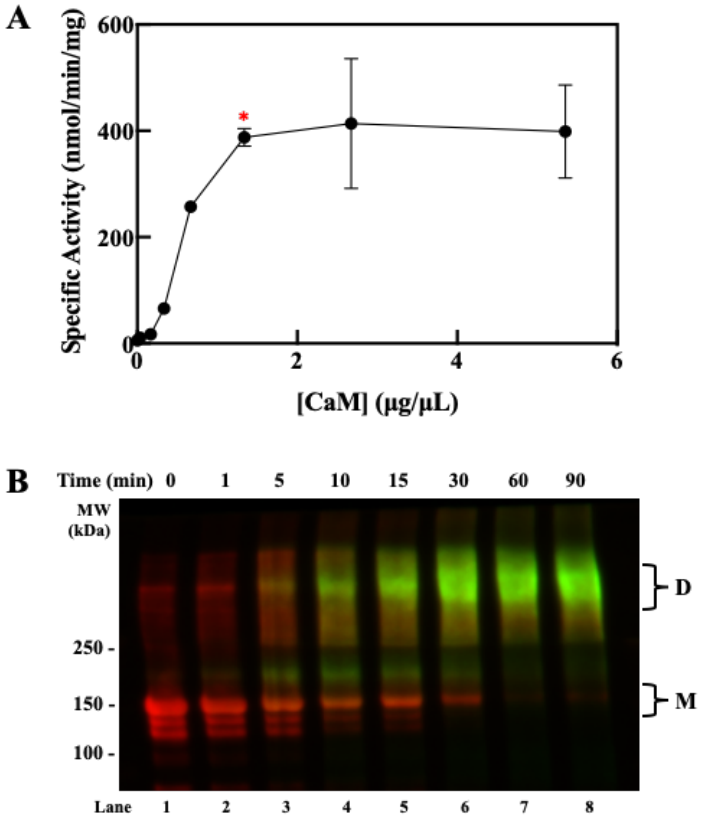


***Figure 3-1.*** *Calmodulin activates and crosslinks to nNOS.*

**(A)**, nNOS (2 µM) was incubated for 5 minutes at 4°C with increasing concentrations of CaM in the presence of $CaCl_2$ (10 µM) and $BH_4$ (10 µM). Aliquots (1.28 µg) of the nNOS:CaM mixtures were removed and nNOS activity was measured as described in Methods. Red asterisk indicates the condition selected for maximal nNOS:CaM assembly without excess CaM. Mean ± SD for n=3 replicates is presented. **(B)**, nNOS (2 µM) was mixed for 5 minutes at 4°C as described in (A) with 1.34 µg/µL CaM (red asterisk, panel A), then treated with 0.1 mM DSBU at room temperature for the described time. Samples were quenched using ammonium bicarbonate and aliquots were examined by SDS-PAGE. The presence of nNOS (red) and CaM (green) were determined by protein-specific western blot. D, crosslinked dimeric nNOS:CaM; M, monomer of nNOS.

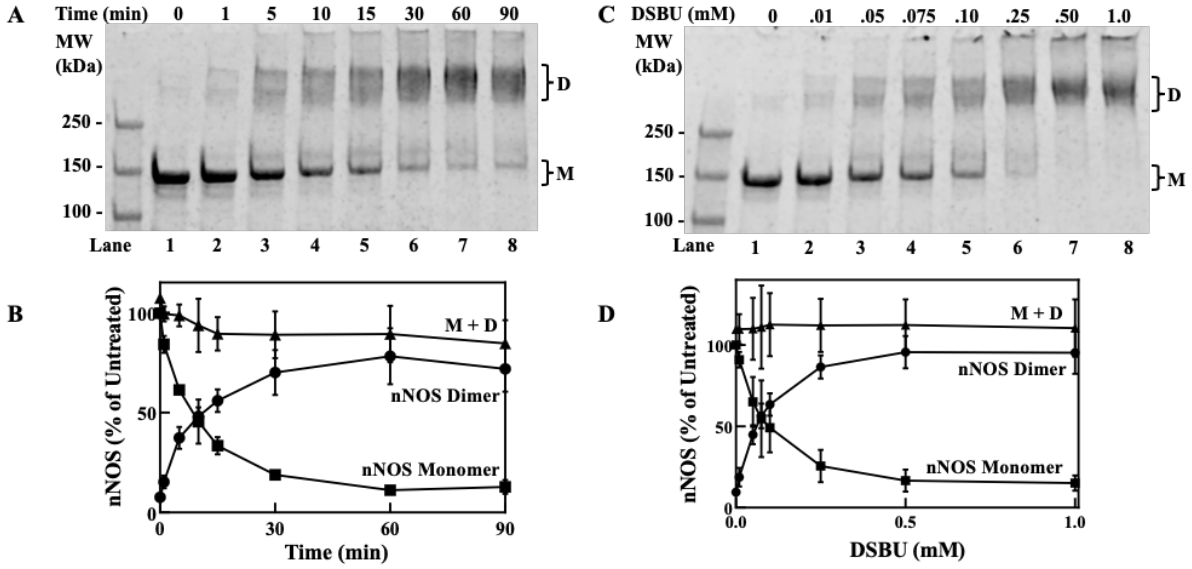


***Figure 3-2.*** *Formation of crosslinked nNOS:CaM dimer after treatment with DSBU.*

**(A)**, Time-dependent formation of crosslinked nNOS:CaM dimeric species after treatment with DSBU. Dimeric nNOS (2 µM) was preincubated for 5 minutes at 4°C with CaM (1.34 µg/µl) in the presence of $CaCl_2$ (10 µM) and BH4 (10 µM) before treatment with 0.1 mM DSBU for the indicated duration. Aliquots (3 µg) of the reaction mixtures were submitted to SDS-PAGE and stained with Coomassie Blue as described in Methods. D, crosslinked nNOS:CaM dimer; M, monomer of nNOS. **(B)**, Quantification of bands seen in A. Bands corresponding to the crosslinked dimer (closed circles) and monomer (closed squares) were quantified by densitometric analysis. The sum of the dimer and monomer was also calculated (closed triangle). Mean ± SD derived from three independent reaction mixtures (n=3). **(C)**, Formation of the crosslinked nNOS:CaM dimer is dependent on the concentration of DSBU. nNOS (2 µM) was preincubated as in (A), treated with the indicated concentrations of DSBU for 10 min, and the reaction mixtures were analyzed as in (A). **(D)**, Quantification of bands seen in (C). The amount of dimeric nNOS:CaM (closed circles), monomeric nNOS (closed squares), and the sum total (closed triangles) was quantified as in B. Mean ± SD (n=3). Densities determined for all bands are within the linear range of detection.

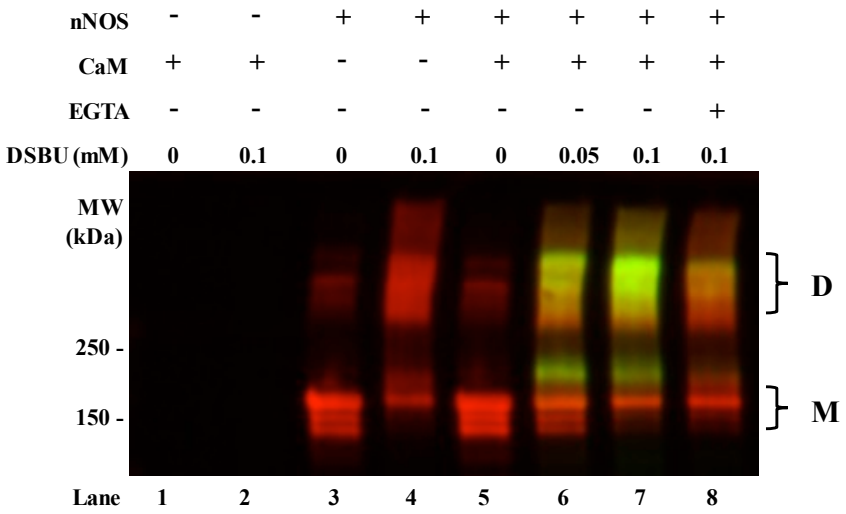


***Figure 3-3.*** *Formation of crosslinked nNOS:CaM dimer is CaM- and calcium-dependent.*

nNOS (2 μM) was preincubated as described in Figure 3-2 in the presence or absence of 1.34 μg/μl CaM and 50 μM EGTA. Samples were then treated for 10 minutes with indicated concentrations of DSBU, quenched using ammonium bicarbonate, and aliquots were examined by SDS-PAGE. The presence of nNOS (red) and CaM (green) were determined by protein-specific western blot as described in Methods. D, crosslinked dimeric nNOS:CaM; M, monomer of nNOS.

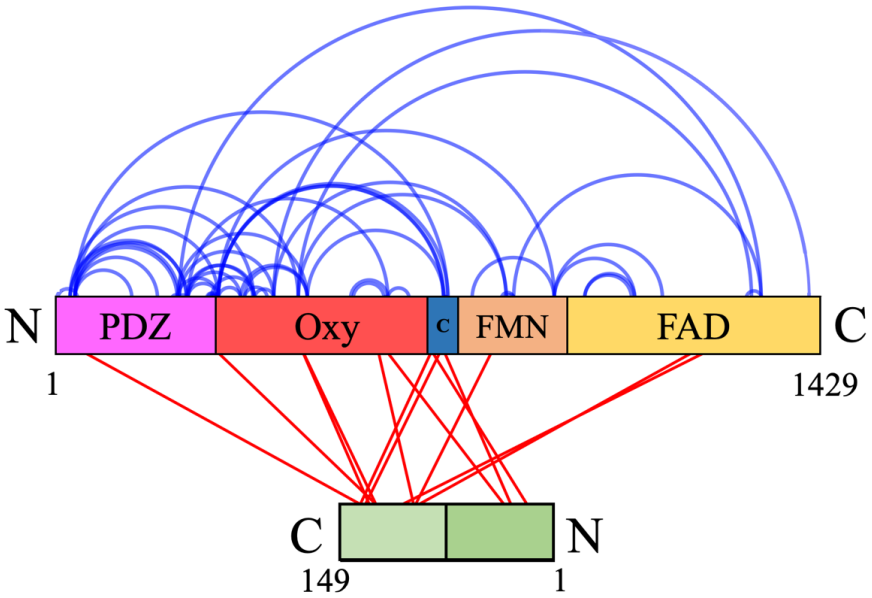


***Figure 3-4.*** *Crosslinks identified in the nNOS:CaM complex are shown in relation to the sequence of each protein.*

Crosslinks that bridged two residues within the nNOS protein are displayed as blue arcs, and crosslinks between residues on both nNOS and CaM are shown in red. Domains are indicated along the nNOS backbone. CaM is colored light and medium green corresponding to its C- and N-lobes.

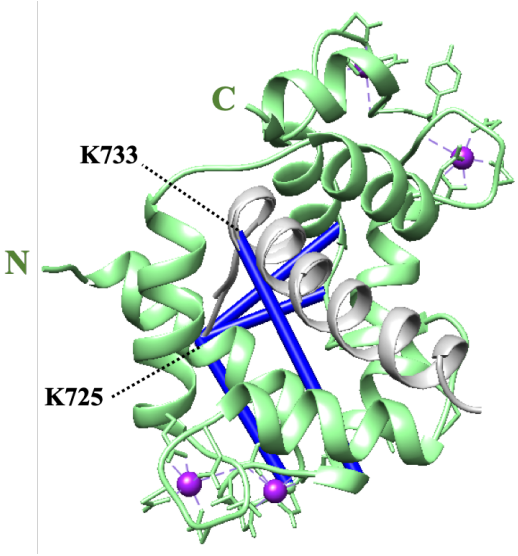


***Figure 3-5.*** *CaM-nNOS crosslinks mapped to crystal structures of CaM bound to the nNOS CaM-binding helix.*

Crosslinks between calmodulin and its binding helix on nNOS mapped to overlaid existing crystal structures of the region [3HR4, 3GOF] renumbered corresponding to nNOS sequence as described in Methods. CaM in shown in green, nNOS in grey, calcium in purple, and crosslinks as blue bars. nNOS residues involved in crosslinks are indicated.

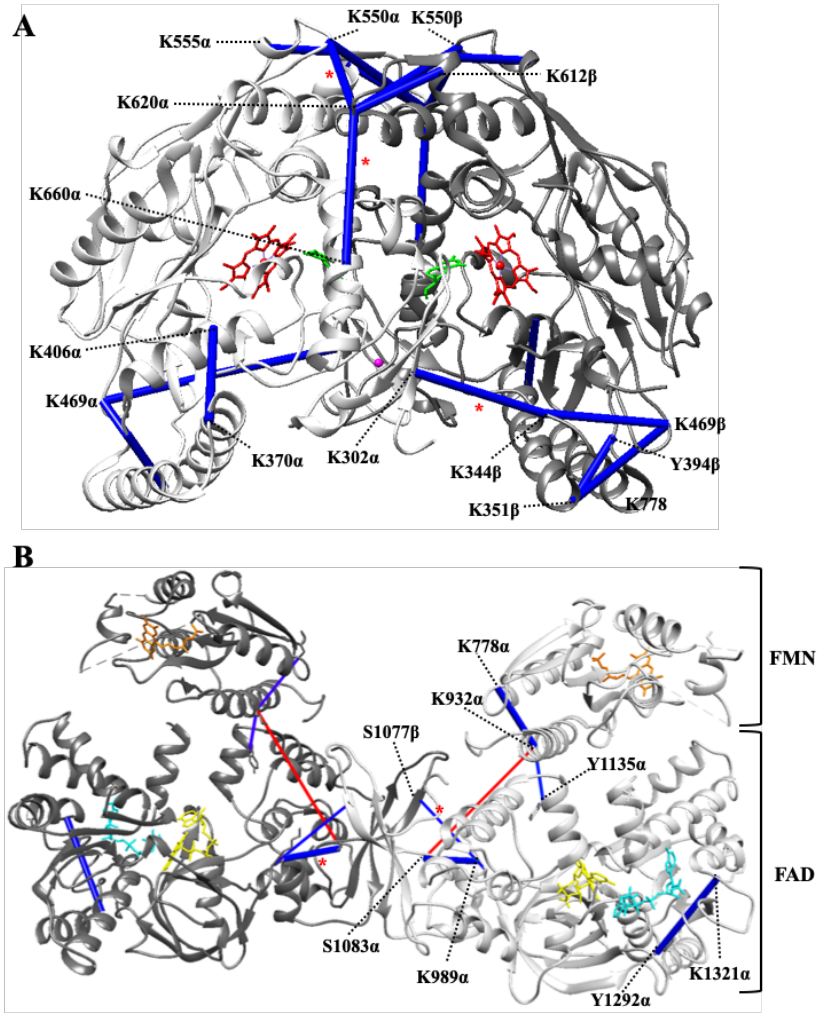


***Figure 3-6.*** *nNOS-nNOS crosslinks mapped to structures of the nNOS oxygenase and reductase domain dimers.*

**(A)**, Crosslinks bridging residues within the nNOS oxygenase domain are mapped to the crystal structure of the oxygenase domain dimer [PDB 1ZVL]. nNOS monomers arbitrarily assigned as α and β are colored in light and dark grey respectively. Prosthetic heme is shown in red, tetrahydrobiopterin in green, and zinc in magenta. Crosslinks all mapped to distances within the 27 Å linker restraint and are shown as blue bars. Crosslinks that mapped to the shortest distance in the inter-protein configuration are marked with a red asterisk (*). Residues involved in crosslinks are labeled. **(B)**, Crosslinks detected within the nNOS reductase domain are shown mapped to the cryo-EM based model of the reductase domain dimer. Monomers are colored as in (A). Crosslinks that mapped to distances within the 27 Å linker restraint are shown as blue bars; crosslinks bridging longer distances are shown as red bars. FMN cofactor is shown in orange, FAD in yellow, and NADP+ in blue.

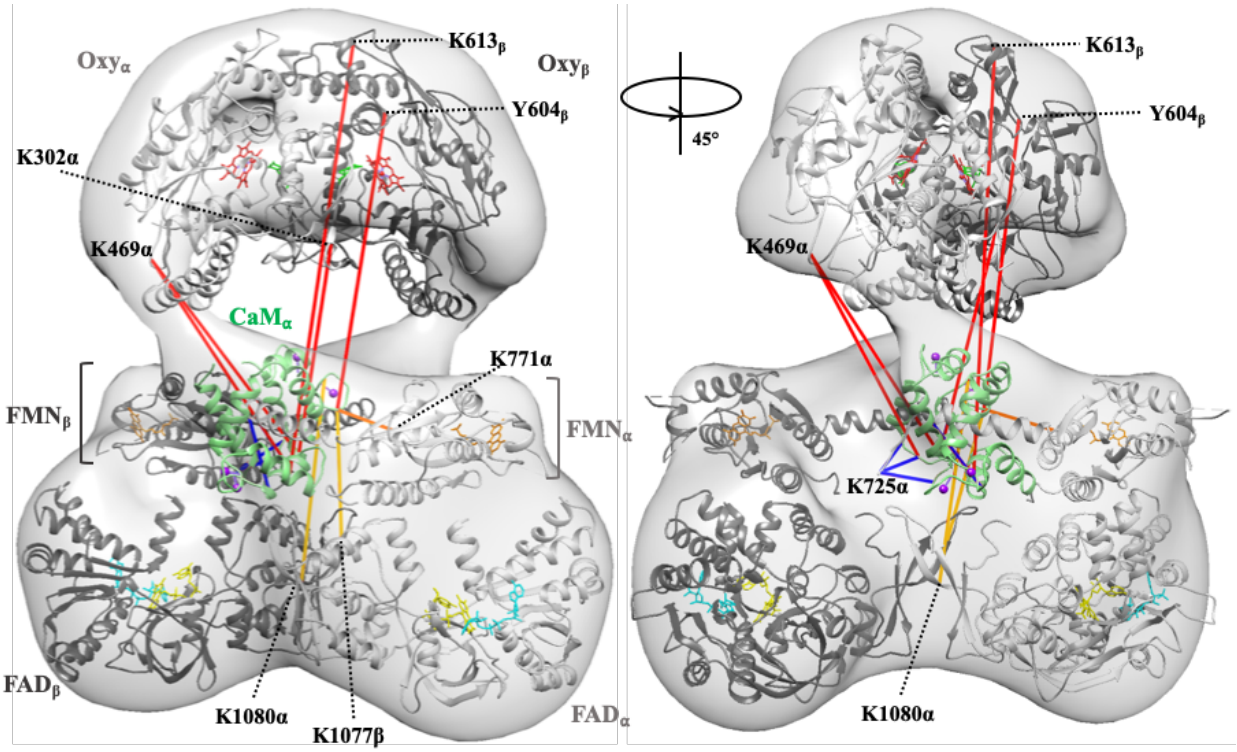


***Figure 3-7.*** *CaM-nNOS crosslinks mapped to cryo-EM based structural model of the nNOS:CaM homodimeric complex.*

A cryo-EM derived model of the nNOS homodimer was generated as described in Methods. nNOS monomers arbitrarily assigned as α and β are colored in light and dark grey respectively within the EM density (shadowed outline). CaM is shown in green. All crosslinks between CaMα and nNOS are shown mapped to their shortest possible distance on the model. Crosslinks between CaM and the nNOS oxygenase domain are shown in red, CaM and its binding helix in blue, CaM-FMN in orange, and CaM-FAD in yellow. Cofactors are colored as in Figure 3-6, and calcium ions are shown in purple.

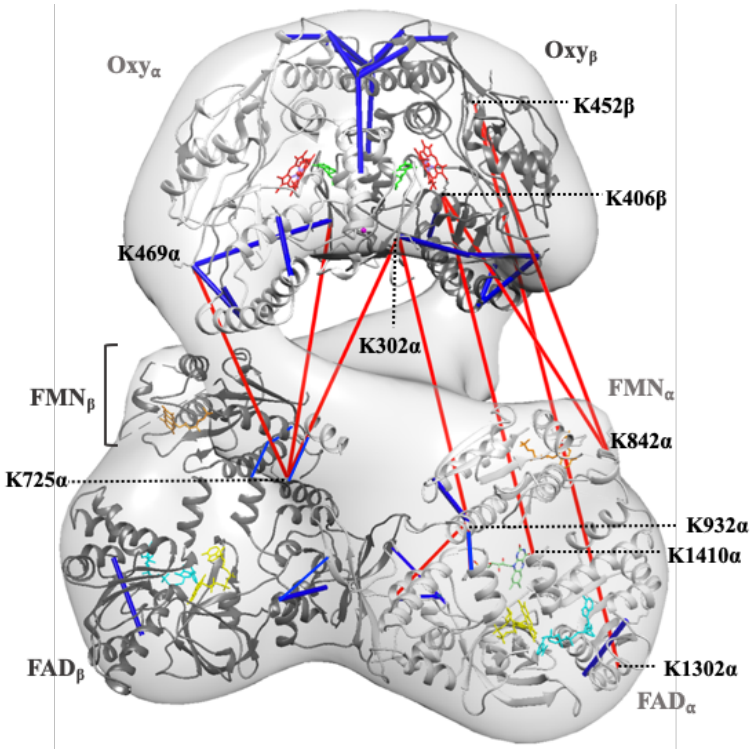


***Figure 3-8.*** *nNOS-nNOS crosslinks mapped to the cryo-EM based model of the nNOS homodimer.*

Crosslinks identified between nNOS residues are shown mapped to the cryo-EM based model of the nNOS homodimer. Crosslinks that bridged $C_\alpha$-$C_\alpha$ Euclidean distances of 27 Å or less are shown as blue bars on both monomers within the dimer. Crosslinks that mapped to distances greater than 27 Å are shown as red bars, mapped only in one monomer to the shortest possible distance. nNOS monomers and cofactors are colored as in Figure 3-6.

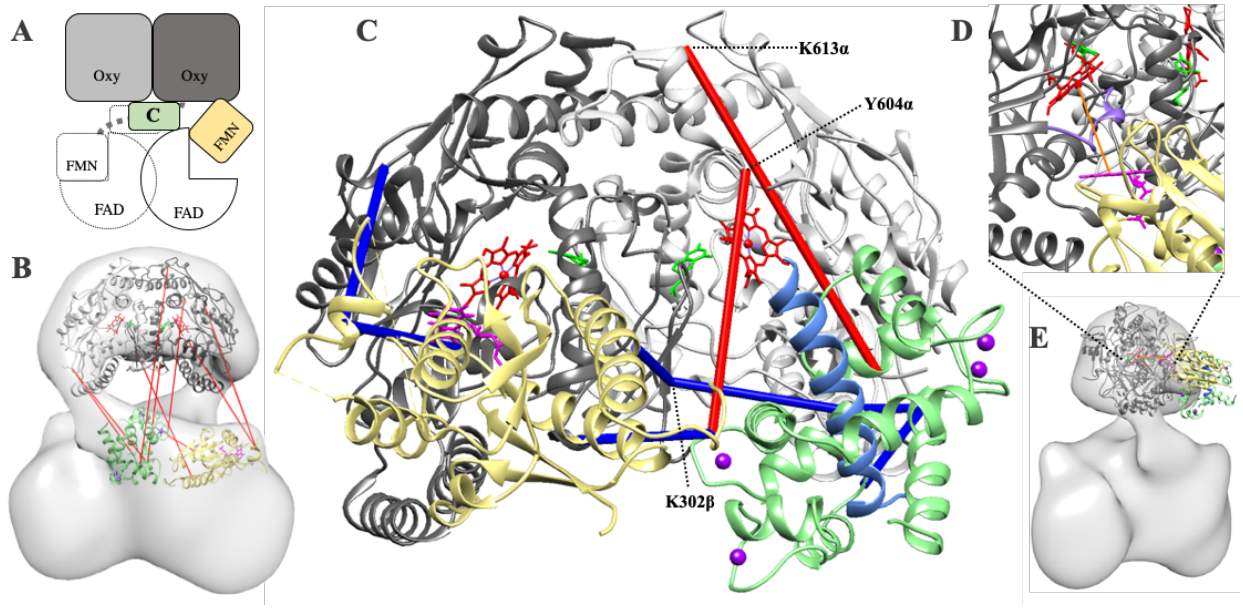


***Figure 3-9.*** *Crosslink-guided intermolecular docking of CaM and nNOS.*

**(A)**, Crystal structures of the nNOS oxygenase domain dimer, nNOS $FMN_{\alpha}$, and $CaM_{\alpha}$ were isolated from the cryo-EM based model of the homodimer. **(B)**, All crosslinks between oxygenase domains, FMN, and CaM were used as restraints to guide docking. These nine total crosslinks are shown mapped as red lines to the structures configured according to the cryo-EM based model of the nNOS:CaM homodimer. HADDOCK was used to perform docking as described in Methods. **(C)**, The result of crosslink-guided docking of $CaM_{\alpha}$ and $FMN_{\alpha}$ to the nNOS oxygenase domain dimer. Oxygenase domains for monomers α and β are shown in light and dark grey, respectively. CaM is shown in green and FMN domain in yellow. The nNOS CaM binding helix corresponding to $CaM_{\alpha}$ is shown in blue, aligned within the CaM docking result according to crystal structure PDB 3HR4. Prosthetic heme is shown in red, calcium in purple, FMN in magenta, and $BH_4$ in green. All crosslinks used to guide the docking experiment are shown mapped to the docking result as blue bars (27 Å or less) or red bars (> 27 Å). **(D)**, Close-up view of the FMN and $heme_{\beta}$ from the rotated angle portrayed in **(E)**. Residues that were previously proposed to make up the lower lip of the heme access point [Hanson et al., 2018] are shown in purple.

# Chapter 4 Discussion

## Contributions

This dissertation research captured transient conformations during structural fluctuations of self-sufficient P450 enzymes in their native states. This work addressed the knowledge gap left by structural analysis of enzymes captured in single conformations, such as x-ray crystallography or cryoelectron microscopy. Novel interactions were identified in this work between reductase and oxygenase domains of both CYP102A1 and nNOS, which likely capture the transient conformational states required for enzyme function. The self-sufficient P450 systems used in this research have proven to be excellent model systems for understanding human P450 function. Strong structural and sequence similarities have been established between the oxygenase domains of CYP102A1, nNOS, and human microsomal P450 systems; similarly, similarities between the reductase domains of these self-sufficient systems and their human cytochrome P450 reductase (CPR) counterpart has been noted in the literature. These studies can therefore serve as models for understanding how human P450 enzyme components interact during conformational shifts necessary for electron transfer and subsequent catalysis.

## Methodological advances

In the course of this dissertation research, I discovered several areas in the CXL-MS workflow where quality could be improved and sources of error minimized. I have optimized these major steps in the process from the reaction of proteins with a covalent crosslinker, to selecting samples for MS analysis, and interpretation of crosslink configuration across protein

monomers. These improvements increase both the fidelity of structural data and the applicability of CXL-MS findings.

***Effective crosslinking reaction quenching is critical.*** In a large portion of the literature applying MS-cleavable crosslinks to protein systems, crosslinkers are quenched by methods I discovered to be inadequate. For example, DSBU quenching with Tris is widely cited in the literature [Jacobsen et al., 2006; Iacobucci et al., 2018; Klykov et al., 2018; Pan et al., 2018; Schäfer et al., 2018; Zhou et al., 2018; Zimmermann et al., 2020]. However, in early studies performed in this dissertation research, a Tris quench was demonstrated via SDS-PAGE to be insufficient to prevent DSBU-induced formation of dimeric species via SDS-PAGE. As shown in Figure 4-1, addition of DSBU in the presence of pre-mixed Tris quench still caused the formation of covalently linked CYP102A1 dimers. This is of concern as numerous studies following the original method put forward by Iacobucci et al. (2018) have utilized Tris quench with MS-cleavable amine-reactive crosslinkers such as DSBU without a control condition demonstrating that an effective quenching of the crosslinking reaction had occurred. Some studies skip the quench entirely, simply adding sample buffer to protein systems while crosslinking reagent is present [Schäfer et al., 2018; Bellia et al., 2019]. In these scenarios as proteins denature, nonspecific crosslinks may form as residues that are not solvent-accessible in the protein's native state. This then causes previously protected residues to be become available for reaction with the un-quenched crosslinker and alters the protein's conformation. These methods allow crosslinking reactions to proceed in an uncontrolled window during protein unfolding. Consequently such procedures have a higher probability of containing inter-residue connectivity that would not be possible in the protein's native conformation, effectively misrepresenting the protein's native state.

***Controlling crosslinking reactions improves data quality.*** Decades of the crosslinking literature contain instances whereby crosslinking reactions have been allowed to proceed to near-total crosslinked product formation as determined by SDS-PAGE. These conditions would be best exemplified by the saturating conditions shown in Figure 4-2A, Lane 8 (*red asterisk*), where over 75% of the original CYP102A1 in the reaction was contained in the crosslinked dimer band (Fig. 4-2B). In my research, it became clear that while this process does generate the maximum amount of crosslinked protein in samples, it also leads to numerous spurious crosslinks formed either nonspecifically across protein complexes due to random collisions in solution or through initial crosslinking "trapping" proteins in conformations not representative of their native conformational state. Once trapped, subsequent crosslink formation within this non-native conformation increases the artificial interconnectivity. An example of this can be seen in Figure 4-2C, which illustrates a number of biologically improbable crosslinks formed in CYP102A1 (red bars) from dimeric sample acquired following 30-minute reaction with DSBU (Fig. 4-2A, black box). This condition was far from the near-complete conversion to dimer typically employed in the crosslinking field, and yet 1/3 of the total crosslinks detected were incompatible with all preexisting structural data on CYP102A1. It is possible the crosslinks seen in red are representative of a never-before-captured conformational state of the CYP102A1 homodimer. However, it is probable that the large numbers of parallel crosslinks between the oxygenase and FAD domains in this sample are due to the homodimer being trapped with these domains in tighter proximity due to crosslinking reactions proceeding unchecked. This contention is reinforced by the fact that these crosslinks did not repeat in samples quenched 15 minutes earlier, even by manually searching at levels below the signal/noise cutoff required for a "hit" within MS data.

The high percentage of spurious crosslinks present in sample with only ~60% of protein crosslinked to dimeric product indicates that a concerning number of non-representative crosslinks in samples analyzed from more saturating reaction conditions (similar to Fig. 2-1A Lane 8) are likely to be commonly presented in the literature. In our studies, limiting the crosslinking reaction to within the linear range of crosslinked product band formation (Figure 2-1A, Lane 4) effectively abolished this issue, resulting in a dataset of highly specific and reproducible crosslinks that were in agreement with orthogonal structural information. As the application of CXL-MS shifts from questions of whether proteins interact to where proteins interact, the fine-tuning of reactions to capture proteins in their native state becomes more relevant. Carefully controlling the crosslink reaction conditions is key to capturing proteins in their endogenous state, and it is essential to validate this conjecture with other structural information when available.

***Crosslink interpretation within homodimeric protein complexes requires complementary structural data.*** The second chapter of this dissertation work included a detailed evaluation of the subtractive method of crosslink assignment when evaluating homodimeric protein complexes. In it, we show that separation by SDS-PAGE before MS analysis was insufficient to separate inter-monomer from intra-monomer crosslinks. A surprising finding in this research was that crosslinks identified in the monomeric band were not consistently reproduced within the dimeric species; this may be due to conformational trapping by the crosslinker, leading to differential crosslink patterns in complexes once inter-monomer crosslinks were formed. Similarly surprising, some intra-monomer crosslinks within the dimer were not detected in the monomeric band. Whether due to biologically relevant conformational differences between these species or artefactual conformations induced by crosslinking, this

phenomenon reinforces our finding that subtracting monomeric from dimeric sample alone is insufficient to appropriately assign crosslinks as intra- versus inter-monomeric in configuration. Instead, integration of structural data from complementary methodologies such as cryo-EM and crystallography are necessary for appropriate assignment of crosslinks in these datasets. The CXL-MS methodology is therefore most effectively applied as a complementary technique to achieve high-fidelity structural information regarding the movement of homomeric protein systems that have been structurally resolved by other methods.

## Commonalities found in dissimilar self-sufficient III P450 systems

***Crosslinks in CYP102A1 and nNOS are consistent with the proposed FMN shuttling model of electron transfer.*** The crosslinking studies in this dissertation research validate the proposed model of self-sufficient P450 interdomain interactions: i.e., that FMN domains shuttle electrons from the intra-protein FAD domain to the active site heme of the opposing monomer. This is indicated in both CYP102A1 and nNOS by the high degree of connectivity observed between the FMN domain and both oxygenase and reductase domains of each system. In order to satisfy all crosslinks detected in these systems, the FMN domain would need to directly contact both oxygenase and reductase domains within its conformational suite; however contacting both at once is unlikely according to existing structural data. Thus, the accepted model of FMN mobility between adjacent domains is supported strongly in this research. With only two crosslinks between FMN and oxygenase domains detected in CYP102A1 that were incompatible with existing structures, triangulating the site of interprotein contact between these domains using crosslinks is likely to be inaccurate [Bullock et al., 2018]. We therefore cannot identify a precise site of interaction between these domains of CYP102A1 from this research. With more intermolecular crosslinks to guide docking, studies examining the nNOS:CaM complex can go

further. Crosslink-guided docking of the FMN and oxygenase in this complex is consistent with FMN domain contacting the oxygenase around oxygenase residue W587 behind the substrate cleft. Although the point of electron transfer cannot be compared across the two self-sufficient P450s examined here, the trajectory of FMN domain appears to be conserved en route to electron transfer.

***Oxygenase-FAD domain crosslink formation in CYP102A1 and nNOS.*** In addition to the expected oxygenase-FMN interconnectivity observed in both enzyme systems, both nNOS and CYP102A1 also underwent oxygenase-FAD domain crosslink formation. This suggests that FAD domain movement toward oxygenase domains occurs during the conformational cycle of both enzymes along with the expected shuttling movement of the FMN domain. The proximity captured by these crosslinks between the oxygenase domain and both reductase domain components of CYP102A1 and nNOS is a surprising finding: although we cannot determine from these studies alone whether this interconnectivity is indicative of direct interdomain contact, it is clearly evident that the FAD domains of self-sufficient P450s experience more orientations relative to oxygenase than previously thought. Direct surface interaction between FAD and oxygenase domains, if confirmed by orthogonal structural methods, would be a novel site of interprotein contact within these complexes.

***Crosslink-guided modeling of both enzymes brings flavins closer to heme.*** In order to examine what conformations were indicated by the oxygenase-reductase domain crosslinks captured in both studies, crosslink-guided intermolecular docking was used [van Zundert et al., 2015]. In these experiments, crosslink distance restraints were used to guide the configuration of domains relative to each other during molecular docking. This method is described in detail in the Chapter 3 Methods. The crosslink-guided docking result of CYP102A1 reductase domain

relative to the oxygenase domain is shown in Figure 4-3A. As seen in panel B, in order to satisfy oxygenase-FAD domain crosslinks the FAD moiety (*blue*) is shifted upward and toward the proximal side of the oxygenase domain away from the opposing reductase. This shift, shown in high resolution in Figure 4-3C, brings the FMN domain into close proximity with the opposing oxygenase. The position of the FMN cofactor in the open II conformation relative to this crosslink-guided model is presented in panel D. The FMN cofactor in the modeled structure (*orange*) is positioned at the edge of the FMN domain, rotated toward the opposing oxygenase (*grey*) and active heme (*red*). This places the FMN 13.3 Å from the iron center of the prosthetic heme, in contrast with the FMN position in the open II structure's 16.8 Å distance. This modeling result orients the FMN in a more favorable position for electron transfer from FMN to heme, and brings both flavins closer to heme than in cryo-EM based structures of the homodimer.

Similar modeling of the nNOS interdomain configuration that best satisfied crosslinks acquired in the nNOS:CaM complex was performed in Chapter 3. The result is shown in Figure 3-9D. The modeling result placed CaM in direct contact with the base of the nNOS oxygenase domain, identifying a novel interprotein interaction within the nNOS:CaM complex. This result also shortened the FMN-heme Euclidean distance to within one third of the 69.4 Å value from the cryo-EM based model. This conformation is much closer to being capable of facilitating electron transfer than the existing cryo-EM based model of the homodimer. While it should not be interpreted as the model for interdomain interaction during electron transfer, it serves as a useful intermediate in understanding the trajectory of the nNOS FMN domain between intraprotein FAD-FMN electron transfer and interprotein FMN-heme transfer. As seen with CYP102A1, having models of multiple conformations of highly flexible proteins greatly

enhances our understanding of the interdomain mechanics necessary for enzyme function. My application of the CXL-MS method helps to build models of additional conformational states, thus enhancing our understanding of domain trajectories during conformational flux.

## Summary & Future Directions

This thesis examined the conformational dynamics of self-sufficient P450 enzymes. In chapter one, a brief context was provided outlining the immense importance of P450 enzymes to human health. As they are involved in the metabolism of a large portion of foreign and endogenous compounds, P450 enzymes are a pillar of biotransformation and detoxification in the body. Within the P450 superfamily, class III enzymes play an important role as model systems for detailed study; insights gained regarding their biomechanics enhance our understanding of the function of membrane-bound systems involved in human metabolism. Covalent crosslinking and mass spectrometry (CXL-MS) utilizing MS-cleavable reagents was presented as an optimal methodology to probe the poorly understood transient conformations of class III systems, and an approach was identified to overcome the unique challenges of applying CXL-MS to homodimeric multiprotein systems such as CYP102A1 and nNOS.

In chapter two, a CXL-MS workflow was developed using the well-studied CYP102A1 homodimer. The subtractive method of crosslink interpretation within homodimeric complexes was examined in detail for efficacy using this system. Crosslinking data were interpreted utilizing recent cryo-EM based models of the homodimer in three different conformational states. Of the 31 total crosslinks detected in CYP102A1, 26 were satisfied by existing conformational models. The remaining five crosslinks do not fit with any existing structural models of the protein and likely captured a conformational state of the protein where the FAD domain is in much closer proximity to the oxygenase domain. Such a conformation would bring

the flavin cofactors much closer to the heme than previously recognized and is thought to enable facile electron transfer from FMN to heme. The subtractive method was found to be inadequate in appropriately assigning crosslinks within vs. across monomers in this system: in addition to the subtractive step, assigning interdomain crosslinks using orthogonal structural and biochemical data was necessary to determine appropriate interdomain crosslink assignment.

In chapter three, the CXL-MS workflow was applied to study the more complex nNOS:CaM multiprotein machinery. nNOS is a critical enzyme responsible for the production of nitric oxide in the brain, and its activity is tightly regulated by the calcium-binding protein CaM. Crystal structures have resolved CaM bound to a truncated helix within the nNOS linker region to which it binds. However, the contacts between CaM and other domains of the full-length nNOS had not been determined. Similarly, individual domains of the nNOS were well resolved by crystallography; however, their interactions during enzymatic turnover were not understood in detail. To address this, the active CaM-bound nNOS dimer was examined by CXL-MS and 74 unique crosslinks were identified within the complex. Thirteen crosslinks between CaM and nNOS were detected, with only four contained within the CaM binding helix of nNOS. Another five crosslinks bridged CaM to the nNOS oxygenase domain, one to the FMN domain, and two to the FAD domain. This large degree of interconnectivity suggests that CaM interacts with both the nNOS oxygenase domain and both components of the nNOS reductase domain. This finding is of particular interest, as CaM association with NOS isozymes is one of the areas of greatest isoform variability. Future research disrupting these interactions could allow the first isoform-specific regulation of nNOS. Within the nNOS homodimer, 11 crosslinks connected the previously unresolved PDZ domain to the nNOS oxygenase domain. This was the first evidence of PDZ domain localization within the active nNOS:CaM complex, indicating it at least

transiently occupies space in close proximity to nNOS oxygenase domains. Three crosslinks between oxygenase and FMN domains allowed the triangulation of FMN domain configuration relative to nNOS oxygenase using crosslink-guided intermolecular docking. This experiment placed the FMN directly adjacent to the previously proposed site of FMN to heme electron transfer. Two crosslinks between oxygenase and FAD domains demonstrated that both components of the nNOS reductase domain come in closer proximity to the oxygenase than previously captured by structural models of the holoenzyme. These studies demonstrated novel interprotein and interdomain connectivity within the nNOS:CaM complex, and provided new insights on nNOS domain trajectories in the complex's transient conformational states.

Several sites of interdomain and interprotein interaction in these vastly different class III P450 protein systems had not been identified previously. While crosslinking studies cannot confirm direct interdomain or interprotein contact at these sites, future research is well positioned to investigate these areas of interaction in closer detail. In particular, determination of whether the oxygenase-FAD domain interaction observed in both P450 systems was representative of direct interdomain contact would change our understanding of how soluble P450 enzymes move during electron shuttling to the active site heme. In addition, the oxygenase-FMN interface must be studied in greater detail. Introduction of bulky side chains within the oxygenase-FMN domain interfaces indicated by these studies would be an expedient way to confirm whether these interactions are critical in catalytic turnover of CYP102A1 and nNOS, and provide target sites for disruption of nNOS electron transport. Similar disruption of the CaM:nNOS oxygenase domain interface by introduction of bulky sidechain could confirm or deny the necessity of this interface in enzyme function, and potentially identify an isoform-specific target site for pharmacologic control of this important multiprotein complex. Application of CXL-MS using

amine-reactive chemical crosslinkers with increasingly short linker arm lengths would be an additional approach to provide insight on the closeness of each multi-domain interaction captured here: as increasingly short linkers lengths are applied to systems, only increasingly close interdomain proximities would be captured by crosslink formation.

Interprotein and interdomain interfaces are effective target sites for pharmacological control of large multiprotein machineries. The research in this dissertation established a sound methodology to explore interprotein interactions in P450 systems of increasing complexity and applicability to human health using the most well-studied, self-sufficient cytochrome P450 systems. Furthermore, this research developed a robust method that could be extended to future investigation of similar homomeric multiprotein systems. The novel interactions identified here in both self-sufficient P450 systems may be conserved across different classes of P450s such as human microsomal systems. Future research applying this CXL-MS method to study less well-characterized systems, such as the human CYP2B4 complexed with CPR, would determine whether the interprotein interactions observed in this research are conserved across different classes of P450 systems sharing similar functional units.

The mechanics of P450 systems are of immense importance in human health. This protein superfamily is responsible for the metabolic processing of foreign compounds in humans, and dictates chemical half-life in the body. Understanding P450 function is therefore vital in understanding the physiologic consequences of environmental exposures. This dissertation work used two model systems to better understand how functional units of P450s interact during transient configurations critical for enzyme function. Through this dissertation work, we gained better insights on how oxygenase and reductase components of P450s orient relative to each other during electron turnover, and identified novel target regions for pharmacologic regulation

of these metabolic protein systems. These findings expand our ability to predict mechanics of P450 systems, which play a vital role in toxicant metabolism, drug development, and bioremediation applications.

## References


Bellia, F.; Lanza, V.; García-Viñuales, S.; Ahmed, I. M. M.; Pietropaolo, A.; Iacobucci, C.; Malgieri, G.; D'Abrosca, G.; Fattorusso, R.; Nicoletti, V. G.; Sbardella, D.; Tundo, G. R.; Coletta, M.; Pirone, L.; Pedone, E.; Calcagno, D.; Grasso, G.; Milardi, D. Ubiquitin Binds the Amyloid β Peptide and Interferes with Its Clearance Pathways. *Chem. Sci.* **2019**, *10* (9), 2732–2742. https://doi.org/10.1039/C8SC03394C.

Bullock, J. M. A.; Sen, N.; Thalassinos, K.; Topf, M. Modeling Protein Complexes Using Restraints from Crosslinking Mass Spectrometry. *Structure* **2018**, *26* (7), 1015-1024.e2. https://doi.org/10.1016/j.str.2018.04.016.

Iacobucci, C.; Götze, M.; Ihling, C. H.; Piotrowski, C.; Arlt, C.; Schäfer, M.; Hage, C.; Schmidt, R.; Sinz, A. A Cross-Linking/Mass Spectrometry Workflow Based on MS-Cleavable Cross-Linkers and the MeroX Software for Studying Protein Structures and Protein–Protein Interactions. *Nat Protoc.* **2018**, *13* (12), 2864–2889. https://doi.org/10.1038/s41596-018-0068-8.

Jacobsen, R. B.; Sale, K. L.; Ayson, M. J.; Novak, P.; Hong, J.; Lane, P.; Wood, N. L.; Kruppa, G. H.; Young, M. M.; Schoeniger, J. S. Structure and Dynamics of Dark-State Bovine Rhodopsin Revealed by Chemical Cross-Linking and High-Resolution Mass Spectrometry. *Protein Sci.* **2006**, *15* (6), 1303–1317. https://doi.org/10.1110/ps.052040406.

Klykov, O.; Steigenberger, B.; Pektaş, S.; Fasci, D.; Heck, A. J. R.; Scheltema, R. A. Efficient and Robust Proteome-Wide Approaches for Cross-Linking Mass Spectrometry. *Nat Protoc.* **2018**, *13* (12), 2964–2990. https://doi.org/10.1038/s41596-018-0074-x.

Pan, D.; Brockmeyer, A.; Mueller, F.; Musacchio, A.; Bange, T. Simplified Protocol for Cross-Linking Mass Spectrometry Using the MS-Cleavable Cross-Linker DSBU with Efficient Cross-Link Identification. *Anal. Chem.* **2018**, *90* (18), 10990–10999. https://doi.org/10.1021/acs.analchem.8b02593.

Schäfer, P.; Tüting, C.; Schönemann, L.; Kühn, U.; Treiber, T.; Treiber, N.; Ihling, C.; Graber, A.; Keller, W.; Meister, G.; Sinz, A.; Wahle, E. Reconstitution of Mammalian Cleavage Factor II Involved in 3′ Processing of MRNA Precursors. *RNA.* **2018**, *24*, 1721–1737.

van Zundert, G. C. P.; Rodrigues, J. P. G. L. M.; Trellet, M.; Schmitz, C.; Kastritis, P. L.; Karaca, E.; Melquiond, A. S. J.; van Dijk, M.; de Vries, S. J.; Bonvin, A. M. J. J. The HADDOCK2.2 Web Server: User-Friendly Integrative Modeling of Biomolecular Complexes. *J Mol Biol.* **2015**, *428* (4), 720–725. https://doi.org/10.1016/j.jmb.2015.09.014.

Zhou, J.; Yang, L.; Ozohanics, O.; Zhang, X.; Wang, J.; Ambrus, A.; Arjunan, P.; Brukh, R.; Nemeria, N. S.; Furey, W.; Jordan, F. A Multipronged Approach Unravels Unprecedented Protein–Protein Interactions in the Human 2-Oxoglutarate Dehydrogenase Multienzyme Complex. *J Biol Chem.* **2018**, *293* (50), 19213–19227. https://doi.org/10.1074/jbc.RA118.005432.

Zimmermann, F.; Serna, M.; Ezquerra, A.; Fernandez-Leiro, R.; Llorca, O.; Luders, J. Assembly of the Asymmetric Human γ-Tubulin Ring Complex by RUVBL1-RUVBL2 AAA ATPase. *Sci. Adv.* **2020**, *6* (51), eabe0894. https://doi.org/10.1126/sciadv.abe0894.

## Acknowledgements

The FP7 WeNMR (project# 261572), H2020 West-Life (project# 675858), the EOSC-hub (project# 777536) and the EGI-ACE (project# 101017567) European e-Infrastructure projects are acknowledged for the use of their web portals, which make use of the EGI infrastructure with the dedicated support of CESNET-MCC, INFN-PADOVA-STACK, INFN-LNL-2, NCG-INGRID-PT, TW-NCHC, CESGA, IFCA-LCG2, UA-BITP, SURFsara and NIKHEF, and the additional support of the national GRID Initiatives of Belgium, France, Italy, Germany, the Netherlands, Poland, Portugal, Spain, UK, Taiwan and the US Open Science Grid.

## Figures

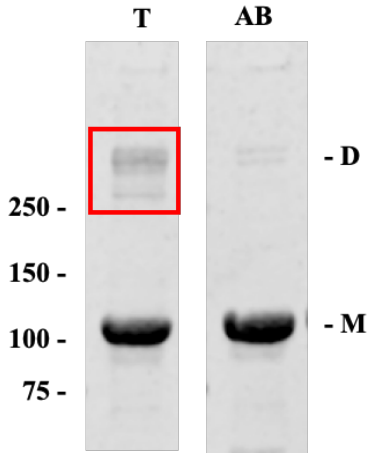


***Figure 4-1.*** *Ineffective quench of DSBU crosslinking of the CYP102A1 homodimer.*

CYP102A1 (10 µM) was quenched with 50 mM Tris (**T**) or ammonium bicarbonate (**AB**) for 5 minutes at 4ºC with mixing, then treated with 0.5 mM DSBU for five minutes at room temperature before addition of sample buffer containing 10% (v/v) β-mercaptoethanol. Aliquots of the reaction mixture corresponding to 3 µg/lane were submitted to SDS-PAGE analysis and stained with Coomassie Blue. Band **–D** corresponds to the crosslinked dimeric CYP102A1 and **–M**- the monomeric. Formation of covalently linked CYP102A1 dimer occurred in the presence of Tris quench (*red box*) but not ammonium bicarbonate.

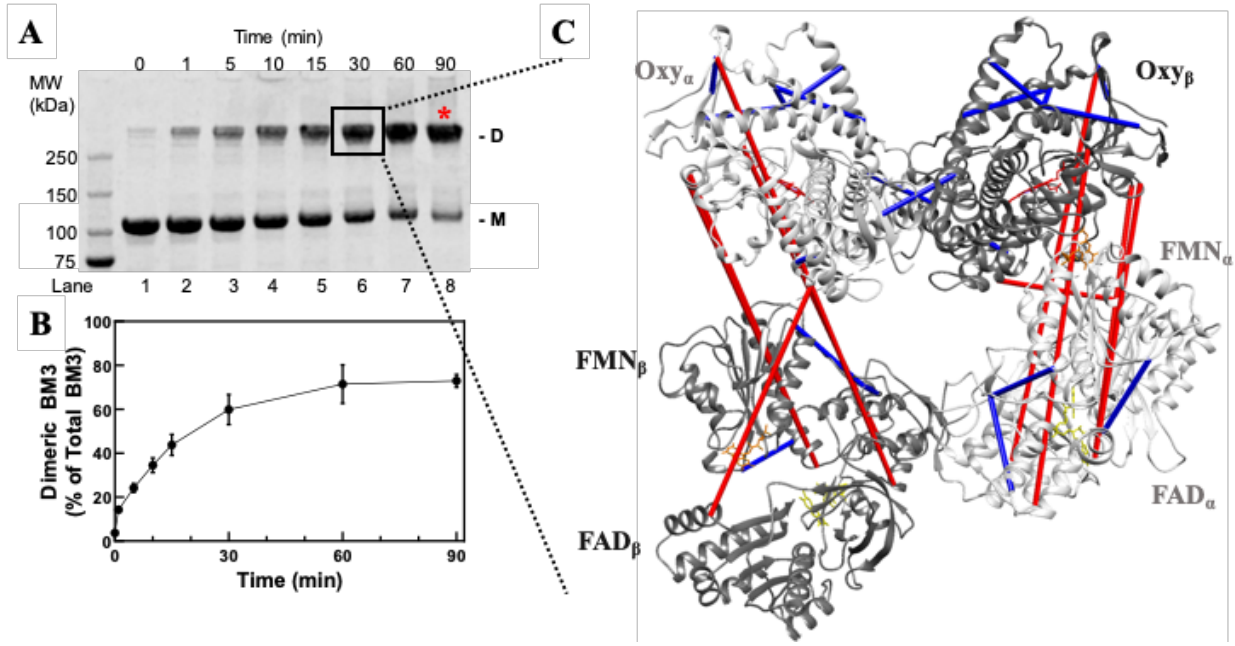


***Figure 4-2.*** *Formation of spurious crosslinks in the CYP102A1 dimeric sample.*

CYP102A1 (10 µM) was treated with 0.5 mM DSBU for the indicated time and quenched as described in Chapter 2 Methods. **(A)**, Aliquots of the reaction mixture corresponding to 3 µg/lane were submitted to SDS-PAGE analysis and stained with Coomassie Blue. Band **–D** corresponds to the crosslinked dimeric CYP102A1 and **–M**- the monomeric. **(B)**, The intensity of the dimeric and monomeric BM3 bands were quantified as described in Chapter 2 Methods. The amount of dimer is expressed as percent of combined monomer and dimer signal for each condition. Signal for all bands was within the linear range of detection for the stain. Results from n=3 gels were quantified and displayed as mean ± SD. **(C)**, Crosslinks identified in the dimeric band following 30-minute reaction with DSBU are shown mapped to the cryo-EM based model of CYP102A1 in its Open I conformation. Crosslinks that mapped to C-C Euclidean distances within the 27Å DSBU linker arm restraint are shown as blue bars, and crosslinks bridging distances greater than 27Å are shown as red bars. The oxygenase, FMN, and FAD domains of monomers arbitrarily assigned as α and β are labeled.

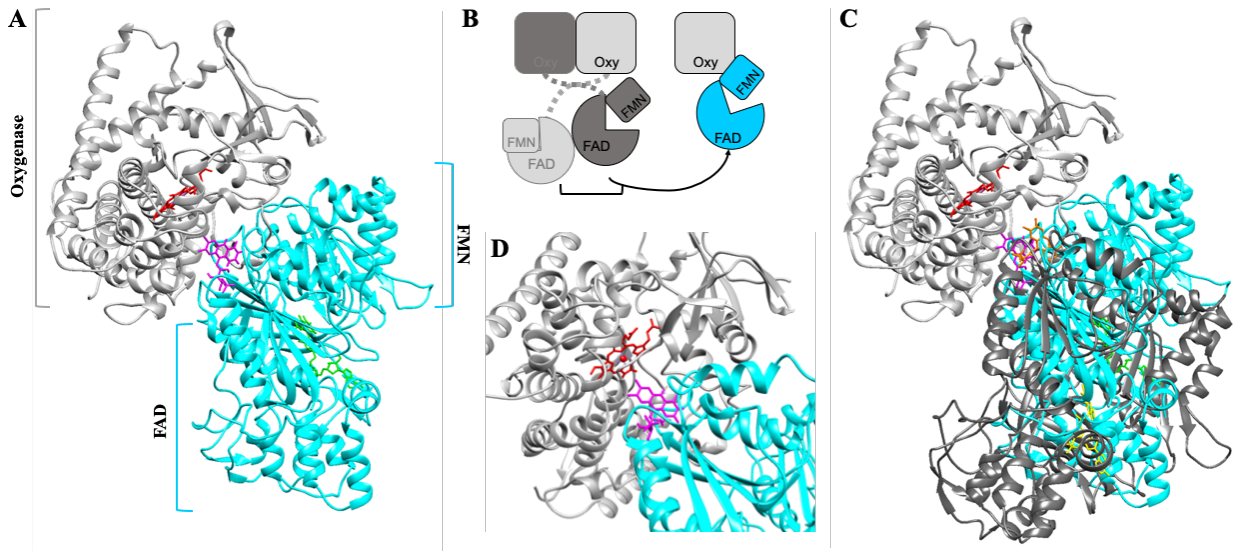


***Figure 4-3.*** *Crosslink-guided docking of CYP102A1 reductase domain in open conformation to opposing oxygenase domain.*

All crosslinks identified in dimeric samples between oxygenase and reductase domains of CYP102A1 were used as distance restraints to guide docking, and interaction of the reductase domain in its open II conformation with its opposing oxygenase domain was predicted using Haddock as described in Chapter 3 Methods. The resulting model of interdomain interaction is shown in **(A)**, with oxygenase domain shown in grey and reductase in blue. Prosthetic heme is shown in red, FMN in magenta, and FAD in green. **(B)**, A schematic depicting the right half of the homodimer in Open II conformation compared to the Haddock output. **(C)**, the Haddock-generated model from Panel A is shown with overlay of reductase domain from the cryo-EM model of the CYP102A1 homodimer in its Open II conformation in dark grey. Both reductase domains are positioned in relation to the same oxygenase domain to highlight the shift reflected from the EM model to the crosslink-guided model. Open II FMN is in orange and FAD in yellow. **(D)**, The FMN domain and cofactor position in the docking result, viewed from bottom right of (A).